Theses and Dissertations

August 2016

Transient Control of Synchronous Machine Active and Reactive Power in Micro-Grid Power Systems

Luke Gerard Weber
University of Wisconsin-Milwaukee

Transient Control of Synchronous Machine Active and Reactive Power in Micro–grid Power Systems

by

Luke G. Weber

A Dissertation Submitted in
Partial Fulfillment of the
Requirements for the Degree of

Doctor of Philosophy
in Engineering

at

The University of Wisconsin–Milwaukee
August 2016

ABSTRACT

TRANSIENT CONTROL OF SYNCHRONOUS MACHINE ACTIVE AND
REACTIVE POWER IN MICRO–GRID POWER SYSTEMS

by

Luke G. Weber

The University of Wisconsin–Milwaukee, 2016
Under the Supervision of Professor Adel Nasiri

There are two main topics associated with this dissertation. The first is to investigate phase–to–neutral fault current magnitude occurring in generators with multiple zero–sequence current sources. The second is to design, model, and tune a linear control system for operating a micro–grid in the event of a separation from the electric power system.

In the former case, detailed generator, AC8B excitation system, and four–wire electric power system models are constructed. Where available, manufacturers data is used to validate the generator and exciter models. A gain–delay with frequency droop control is used to model an internal combustion engine and governor. The four wire system is connected through a transformer impedance to an infinite bus. Phase–to–neutral faults are imposed on the system, and fault magnitudes analyzed against three–phase faults to gauge their severity.

In the latter case, a balanced three–phase system is assumed. The model structure from the former case – but using data for a different generator – is incorporated with a model for an energy storage device and a net load model to form a micro–grid. The primary control model for the energy storage device has a high level of detail, as does the energy storage device plant model in describing the LC filter and transformer. A gain–delay battery and inverter model is used at the front end.

The net load model is intended to be the difference between renewable energy sources and load within a micro–grid system that has separated from the grid. Given the variability of

both renewable generation and load, frequency and voltage stability are not guaranteed. This work is an attempt to model components of a proposed micro–grid system at the University of Wisconsin Milwaukee, and design, model, and tune a linear control system for operation in the event of a separation from the electric power system. The control module is responsible for management of frequency and active power, and voltage and reactive power.

The scope of this work is to

- develop a mathematical model for a salient pole, 2 damper winding synchronous generator with d axis saturation suitable for transient analysis,

- develop a mathematical model for a voltage regulator and excitation system using the IEEE AC8B voltage regulator and excitation system template,

- develop mathematical models for an energy storage primary control system, LC filter and transformer suitable for transient analysis,

- combine the generator and energy storage models in a micro–grid context,

- develop mathematical models for electric system components in the stationary abc frame and rotating dq reference frame,

- develop a secondary control network for dispatch of micro–grid assets,

- establish micro–grid limits of stable operation for step changes in load and power commands based on simulations of model data assuming net load on the micro–grid, and

- use generator and electric system models to assess the generator current magnitude during phase–to–ground faults.

iv

To my wife Linda K. Nelson

TABLE OF CONTENTS

List of Figures

LIST OF TABLES

Acknowledgements

Chapter 1

Introduction

The objectives for this dissertation are two–fold. The first objective entails the construction of a detailed synchronous machine model including an accurate representation of the zero–sequence network, d axis saturation, and voltage regulation. The prime mover and governor model is less sophisticated, incorporating speed droop control ahead of a gain and delay. The generator stator terminals feed a four–wire electrical system which is connected via a transformer to the outside electric power system, commonly referred to as the grid. Simulations are performed to determine the effects interconnecting with the grid has on generator current magnitude during line–to–neutral faults occurring at the generator terminals.

The second objective revolves around the idea of connecting synchronous generators to systems otherwise fed through power electronic inverter devices. When there is no connection to the grid, this is commonly referred to as a micro–grid. To accomplish this task, a detailed model of major components of the energy storage device is developed – the LC filter and transformer, and primary control mechanisms. A gain and delay is used to model the battery and inverter.

Much of the work from the first objective is incorporated into the second. However, the design of the energy storage device is such that the transformer connecting the 208 [V] energy storage system to the 480/277 [V] four–wire electrical system does not permit the flow of zero–sequence current to the load. As a result, a balanced system load is assumed in developing the controls for this objective.

A secondary control system is developed to weigh several inputs in the active and reactive power dispatch of the synchronous machine and energy storage device while operating

as a micro–grid. The inputs for dispatch of active power are frequency and active power loading, and reactive power dispatch depends on voltage and reactive power loading.

1.1 Problem Statements

Per NEMA design standards [22], synchronous machines are braced for fault magnitudes equal to three phase bolted fault at the generator terminals. A phase–to–neutral fault at the generator terminals will in general exceed the magnitude of the three phase value. Further, it has been advanced by several authors [23, 37, 2] that a connection to another source of zero–sequence current further increases the fault magnitude.

Under normal conditions, micro–grids are connected to a distribution, subtransmission or transmission system. The connection serves as a swing bus for power flow, supports stable frequency and voltage, and provides fault current for protective device coordination and operation. When the micro–grid separates from the grid proper, it may be susceptible to frequency and voltage instability, and maintaining electric service to critical loads becomes non–trivial.

Assuring long term viability of the micro–grid is essential as electric power system outages may extend for some time. Hurricanes Katrina in August, 2005 and Sandy in October and November, 2012 in the United States, and the earthquake and ensuing tsunami in Japan March 11, 2011 are taken as examples.

1.2 Literature Review

1.2.1 Generator Model

The generator model selected for this dissertation primarily is defined in [6] for a salient pole generator with one (1) field winding, one (1) d–axis damper winding, and one (1) q–axis damper winding. Using the rotating 0dq reference frame, the model permits usage

of readily available test data for most generators. The model contains a total of eight (8) states: six (6) current states, a velocity state, and a position state. Inputs to the model are voltages on the 0, d, and q axes, field voltage, and mechanical power. This model was chosen because it is intuitive to the author, and with additional data and programming allows for modeling saturation along the d–axis and q–axis.

One model considered replaces the six (6) current states in the chosen model with flux linkage states as seen in [15]. Here the inputs are currents in the 0, d and q axes, field current, and mechanical power or torque. Another model found in [13, 34] utilizes impedances referred to the positive, negative and zero sequence axes, and takes advantage of phasor terminology for expressing state variables. In [13], a dynamic model is not thoroughly developed, but in [34], the states are a mix of voltages and flux linkages.

Generators with cylindrical rotors are often modeled using nine (9) states with the addition of a second q–axis damper winding [36]. Higher order models may be appropriate for modeling the damping effects of eddy currents in the rotor iron [14].

The citations herein used comparable model complexity to the eight (8) state model. Standard generator testing for salient pole and cylindrical rotor machines generally produces sufficient data to create a eight (8) and nine (9) state models respectively, and simplification at the outset was deemed unnecessary.

1.2.2 Generator Mechanical Forces

In [23, 37, 2] concern is expressed for mechanical stresses experienced by synchronous generators under line–to–ground fault conditions when neutral connections are made without intentional impedance. Roughly half this dissertation is dedicated to developing generator and electric power system models that may be used to model this phenomenon. As a byproduct, a nonlinear model capable of simulating four wire systems with phase load imbalance is created.

Statements regarding the superiority of Time–Phase Domain generator models over

stationary frame 0dq generator models for transient analysis [8, 31] are countered by claims that the two modeling techniques produce comparable results [32, 36]. Authors in [36] state that since the models are directly drawn from each other, the close match is expected.

1.2.3   Electric Power System Model

Two model representations of electric power systems will be used in this dissertation. For the unbalanced system model of the generator with connections to an electric power system, the electric power system is modeled in the stationary abc reference frame. Here the equations for state variables are linear, but steady state conditions produce sinusoidal states. Electric power system parameters are often expressed as positive, negative and zero sequence values which are readily converted to stationary abc frame parameters.

For the balanced system control development section, the electric power system is represented in the rotating 0dq reference frame, and the equations become non–linear due to a cross coupling frequency term.

Lumped parameter equivalent π models are used for electric power system cables, and series resistance and inductance models for transformers.

1.2.4   Synchronous Generator Prime Mover Model

It is recognized that the synchronous generator prime mover contributes to the overall system response characteristics. It is also recognized that internal combustion engine models can be very complex, for example [11, 29]. For this dissertation, a simple gain and delay will be used to model the prime mover.

1.2.5   Micro–grid Stability Analysis

In [18] micro–grid energy sources interconnect using inverters. A natural gas fueled permanent magnet generator used for combined heat and power is equipped with a rectifier and inverter. Each source is equipped with batteries on the DC bus to provide energy

bursts for transient ride–through. Local power versus frequency droop and reactive power control are used exclusively for grid control. In [17], a similar control approach is used with the addition of a central communication system to dispatch distributed generation set points. The authors indicate the dispatch element is intended to improve steady state operation, not for improving dynamic operation. Convincing field test data are provided to the exclusion of frequency regulation. The bulk of [24] is the detail behind the operation of the surge module used in [18] and [17]. The authors describe droop settings that could cause a 0.5 [Hz] (0.83%) frequency decline for a load increase of 60 [kW].

The control scheme described in [10] uses a concept called angle droop to control active power, and voltage droop to control reactive power. Simulations are used to characterize real power flow and current flow during normal and faulted conditions. Analysis of frequency deviation is not included. In [38] the control architecture does not require a centralized control device. Rather, each energy source including renewable sources participates in the regulation of frequency using frequency thresholds to alter the control characteristics. Authors in [9] develop a hierarchy of control systems for single phase inverters operating in parallel within a micro–grid. In [20] a master inverter in voltage mode and a slave inverter in current mode is established for inverters located near to each other. Inverters remote from the voltage mode unit employ voltage and frequency droop for control. In [21], data communications between inverters is used in conjunction with locally measured quantities to generate the control set points for fundamental and harmonic load sharing.

Based on the assumption that an energy storage inverter operating in voltage control mode will respond more quickly to changes in grid loading than will synchronous machines, the authors in [35] propose a virtual droop control system that dispatches assets based on virtual frequency and voltage calculations. Dispatchable energy sources within the micro–grid are assigned frequency and voltage droops that determine the participation of each in the restoration of desired voltage and frequency in the event of changes in net loading. Simulations and field test data provide convincing evidence the method works as posited,

demonstrating near isochronous control and tight voltage regulation. A control design for unit commitment is included in the work.

1.2.6   Limitations of Past Work

The limitations of past work are the exclusion of saturation in considering synchronous machine voltage regulation and fault contributions. Past work has also focused on balanced three–phase systems, while model structures developed permit modeling of saturation and zero–sequence networks.

Chapter 2

Transformer Connections and Grounding

2.1 Electric Power System Interfaces

Disregarding utility conventions and restrictions, conceivable transformer connections are detailed in Table 2.1. Analysis of faults occurring on the Electric Power System show that micro–grid resources can contribute current during line–to–ground faults for transformer connections 1, 2 and 3[1] only. If any other connection in Table 2.1 is used, the micro–grid will see infinite zero–sequence impedance to the Electric Power System, and cannot contribute current during line–to–ground faults. Fault detection schemes for micro–grids should not rely on fault current magnitude alone since power electronic interfaces are current limited to near 1 per–unit.

2.2 Grounding Systems

Capacitance grounded (ungrounded) systems are used when continuity of service is paramount, but locating ground faults is time consuming, and there are risks to personnel and equipment should another phase fault to ground. The main reason capacitance grounded systems are no longer recommended is to prevent transient overvoltages that result during restriking faults [5].

Systems which have a solid connection to the grounding system present low impedance paths for current during line–to–ground faults. Transformers without zero sequence paths to the source present systems with maximum fault currents available for line–to–ground

---

[1]Transformers using connection 3 are susceptible to burnout on Electric Power System faults, and the transformer will act as a grounding transformer for Electric Power System imbalance, reducing capacity to serve load or supply power, possibly leading to burnout.

Transformer Connection Number	Electric Power System Configuration	Transformer Winding Configuration	Transformer Winding Configuration	Micro Grid System Configuration
1	4 Wire	Gnd–Y	Gnd–Y	4 Wire
2	4 Wire	Gnd–Y	Y	3 or 4 Wire
3	4 Wire	Gnd–Y	Δ	3 or 4 Wire
4	4 Wire	Y	Gnd–Y	4 Wire
5	4 Wire	Y	Y	3 or 4 Wire
6	4 Wire	Y	Δ	3 or 4 Wire
7	4 Wire	Δ	Gnd–Y	4 Wire
8	4 Wire	Δ	Y	3 or 4 Wire
9	4 Wire	Δ	Δ	3 or 4 Wire
10	3 Wire	Y	Gnd–Y	4 Wire
11	3 Wire	Y	Y	3 or 4 Wire
12	3 Wire	Y	Δ	3 or 4 Wire
13	3 Wire	Δ	Gnd–Y	4 Wire
14	3 Wire	Δ	Y	3 or 4 Wire
15	3 Wire	Δ	Δ	3 or 4 Wire

Table 2.1: Conceivable transformer connections between Electric Power Systems and Micro Grid Systems.

faults. The preponderance of interruptions in plant distribution systems are caused by line–to–ground faults [37]. Potential concerns with using solidly grounded systems:

- High arc fault energy could cause injuries, or damage equipment

- Line–to–ground faults cause voltage dips which may interrupt critical loads

- Generators designed to NEMA MG–1 are not braced to withstand ground faults that exceed the three–phase fault capability [37, 23]

- Ground fault coordination requires relaying equipment and coordination studies. In the context of a micro–grid, coordination will be difficult if separation occurs and power electronic sources are prominent.

High resistance grounding offers the same resilience to ground faults as capacitance grounding, with the benefit of limiting steady state and severe transient overvoltages inherent in capacitance grounded systems [1]. Commonly used at synchronous generators

to limit current flow during ground faults, high impedance grounding systems are gaining traction for industrial and commercial power systems. Low voltage systems without line–to–neutral loads, medium voltage systems where continuity of service is critical, and retrofits of ungrounded systems are all candidates [5]. Ground fault locating is done by altering the grounding resistance between two values, creating a pulse signal which can be traced to the ground fault. Reducing the current magnitude of ground faults using high impedance grounding is beneficial for several reasons:

- Limits arc fault energy eliminating equipment damage and providing a safer workplace

- Does not cause a disturbance in the system voltage

- Generators designed to NEMA MG–1 are not designed for solidly grounded systems [37, 23]

> "The reasons for limiting the current by resistance grounding include the following: a) To reduce burning and melting effects in faulted electric equipment, such as switchgear, transformers, cables, and rotating machines. b) To reduce mechanical stresses in circuits and apparatus carrying fault currents. c) To reduce electric-shock hazards to personnel caused by stray ground-fault currents in the ground–return path. d) To reduce the arc blast or flash hazard to personnel who may have accidentally caused or happen to be in close proximity to the ground fault. e) To reduce the momentary line–voltage dip occasioned by the occurrence and clearing of a ground fault. f) To secure control of transient overvoltages while at the same time avoiding the shutdown of a faulted circuit on the occurrence of the first ground fault (high–resistance grounding)." [5]

2.3 Synchronous Generators

Synchronous generators connected to the bulk electric system through a single transformation normally utilize impedance grounding to protect the generator from terminal ground fault current exceeding generator mechanical design limitations. Further, these bulk electric system generators are protected from transmission system zero–sequence currents by the interconnecting transformer winding arrangement.

Largely due to the conditions stated, academic textbooks focus on simulation of generators connected to balanced systems [16, 26, 15, 6], and calculation of negative sequence current flow during fault conditions is developed in [19, 27, 7]. An assumption of balanced voltage, current, impedance, and load characteristic of transmission systems leads to many simulation software realizations using a single phase system model to assess electromechanical phenomena [30].

Following the passage of the Public Utilities Regulatory Policy Act (PURPA) of 1978, it made business sense for some manufacturing plants in the US to install local generation burning byproduct fuels. As a consequence, mechanical stresses experienced by synchronous generators under line–to–ground fault conditions when neutral connections are made without intentional impedance became a concern [23, 37, 2]. More recently, the growth of distributed generation connected to unbalanced low voltage systems fuels an interest in models capable of accurately predicting generator and other power system component transient behavior in that context [33, 34, 32, 36]. The stated trend – using generators without intentional impedance between the generator neutral and electric power system neutral – is consistent with discussions with generator manufacturer Regal Beloit for system voltages up to 4 [kV]. At the University of Wisconsin Milwaukee, a micro–grid project includes two Kohler natural gas generators that are connected directly to the 480Y/277 [V] bus without intentional impedance in the generator neutral connection.

Authors of [8, 31] assert the superiority of time phase domain generator models over rotating frame 0dq generator models for transient analysis, while in [32, 36] the authors

claim either technique produces comparable results. Authors in [36] state that since the time phase domain, 0dq axes, and voltage behind reactance models are directly drawn from each other, a close match is expected, provide proper care is taken in the model development and simulation time step considerations.

Chapter 3

General Equations for Electrical System States and Parameters in the abc Reference Frame

J.E. Hobson and D. L. Whitehead write in [25]

> "The analysis of a three–phase circuit in which phase voltages and currents are balanced (of equal magnitude in three phases and displaced 120° from each other), and in which all circuit elements in each phase are balanced and symmetrical, is relatively simple since the treatment of a single–phase leads directly to the three–phase solution. The analysis by Kirchoff's laws is much more difficult, however, when the circuit is not symmetrical, as a result of unbalanced loads, unbalanced faults or short–circuits that are not symmetrical in the three phases."

Toward the end of simplifying the analysis of unbalanced three–phase systems, transformations to frames of reference other than the rotating abc frame have been developed. Use of abc to zero (0), positive (+) and negative (-) sequence components by software developers, electrical utilities, transmission system owners and operators, and independent market operators is at a mature stage. Generator owners and operators typically use transformations to zero (0), direct (d) quadrature (q) axes under the assumption of symmetrical electrical power systems.

Attention has focused on simulation of generators connected to balanced systems [15, 26, 6, 16], and calculation of negative sequence [7, 19] and zero sequence [37, 23] current flow during fault conditions. There has not been an exhaustive treatment and simulation of generators that connect to systems which may be exposed to unbalanced conditions –

due either to load connections, or the inception of line–to–neutral faults at the generator level. Simulation software to the inclusion of Mathworks Matlab® Simulink®, ANSYS Simplorer®, Manitoba Hydro International Ltd. PSCAD®, and Siemens PSSE® do not provide dynamic simulation models that include connections to the neutral point of the generator. Some of the packages offer a simple voltage–behind–impedance model with access to the neutral point, without modeling the field and damper winding interactions of a synchronous machine.

There is good reason for these model limitations. Generators connected to the transmission system are normally configured with grounding impedance to limit the magnitude of line–to–ground fault currents, and disconnection is initiated based on the voltage appearing across the grounding impedance. Similar recommendations apply for generators connected at the customer level with or without transformation between the local electric power system [1, 37, 23].

In contrast, customers of the Regal Beloit Corporation indicate using generators without impedance between the generator neutral and system neutral at voltages up to 4 [kV]. At the University of Wisconsin Milwaukee, a micro–grid project includes two Kohler Company natural gas generators that are connected directly to the 480Y/277 [V] bus without impedance in the generator neutral connection.

3.1   Series Resistance and Inductance

The series elements of an electrical transmission line may be represented in the abc reference frame by the the resistances and inductances as shown in Figure 3.1 on Page 14 [26]. At power frequencies of 50 or 60 [Hz], lumped parameter models have proven sufficient for
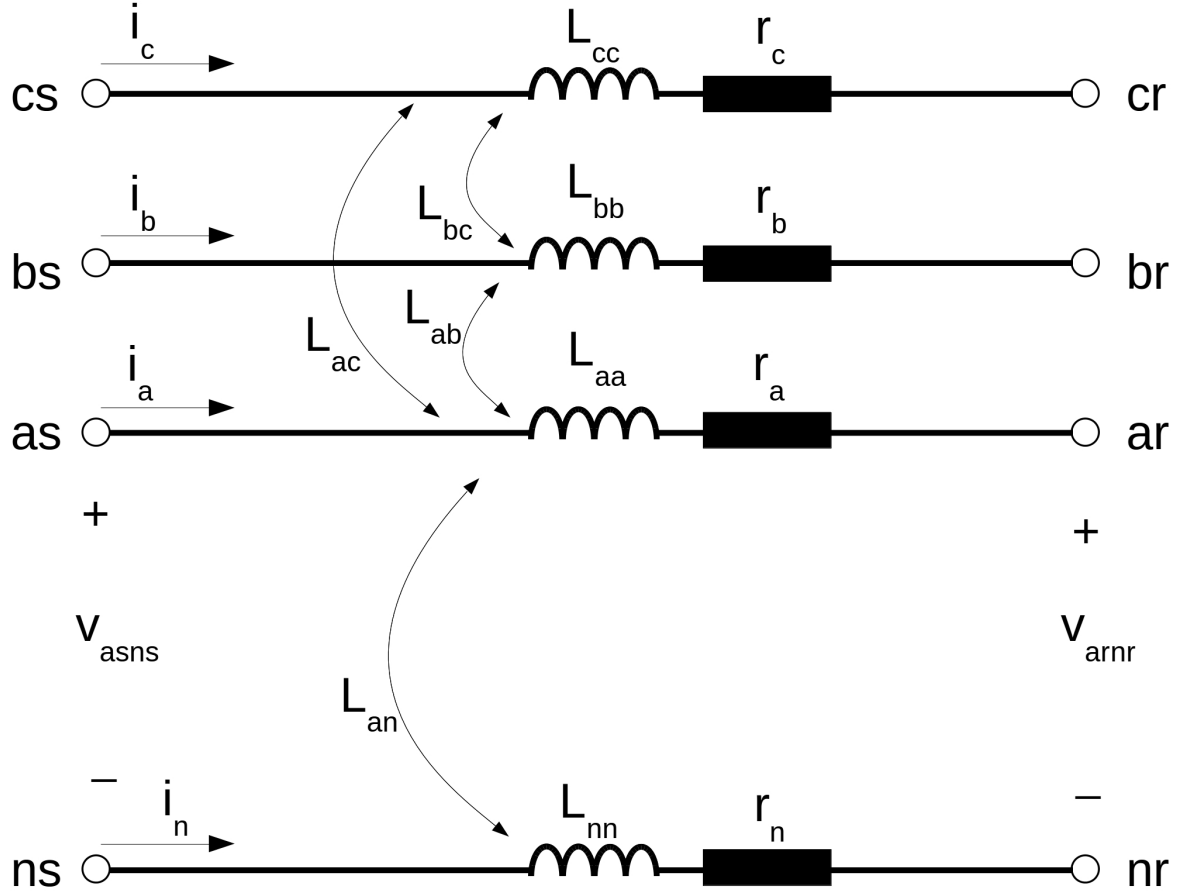
Figure 3.1: An abc reference frame transmission line series component lumped parameter model.

modeling and analysis of transient phenomena. In equation form

$$v_{asns} - v_{arnr} = i_a r_a + L_{aa}\frac{di_a}{dt} + L_{ab}\frac{di_b}{dt} + L_{ac}\frac{di_c}{dt} + L_{ag}\frac{di_n}{dt} + v_{nrns}$$

$$v_{bsns} - v_{brnr} = i_b r_b + L_{bb}\frac{di_b}{dt} + L_{bc}\frac{di_c}{dt} + L_{ba}\frac{di_a}{dt} + L_{bg}\frac{di_n}{dt} + v_{nrns} \qquad (3.1)$$

$$v_{csns} - v_{crnr} = i_c r_c + L_{cc}\frac{di_c}{dt} + L_{ca}\frac{di_a}{dt} + L_{cb}\frac{di_b}{dt} + L_{cg}\frac{di_n}{dt} + v_{nrns}$$

Since $i_g = -(i_a + i_b + i_c)$

$$L_{an}\frac{di_n}{dt} = -L_{an}\frac{di_a}{dt} - L_{an}\frac{di_b}{dt} - L_{an}\frac{di_c}{dt}$$

$$L_{bn}\frac{di_n}{dt} = -L_{bn}\frac{di_a}{dt} - L_{bn}\frac{di_b}{dt} - L_{bn}\frac{di_c}{dt} \tag{3.2}$$

$$L_{cn}\frac{di_n}{dt} = -L_{cn}\frac{di_a}{dt} - L_{cn}\frac{di_b}{dt} - L_{cn}\frac{di_c}{dt}$$

and

$$v_{nrns} = i_a r_g + (L_{nn} - L_{an})\frac{di_a}{dt} + i_b r_n + (L_{nn} - L_{bn})\frac{di_b}{dt} + i_c r_n + (L_{nn} - L_{cn})\frac{di_c}{dt} \tag{3.3}$$

Substituting (3.2) and (3.3) into (3.1) and writing in matrix form

$$
\begin{bmatrix} v_{asns} - v_{arnr} \\ v_{bsns} - v_{brnr} \\ v_{csns} - v_{crnr} \end{bmatrix} =
$$

$$
\begin{bmatrix} r_a + r_n & r_n & r_n \\ r_n & r_b + r_n & r_g \\ r_n & r_n & r_c + r_n \end{bmatrix} \begin{bmatrix} i_a \\ i_b \\ i_c \end{bmatrix} + \tag{3.4}
$$

$$
\begin{bmatrix} L_{aa} + L_{nn} - 2L_{an} & L_{ab} + L_{nn} - L_{bn} - L_{an} & L_{ac} + L_{nn} - L_{cn} - L_{an} \\ L_{ba} + L_{nn} - L_{an} - L_{bn} & L_{bb} + L_{nn} - 2L_{bn} & L_{bc} + L_{nn} - L_{cn} - L_{bn} \\ L_{ca} + L_{nn} - L_{an} - L_{cn} & L_{cb} + L_{nn} - L_{bn} - L_{cn} & L_{cc} + L_{nn} - 2L_{cn} \end{bmatrix} \begin{bmatrix} \dot{i}_a \\ \dot{i}_b \\ \dot{i}_c \end{bmatrix}
$$

An assumption of uniform conductor size and transposition yields $r_a = r_b = r_c$, $L_{aa} = L_{bb} = L_{cc}$, $L_{ab} = L_{ba} = L_{bc} = L_{cb} = L_{ca} = L_{ac}$, and $L_{an} = L_{bn} = L_{cn}$. Setting $L_s = L_{aa} + L_{nn} - 2L_{an}$, $L_m = L_{ab} + L_{nn} - 2L_{an} = L_s + L_{ab} - L_{aa}$, $r_s = r_a + r_n$, $r_m = r_n$, and the resistance matrix may be written

$$
\mathbf{r_{ln}} = \begin{bmatrix} r_s & r_m & r_m \\ r_m & r_s & r_m \\ r_m & r_m & r_s \end{bmatrix} \tag{3.5}
$$

15

and the inductance matrix

$$\mathbf{L_{ln}} = \begin{bmatrix} L_s & L_m & L_m \\ L_m & L_s & L_m \\ L_m & L_m & L_s \end{bmatrix} \tag{3.6}$$

In first order differential equation form assuming $\mathbf{L}$ is invertible,

$$\dot{\mathbf{i}}_{abcn} = -\mathbf{L_{ln}^{-1}} \mathbf{r_{ln}} \mathbf{i}_{abcn} + \mathbf{L_{ln}^{-1}} \left(\mathbf{v}_{s,abcn} - \mathbf{v}_{r,abcn} \right) \tag{3.7}$$

where $\mathbf{v}_{s,abcn} - \mathbf{v}_{r,abcn}$ is the voltage drop measured across the series connection of line resistance and inductance, and the letter "n" is appended to the subscripts as a reminder of a four wire electric power system.

3.2   Leakage Capacitance

Alternating current distribution and transmission circuits exhibit leakage capacitance between phases and from each phase to neutral and ground. Cable circuits typically have higher capacitance per unit length than do overhead circuits due to the close proximity of phase conductors and dielectric characteristics of insulating media. Lumped parameters for this model component are normally divided by 2 and placed at either end of the cable run or overhead circuit. The approach will be to separate the line–to–neutral leakage capacitance from the line–to–line leakage capacitance and write the first order differential equations for each. This representation could also be used to model power factor correction capacitor banks.

Referring to Figure 3.2 on Page 17, the model equations for one end of the circuit are

$$i_{lca} = \dot{v}_{an} c_{an} + (\dot{v}_{an} - \dot{v}_{bn}) c_{ab} + (\dot{v}_{an} - \dot{v}_{cn}) c_{ca}$$

$$i_{lcb} = \dot{v}_{bn} c_{bn} + (\dot{v}_{bn} - \dot{v}_{cn}) c_{bc} + (\dot{v}_{bn} - \dot{v}_{an}) c_{ab} \tag{3.8}$$

$$i_{lcc} = \dot{v}_{cn} c_{cn} + (\dot{v}_{cn} - \dot{v}_{an}) c_{ca} + (\dot{v}_{cn} - \dot{v}_{bn}) c_{bc}$$
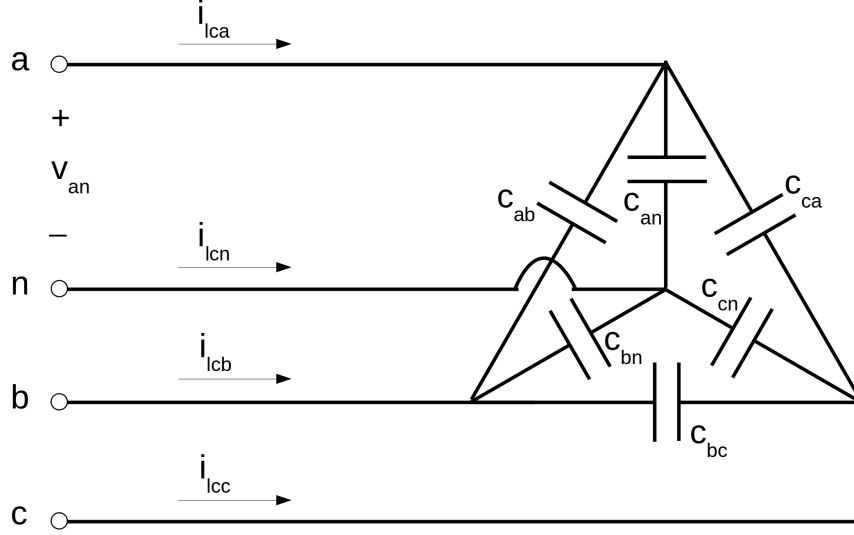
Figure 3.2: One terminal of an abc reference frame distribution circuit leakage capacitance lumped parameter model.

Assuming $c_{an} = c_{bn} = c_{cn}$ and $c_{ab} = c_{bc} = c_{ca}$ and rearranging (3.8)

$$i_{lca} = (c_{an} + 2c_{ab})\dot{v}_{an} - c_{ab}\dot{v}_{bn} - c_{ab}\dot{v}_{cn}$$

$$i_{lcb} = -c_{ab}\dot{v}_{an} + (c_{an} + 2c_{ab})\dot{v}_{bn} - c_{ab}\dot{v}_{cn} \qquad (3.9)$$

$$i_{lcc} = -c_{ab}\dot{v}_{an} - c_{ab}\dot{v}_{bn} + (c_{an} + 2c_{ab})\dot{v}_{cn}$$

Setting $c_m = c_{ab}$ and $cs = c_{an} + 2c_{ab}$, and writing in matrix form

$$\begin{bmatrix} i_{lca} \\ i_{lcb} \\ i_{lcc} \end{bmatrix} = \begin{bmatrix} c_s & -c_m & -c_m \\ -c_m & c_s & -c_m \\ -c_m & -c_m & c_s \end{bmatrix} \begin{bmatrix} \dot{v}_{an} \\ \dot{v}_{bn} \\ \dot{v}_{cn} \end{bmatrix} \qquad (3.10)$$

Expressed in first order differential form

$$\begin{bmatrix} \dot{v}_{an} \\ \dot{v}_{bn} \\ \dot{v}_{cn} \end{bmatrix} = \begin{bmatrix} c_s & -c_m & -c_m \\ -c_m & c_s & -c_m \\ -c_m & -c_m & c_s \end{bmatrix}^{-1} \begin{bmatrix} i_{lca} \\ i_{lcb} \\ i_{lcc} \end{bmatrix} \qquad (3.11)$$

3.3 Wye Connected Load with Resistance and Inductance

A load composed of resistive and inductive elements may be modeled similar to the distribution line series electrical elements. In the case of wye connections, the main diagonal terms of the resistance and inductance matrices represent load parameters, while off diagonal terms are trivial. The "receiving" end voltage is set to zero (0). Unbalanced conditions may be modeled using loads of differing magnitude in one or more legs. The wye connection is useful for modeling line–to–neutral, line–to–line–to–neutral, and three–phase faults by presenting small values of resistance and inductance. Refer to Figure 3.3 on Page 19. For this case, the first order differential equation representation is

$$
\begin{bmatrix} \dot{i}_{Ya} \\ \dot{i}_{Yb} \\ \dot{i}_{Yc} \end{bmatrix} = - \begin{bmatrix} r_{ldan}/l_{ldan} & 0 & 0 \\ 0 & r_{ldbn}/l_{ldbn} & 0 \\ 0 & 0 & r_{ldcn}/l_{ldcn} \end{bmatrix} \begin{bmatrix} i_{Ya} \\ i_{Yb} \\ i_{Yc} \end{bmatrix}
$$
$$
+ \begin{bmatrix} 1/l_{ldan} & 0 & 0 \\ 0 & 1/l_{ldbn} & 0 \\ 0 & 0 & 1/l_{ldcn} \end{bmatrix} \begin{bmatrix} v_{ldan} \\ v_{ldbn} \\ v_{ldcn} \end{bmatrix} \tag{3.12}
$$

where r_{ldan}, r_{ldbn} and r_{ldcn} are resistive elements connected respectively in series with l_{ldan}, l_{ldbn} and l_{ldcn} inductive elements in the a, b and c phase legs of the wye connected load. Setting

$$
\boldsymbol{r}_{ld} = \begin{bmatrix} r_{ldan} & 0 & 0 \\ 0 & r_{ldbn} & 0 \\ 0 & 0 & r_{ldcn} \end{bmatrix} \tag{3.13}
$$
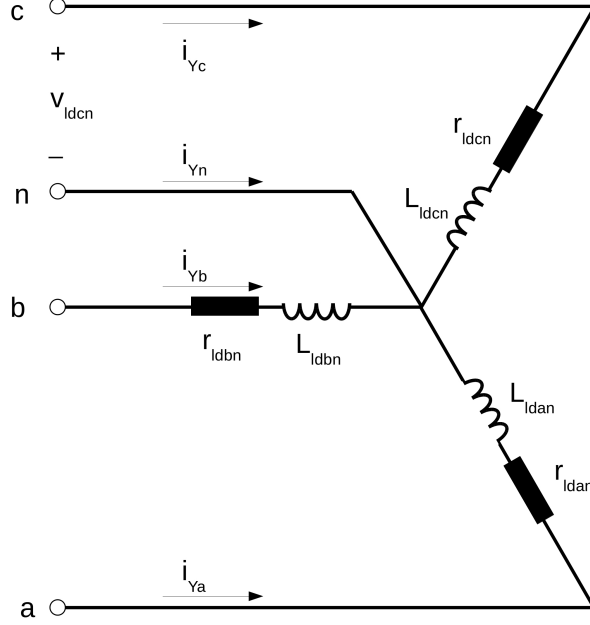
Figure 3.3: An abc reference frame wye connected series resistance and inductance load representation.

and

$$\boldsymbol{L}_{ld} = \begin{bmatrix} L_{ldan} & 0 & 0 \\ 0 & L_{ldbn} & 0 \\ 0 & 0 & L_{ldcn} \end{bmatrix} \tag{3.14}$$

equation (3.12) may be written

$$\dot{\boldsymbol{i}}_Y = -\boldsymbol{r}_{ld}\boldsymbol{L}_{ld}^{-1}\boldsymbol{i}_Y + \boldsymbol{L}_{ld}^{-1}\boldsymbol{v}_{ld} \tag{3.15}$$

3.4 Δ Connected Load with Resistance and Inductance

For series resistive and inductive loads using delta connections, the construction is fundamentally altered. This connection is useful for modeling line–to–line faults and three–phase
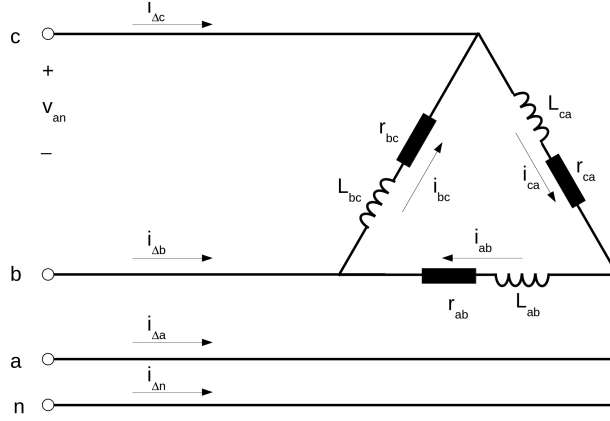
Figure 3.4: Resistive and inductive model for delta connected load in the abc reference frame.

faults. Referring to Figure 3.4 on Page 20, the circuit equations are

$$v_{an} - v_{bn} = r_{ab}i_{ab} + L_{ab}\dot{i}_{ab}$$

$$v_{bn} - v_{cn} = r_{bc}i_{bc} + L_{bc}\dot{i}_{bc} \qquad (3.16)$$

$$v_{cn} - v_{an} = r_{ca}i_{ca} + L_{ca}\dot{i}_{ca}$$

In first order differential form, (3.16) is

$$\dot{i}_{ab} = -\frac{r_{ab}}{L_{ab}}i_{ab} + \frac{1}{L_{ab}}v_{an} - \frac{1}{L_{ab}}v_{bn}$$

$$\dot{i}_{bc} = -\frac{r_{bc}}{L_{bc}}i_{bc} + \frac{1}{L_{bc}}v_{bn} - \frac{1}{L_{bc}}v_{cn} \qquad (3.17)$$

$$\dot{i}_{ca} = -\frac{r_{ca}}{L_{ca}}i_{ca} + \frac{1}{L_{ca}}v_{cn} - \frac{1}{L_{ca}}v_{an}$$

and in first matrix form

$$\begin{bmatrix} \dot{i}_{ab} \\ i_{bc} \\ i_{ca} \end{bmatrix} = - \begin{bmatrix} \frac{r_{ab}}{L_{ab}} & 0 & 0 \\ 0 & \frac{r_{bc}}{L_{bc}} & 0 \\ 0 & 0 & \frac{r_{ca}}{L_{ca}} \end{bmatrix} \begin{bmatrix} i_{ab} \\ i_{bc} \\ i_{ca} \end{bmatrix} + \begin{bmatrix} \frac{1}{L_{ab}} & -\frac{1}{L_{ab}} & 0 \\ 0 & \frac{1}{L_{bc}} & -\frac{1}{L_{bc}} \\ -\frac{1}{L_{ca}} & 0 & \frac{1}{L_{ca}} \end{bmatrix} \begin{bmatrix} v_{an} \\ v_{bn} \\ v_{cn} \end{bmatrix} \qquad (3.18)$$

Line currents $i_{\Delta a}$, $i_{\Delta b}$, and $i_{\Delta c}$ are

$$i_{\Delta a} = i_{ab} - i_{ca}; \quad i_{\Delta b} = i_{bc} - i_{ab}; \quad i_{\Delta c} = i_{ca} - i_{bc} \qquad (3.19)$$

3.5 Transformer and Electric Power System Models

The transformer – and the electric power system it connects with – are modeled as series resistances and inductances. The source feeding the electric power systems is modeled as a constant frequency zero–impedance voltage source. The first order differential equations describing the system are similar in form to (3.7). Arriving at r_s, r_m, L_s, and L_m for the combined transformer and electric power system impedance is addressed in Section 4.2

Chapter 4

Transforming Zero, Positive, and Negative Sequence Parameters to abc

Transmission and distribution system parameters are often given in terms of zero, positive and negative sequence components. The impedance matrices are diagonal and power system professionals are accustomed to working in this reference frame. For this work, converting from zero, positive and negative sequence parameters to the abc frame is accomplished using the transformation from [25]

$$\boldsymbol{S} = \frac{1}{3} \begin{bmatrix} 1 & 1 & 1 \\ 1 & a & a^2 \\ 1 & a^2 & a \end{bmatrix} \tag{4.1}$$

where $a = e^{j2\pi/3}$.

Given a set of states $\boldsymbol{X_{abc}}$ in the abc reference frame, the relationship to states $\boldsymbol{X_{012}}$ in the zero, positive, and negative sequence frame is:

$$\boldsymbol{X_{012}} = \boldsymbol{S}\boldsymbol{X_{abc}} \tag{4.2}$$

4.1 Series RL Circuits

Applying (4.2) to a set of abc frame current states $\mathbf{i_{abc}}$ and equating to voltage states $\mathbf{v_{012}}$ in the 012 frame

$$\begin{bmatrix} v_0 \\ v_1 \\ v_2 \end{bmatrix} = \mathbf{S} \begin{bmatrix} z_s & z_m & z_m \\ z_m & z_s & z_m \\ z_m & z_m & z_s \end{bmatrix} \begin{bmatrix} i_a \\ i_b \\ i_c \end{bmatrix} = \frac{1}{3} \begin{bmatrix} 1 & 1 & 1 \\ 1 & a & a^2 \\ 1 & a^2 & a \end{bmatrix} \begin{bmatrix} z_s i_a + z_m i_b + z_m i_c \\ z_m i_a + z_s i_b + z_m i_c \\ z_m i_a + z_m i_b + z_s i_c \end{bmatrix} \tag{4.3}$$

Expanding (4.3) by line

$$v_0 = \frac{1}{3}\left[z_s(i_a + i_b + i_c) + 2z_m(i_a + i_b + i_c) \right]$$
$$v_1 = \frac{1}{3}\left\{ z_s(i_a + ai_b + a^2 i_c) + z_m\left[(a + a^2)i_a + (1 + a^2)i_b + (1 + a)i_c \right] \right\} \tag{4.4}$$
$$v_2 = \frac{1}{3}\left\{ z_s(i_a + a^2 i_b + ai_c) + z_m\left[(a + a^2)i_a + (1 + a)i_b + (1 + a^2)i_c \right] \right\}$$

Because $1 + a + a^2 \equiv 0$ [12]

$$a + a^2 = -1; \quad 1 + a^2 = -a; \quad 1 + a = -a^2 \tag{4.5}$$

and (4.4) becomes

$$v_0 = \frac{1}{3}\left[z_s(i_a + i_b + i_c) + 2z_m(i_a + i_b + i_c) \right]$$
$$v_1 = \frac{1}{3}\left[z_s(i_a + ai_b + a^2 i_c) - z_m(i_a + ai_b + a^2 i_c) \right] \tag{4.6}$$
$$v_2 = \frac{1}{3}\left[z_s(i_a + a^2 i_b + ai_c) - z_m(i_a + a^2 i_b + ai_c) \right]$$

From (4.2)

$$i_0 = \frac{1}{3}(i_a + i_b + i_c)$$
$$i_1 = \frac{1}{3}(i_a + ai_b + a^2 i_c) \tag{4.7}$$
$$i_2 = \frac{1}{3}(i_a + a^2 i_b + ai_c)$$

Substituting (4.7) into (4.6)

$$v_0 = (z_s + 2z_m)i_0$$

$$v_1 = (z_s - z_m)i_1 \tag{4.8}$$

$$v_2 = (z_s - z_m)i_2$$

Given a set of series impedance system parameters as shown in Figure 3.1 on Page 14 in the zero, positive and negative reference frame, the values for (3.5) and (3.6) can be calculated. Starting with

$$z_0 = (z_s + 2z_m); \quad r_0 = r_s + 2r_m; \quad x_0 = x_s + 2x_m$$

$$z_1 = (z_s - z_m); \quad r_1 = r_s - r_m; \quad x_1 = x_s - x_m \tag{4.9}$$

Using elimination techniques and solving for r_s, r_m, x_s and x_m

$$r_s = \frac{1}{3}(r_0 + 2r_1); \quad x_s = \frac{1}{3}(x_0 + 2x_1)$$

$$r_m = \frac{1}{3}(r_0 - r_1); \quad x_m = \frac{1}{3}(x_0 - x_1) \tag{4.10}$$

Working with the inductive reactances and expressing in terms of inductance

$$L_s = \frac{1}{3\omega}(x_0 + 2x_1)$$

$$L_m = \frac{1}{3\omega}(x_0 - x_1) \tag{4.11}$$

where $\omega = 2\pi f \left[\frac{rad}{second}\right]$, and f [Hz] is the nominal system frequency.

4.2   Transformer and Electric Power System Models

A two winding transformer with a turns ratio of one (1) is assumed, and phase shift resulting from coil connections is ignored. The transformer core assemblies and coil connections determine the sequence impedances seen by the micro–grid 480Y/277 [V] system bus.

This breaks down into three (3) categories for the transformer and electric power system impedances [25]:

1. Positive, negative and zero sequences add (i.e. grounded–wye to grounded–wye connections)

2. Positive and negative sequences add, zero sequence equals transformer positive sequence (i.e. Δ to grounded–wye connections)

3. Positive and negative sequences add, zero sequence is infinite (any transformer with an ungrounded secondary in the absence of grounding transformers)

The case at hand is a Δ to grounded–wye transformation, so the positive sequence impedance of the electric power system is added to the positive sequence impedance of the transformer to arrive at the cumulative positive and negative sequence impedances seen by the micro–grid bus. The zero sequence impedance is the equal to the transformer positive sequence impedance. These values are then used in (4.10) and (4.11) to calculate r_s, r_m, L_s, and L_m for the combined transformer and electric power system impedance.

4.3   Leakage Capacitance

For leakage capacitance, applying (4.2) to a set of abc frame voltage states $\mathbf{v_{abc}}$ and equating to current states $\mathbf{i_{012}}$ in the 012 frame

$$
\begin{bmatrix} i_0 \\ i_1 \\ i_2 \end{bmatrix} = \mathbf{S} \begin{bmatrix} y_s & -y_m & -y_m \\ -y_m & y_s & -y_m \\ -y_m & -y_m & y_s \end{bmatrix} \begin{bmatrix} v_a \\ v_b \\ v_c \end{bmatrix} = \frac{1}{3} \begin{bmatrix} 1 & 1 & 1 \\ 1 & a & a^2 \\ 1 & a^2 & a \end{bmatrix} \begin{bmatrix} y_s v_a - y_m v_b - y_m v_c \\ -y_m v_a + y_s v_b - y_m v_c \\ -y_m v_a - y_m v_b + y_s v_c \end{bmatrix}
\tag{4.12}
$$

Expanding (4.12) by line

$$i_0 = \frac{1}{3}[y_s(v_a + v_b + v_c) - 2y_m(v_a + v_b + v_c)]$$

$$i_1 = \frac{1}{3}\{y_s(v_a + av_b + a^2v_c) - y_m[(a + a^2)v_a + (1 + a^2)v_b + (1 + a)v_c]\} \qquad (4.13)$$

$$i_2 = \frac{1}{3}\{y_s(v_a + a^2v_b + av_c) - y_m[(a + a^2)v_a + (1 + a)v_b + (1 + a^2)v_c]\}$$

Using (4.5) in (4.4)

$$i_0 = \frac{1}{3}[y_s(v_a + v_b + v_c) - 2y_m(v_a + v_b + v_c)]$$

$$i_1 = \frac{1}{3}[y_s(v_a + av_b + a^2v_c) + y_m(v_a + av_b + a^2v_c)] \qquad (4.14)$$

$$i_2 = \frac{1}{3}[y_s(v_a + a^2v_b + av_c) + y_m(v_a + a^2v_b + av_c)]$$

Invoking (4.2) and substituting into (4.14)

$$i_0 = (y_s - 2y_m)v_0$$

$$i_1 = (y_s + y_m)v_1 \qquad (4.15)$$

$$i_2 = (y_s + y_m)v_2$$

Given the charging capacitance of a transmission or distribution circuit in 012 coordinates, the capacitance matrix in abc coordinates can be calculated by elimination techniques applied to (4.16)

$$y_0 = y_s - 2y_m$$

$$y_1 = y_2 = y_s + y_m \qquad (4.16)$$

Solving for y_s and y_m

$$y_m = \frac{1}{3}(y_1 - y_0)$$

$$y_s = \frac{1}{3}(2y_1 + y_0) \qquad (4.17)$$

26

Expressing in terms of capacitance

$$c_m = \frac{1}{3\omega}(y_1 - y_0)$$

$$c_s = \frac{1}{3\omega}(2y_1 + y_0)$$

(4.18)

where $\omega = 2\pi f \left[\frac{rad}{s}\right]$, and f [Hz] is the nominal system frequency.

Chapter 5

Synchronous Machine Model

In his seminal 1929 work [28], R. H. Park defines a transformation from the three–phase abc coordinate stationary reference frame to the 0dq rotating reference frame

$$\boldsymbol{x_{0dq}} = \boldsymbol{Q}\boldsymbol{x_{abcn}} \tag{5.1}$$

where $\mathbf{Q}$ is the 3x3 Park's transformation matrix and $\mathbf{x}$ is a 3x1 vector of electrical states. In matrix form the equation becomes

$$\boldsymbol{Q} = 2/3 \begin{bmatrix} 1/2 & 1/2 & 1/2 \\ \cos(\omega t) & \cos(\omega t - 2\pi/3) & \cos(\omega t + 2\pi/3) \\ -\sin(\omega t) & -\sin(\omega t - 2\pi/3) & -\sin(\omega t + 2\pi/3) \end{bmatrix} \tag{5.2}$$

$\mathbf{Q}$ is not power invariant and does not result in a reciprocal (symmetric) inductance matrix [6].

Referring to Figure 5.1 on Page 29, subscripts a, b and c apply to the stator phase windings, F applies to the field winding, D to the d axis damper winding, and Q to the q axis damper winding. Field flux is directed along the d axis, with voltage induction along the q axis. The angle δ represents the power angle and should have a steady state value greater than zero (0) for generating conditions. Using the a phase magnetic field axis as reference, the projections of abc quantities onto the d and q axes respectively are

$$x_d = 2/3 \left[x_a cos(\theta) + x_b cos(\theta - 2\pi/3) + x_c cos(\theta + 2\pi/3) \right]$$
$$x_q = 2/3 \left[x_a \sin(\theta) + x_b \sin(\theta - 2\pi/3) + x_c \sin(\theta + 2\pi/3) \right] \tag{5.3}$$
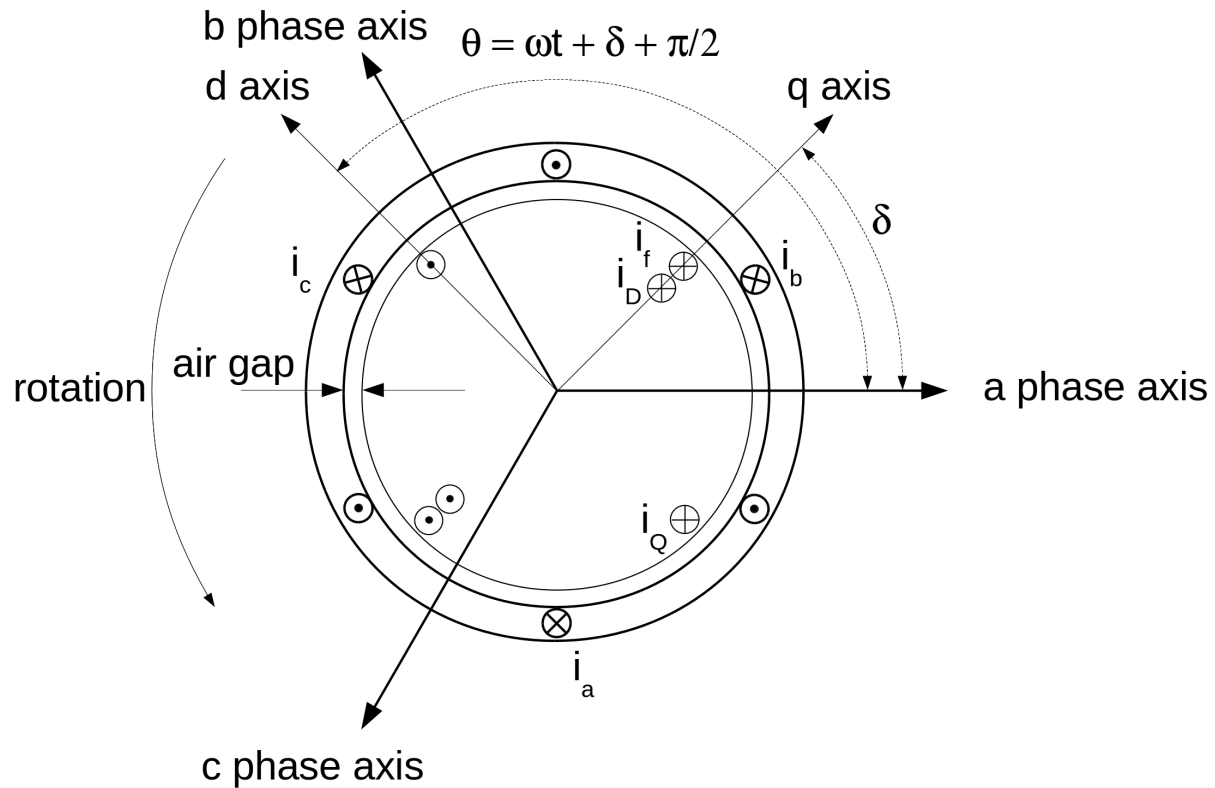
Figure 5.1: A representation of the synchronous machine assuming sinusoidal winding distribution.

Other transforms are equally valid, including the arbitrary selection of d and q axes, and selection of constants to yield power invariance. After [6], the transform from abc to 0dq coordinates is written

$$\boldsymbol{P} = \sqrt{2/3} \begin{bmatrix} 1/\sqrt{2} & 1/\sqrt{2} & 1/\sqrt{2} \\ \cos(\omega t) & \cos(\omega t - 2\pi/3) & \cos(\omega t + 2\pi/3) \\ \sin(\omega t) & \sin(\omega t - 2\pi/3) & \sin(\omega t + 2\pi/3) \end{bmatrix} \qquad (5.4)$$

Synchronous machines models exhibit nonlinear behavior due to:

- the appearance of speed voltages in the d and q axes

- mutual inductance saturation

29

– along the d axis for salient pole machines

– along the d axis and q axis for cylindrical rotor machines

For nonlinear simulations, the objective is to develop a synchronous generator model in the form

$$\dot{\boldsymbol{x}} = f(x, u, t). \tag{5.5}$$

Since frequency will be relatively constant, nonlinearities due to changes in rotor speed will be minimal. The model shall include the zero–sequence network, and be suitable for analysis of unbalanced load conditions (i.e. line–to–neutral load connections and faults, and line–to–line load connections and faults).

5.1   Main Generator Electrical Model

In Figure 5.2 on Page 31, the generator parameters are shown in the abc reference frame. Not all mutual inductances have been included in the figure. For example, the mutual inductance L_{Fc} between the field winding and the c phase winding is shown, but L_{Fa} and L_{Fb} between the field winding and the a and b phase windings have not. Similarly, the mutual inductance L_{Da} (L_{Qa}) between the d axis (q axis) damper winding and the a phase winding is shown, but L_{Db} (L_{Qb}) and L_{Dc} (L_{Qc}) are not. The exclusion of mutual inductance between the q axis damper winding and the two windings on the d axis is due to the quadrature relationship: there is no mutual coupling between these windings. It is also the case that not all voltages are indicated, rather one phase is shown, and the others may be surmised by inspection.

It is assumed that generator mutual inductances are symmetrical: $L_{Da} = L_{aD}$, L_{FD} $= L_{DF}$, $L_{Fa} = L_{aF}$, etcetera. After [6], symmetry properties will be used to simplify the model. It is also the case that the most general model will permit the inclusion of electrical elements r_n and L_n between the generator neutral and the electrical system neutral as shown in Figure 5.2 on Page 31.
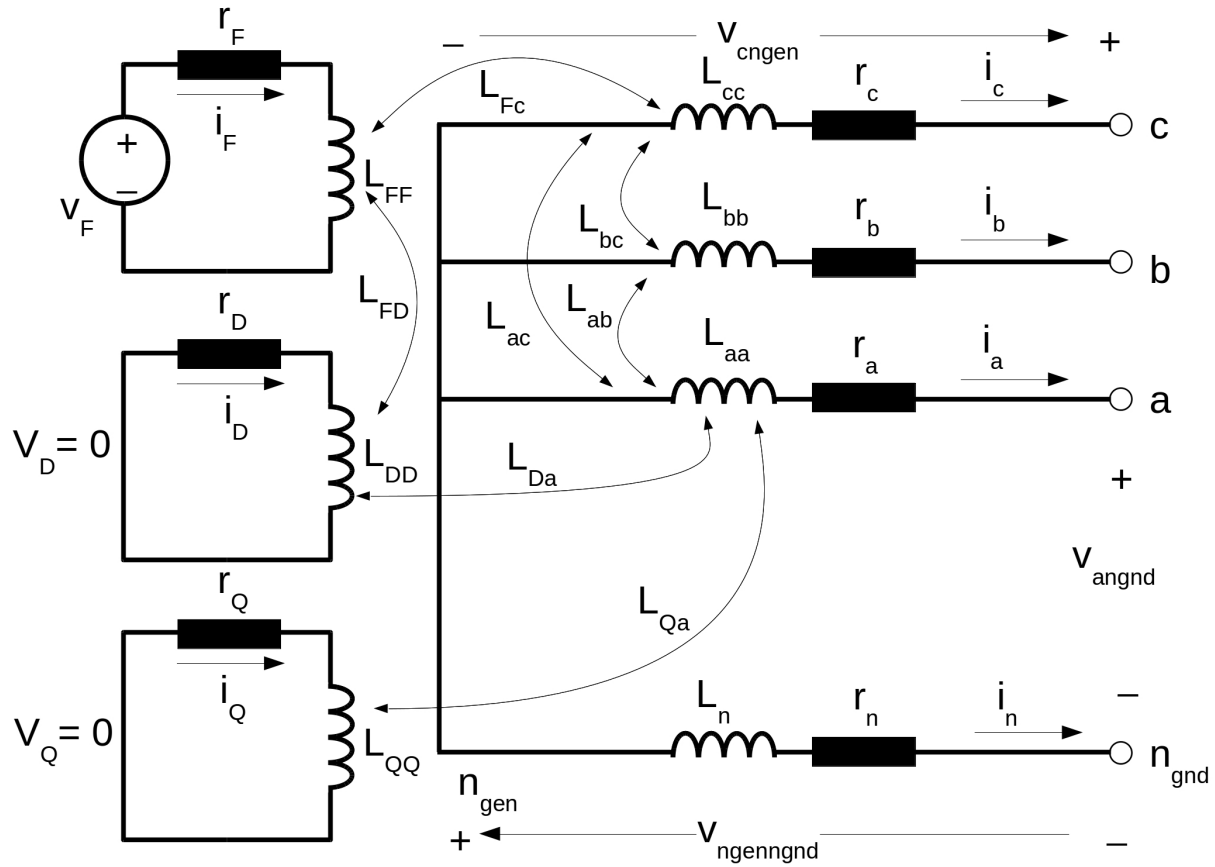
Figure 5.2: The generator electrical system model in the abc reference frame. Not all mutual inductances are shown.

Following the convention established in [6], inductances with two subscripts are time varying, and those with single subscripts are constant. Also after [6], the rotor parameters are denoted with single upper case letter subscripts:

- F – field winding

- D – d axis damper winding

- Q – q axis damper winding.

Following the development in [6], the generator voltage equations in the 0dq frame are

$$
\begin{bmatrix} v_0 \\ v_d \\ v_q \\ -v_F \\ v_D \\ v_Q \end{bmatrix} = -
\begin{bmatrix}
r + 3r_n & 0 & 0 & 0 & 0 & 0 \\
0 & r & \omega L_q & 0 & 0 & \omega k M_Q \\
0 & -\omega L_d & r & -\omega k M_F & -\omega k M_D & 0 \\
0 & 0 & 0 & r_F & 0 & 0 \\
0 & 0 & 0 & 0 & r_D & 0 \\
0 & 0 & 0 & 0 & 0 & r_Q
\end{bmatrix}
\begin{bmatrix} i_0 \\ i_d \\ i_q \\ i_F \\ i_D \\ i_Q \end{bmatrix}
$$
$$
-
\begin{bmatrix}
L_0 + 3L_n & 0 & 0 & 0 & 0 & 0 \\
0 & L_d & 0 & k M_F & k M_D & 0 \\
0 & 0 & L_q & 0 & 0 & k M_Q \\
0 & k M_F & 0 & L_F & M_R & 0 \\
0 & k M_D & 0 & M_R & L_D & 0 \\
0 & 0 & k M_Q & 0 & 0 & L_Q
\end{bmatrix}
\begin{bmatrix} \dot{i}_0 \\ \dot{i}_d \\ \dot{i}_q \\ \dot{i}_F \\ \dot{i}_D \\ \dot{i}_Q \end{bmatrix}
\tag{5.6}
$$

Referring all values to the stator:

- v_{0dq} are the generator stator 0, d and q axis voltages,

- v_{FDQ} are the generator rotor field, d axis damper winding and q axis damper winding voltages,

- i_{0dq} are the generator stator 0, d and q axis currents,

- i_{FDQ} are the generator rotor field, d axis damper winding and q axis damper winding currents,

- r, r_F, r_D and r_Q are the stator armature, and rotor field, d axis damper and q axis damper resistances,

- r_n is the resistance inserted in the neutral connection between the generator and system neutral,

- L_n is the inductance inserted in the neutral connection between the generator and system neutral,

- ω is the electrical frequency,

- L_{0dq} are the generator stator 0, d and q axis synchronous inductances,

- L_{FDQ} are the generator rotor field, d axis damper and q axis damper synchronous inductances,

- kM_F is the stator d axis to rotor field mutual inductance,

- kM_D is the stator d axis to rotor d axis damper mutual inductance,

- kM_Q is the stator q axis to q rotor axis damper mutual inductance,

- $L_{AD} = kM_F = kM_D = M_R$ and

- $L_{AQ} = kM_Q$ is the stator q axis to q rotor axis damper mutual inductance.

This representation is shown in Figure 5.3 on Page 34. Setting

$$
\mathbf{r} =
\begin{bmatrix}
r + 3r_n & 0 & 0 & 0 & 0 & 0 \\
0 & r & \omega L_q & 0 & 0 & \omega k M_Q \\
0 & -\omega L_d & r & -\omega k M_F & -\omega k M_D & 0 \\
0 & 0 & 0 & r_F & 0 & 0 \\
0 & 0 & 0 & 0 & r_D & 0 \\
0 & 0 & 0 & 0 & 0 & r_Q
\end{bmatrix}
\tag{5.7}
$$
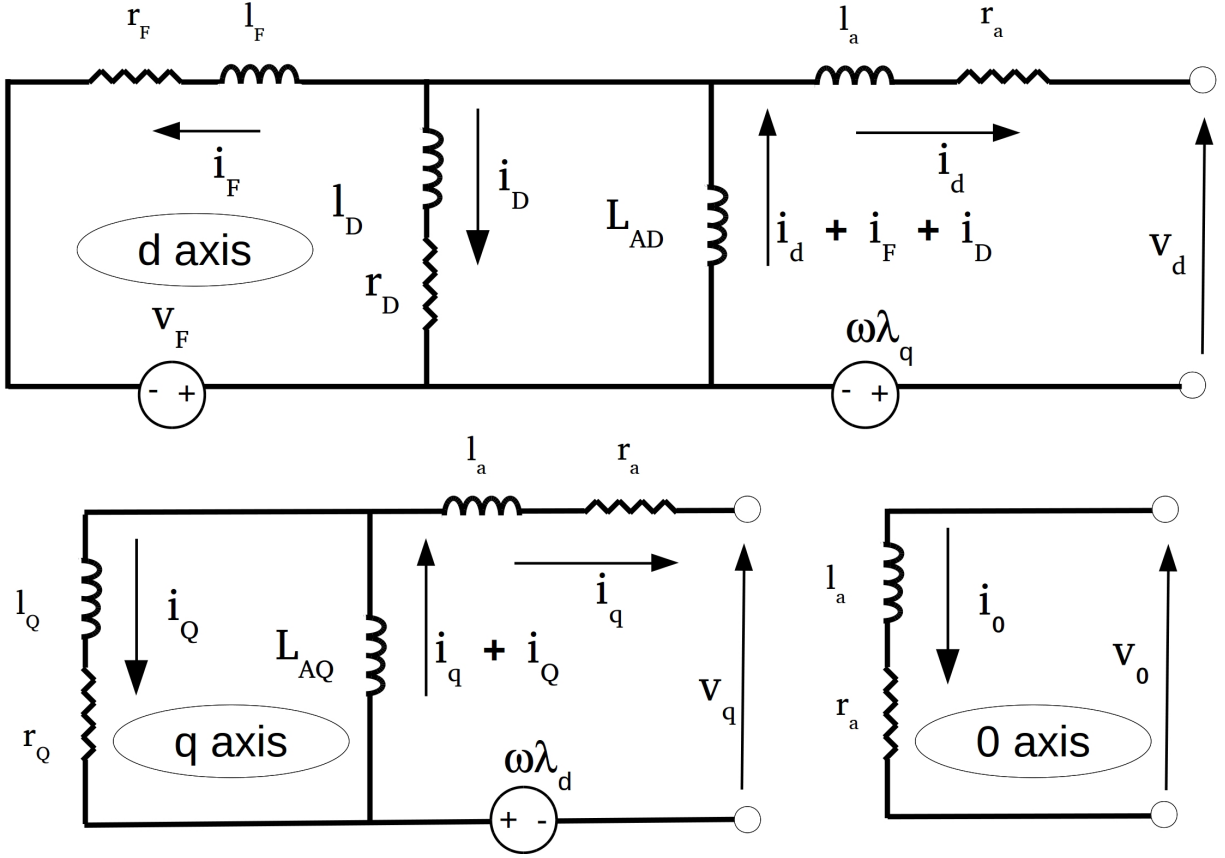
Figure 5.3: The generator electrical system model in the 0dq reference frame.

and

$$\mathbf{L} = \begin{bmatrix} L_0 + 3L_n & 0 & 0 & 0 & 0 & 0 \\ 0 & L_d & 0 & kM_F & kM_D & 0 \\ 0 & 0 & L_q & 0 & 0 & kM_Q \\ 0 & kM_F & 0 & L_F & M_R & 0 \\ 0 & kM_D & 0 & M_R & L_D & 0 \\ 0 & 0 & kM_Q & 0 & 0 & L_Q \end{bmatrix}, \qquad (5.8)$$

rearranging into first order differential equation form, recognizing $v_D = v_Q = 0$, and treating

v_F as an input

$$\begin{bmatrix} \dot{i_0} \\ i_d \\ i_q \\ i_F \\ i_D \\ i_Q \end{bmatrix} = -\boldsymbol{L}^{-1}\boldsymbol{r}\begin{bmatrix} i_0 \\ i_d \\ i_q \\ i_F \\ i_D \\ i_Q \end{bmatrix} - \boldsymbol{L}^{-1}\begin{bmatrix} v_0 \\ v_d \\ v_q \\ 0 \\ 0 \\ 0 \end{bmatrix} + \boldsymbol{L}^{-1}\begin{bmatrix} 0 \\ 0 \\ 0 \\ v_F \\ 0 \\ 0 \end{bmatrix} \tag{5.9}$$

Since the generator terminal voltage will be modeled in the abc reference frame, (5.9) is written

$$\begin{bmatrix} \dot{i_0} \\ i_d \\ i_q \\ i_F \\ i_D \\ i_Q \end{bmatrix} = -\boldsymbol{L}^{-1}\boldsymbol{r}\begin{bmatrix} i_0 \\ i_d \\ i_q \\ i_F \\ i_D \\ i_Q \end{bmatrix} - \boldsymbol{L}^{-1}\begin{bmatrix} \boldsymbol{P}\begin{bmatrix} v_a \\ v_b \\ v_c \end{bmatrix} \\ 0 \\ 0 \\ 0 \end{bmatrix} + \boldsymbol{L}^{-1}\begin{bmatrix} 0 \\ 0 \\ 0 \\ v_F \\ 0 \\ 0 \end{bmatrix} \tag{5.10}$$

where $\boldsymbol{P}$ is the Park transform (5.4).

5.2 Main Generator Saturation

It is generally the case that saturation occurs along the d and q axes for cylindrical rotor synchronous machines. For salient pole machines, it is sufficient to consider saturation along the d axis only [6, 14, 16, 3]. Is is also generally accepted that leakage inductance saturation is minimal due to the flux path being composed mostly of air. From [3] and referring to Figure 5.4 on Page 36 a per unit saturation function S_G is one way to model the circuit behavior at V_{t1}

$$S_G(V_{t1}) = (I_{FD2} - I_{FD1})/I_{FD1} \tag{5.11}$$
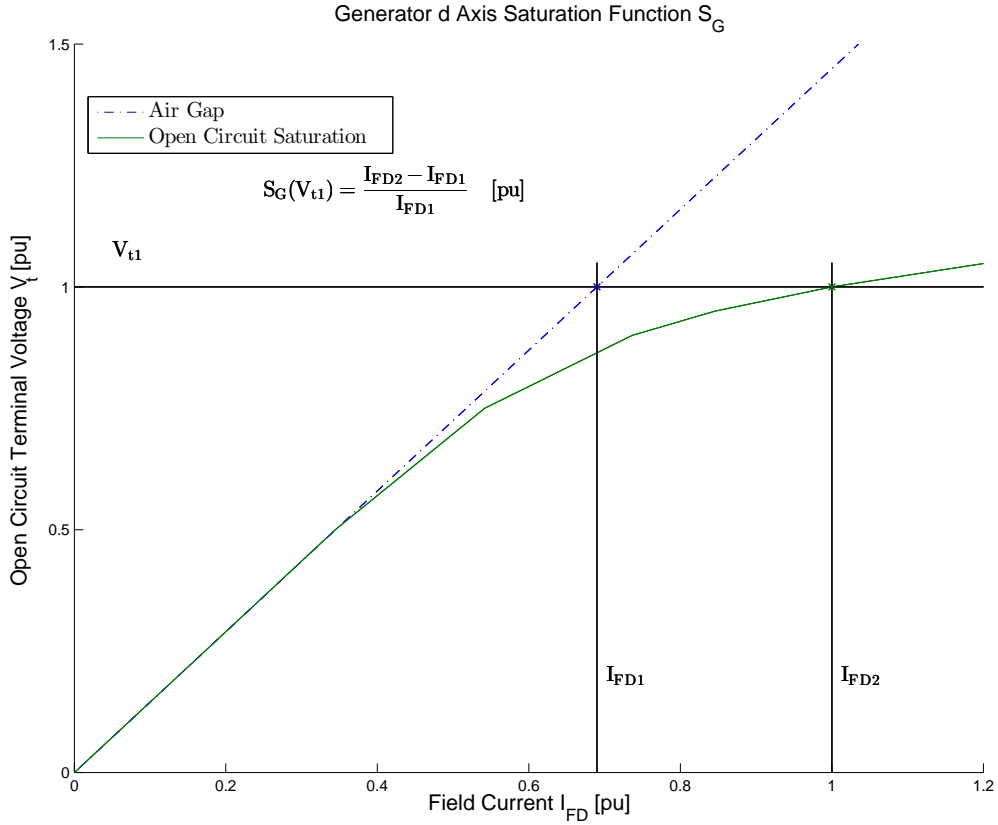
Figure 5.4: Generator air gap line, open circuit saturation curve, and saturation function S_G.

It is assumed that generator saturation under operating conditions is completely described by the open circuit saturation characteristic. The Generator saturation may be represented in several ways, including look–up table, polynomial function, or an exponential. Exponential and polynomial forms will be compared for accuracy.

Starting with the exponential form specified in terms of a generator saturation function S_G

$$S_G \triangleq A_G \exp^{B_G V_\Delta} \tag{5.12}$$

where A_G and B_G are constants, and

$$V_\Delta = V_t - 0.8 \tag{5.13}$$

36

Here, V_Δ and terminal voltage V_t are expressed as per unit values.

Generator manufacturers normally provide two values for S_G – call them S_{G1} and S_{G2} – at two values of terminal voltage V_{t1} and V_{t2} respectively. A typical value for V_{t1} is 1.0 [pu], and for V_{t2} 1.2 [pu].

Solving for A_G and B_G

$$B_G = \log(S_{G1}/S_{G2})/(V_{\Delta 1} - V_{\Delta 2}) \qquad (5.14)$$

and

$$A_G = S_{G2}/\exp^{B_G V_{\Delta 2}} \qquad (5.15)$$

where *log* is the natural logarithm and *exp* the natural exponent in (5.14)–(5.15).

Since the flux linkage $\lambda_{AD} = \sqrt{3}V_t$ under open circuit conditions, (5.12) may be written

$$S_G = A_G \exp^{[(\lambda_{AD}/\sqrt{3})-0.8]} \qquad (5.16)$$

Based on design program data for a Regal Beloit main generator HSG740066 shown in Figure 5.4, a comparison between use of the generator saturation function $S_G = A_G e^{B_G V_\Delta}$ and polynomial fits was conducted. Since the model uses the saturated mutual inductance, that parameter is used to judge the efficacy of the fitting methods. Figures 5.5 through 5.8 compare the test saturated inductance values and estimated values versus open circuit voltage, and include a plot of open circuit terminal voltage versus field current.

In Figure 5.5, a comparison between design program data from Regal Beloit Corporation and use of generator saturation function of the form $S_G = A_G e^{B_G V_\Delta}$ is plotted. The upper plot shows the d–axis saturated inductance versus terminal voltage. The fit is best near 1 [pu] voltage, but diverges on either side. The residual calculated for this fit is 3.8×10^{-7}. The lower half of Figure 5.5 is a calculation of rated frequency open circuit terminal voltage versus field current based on the inductance values from the upper plot.

Figures 5.6 through 5.8 use ploynomial fits of increasing order to characterize the sat-

37
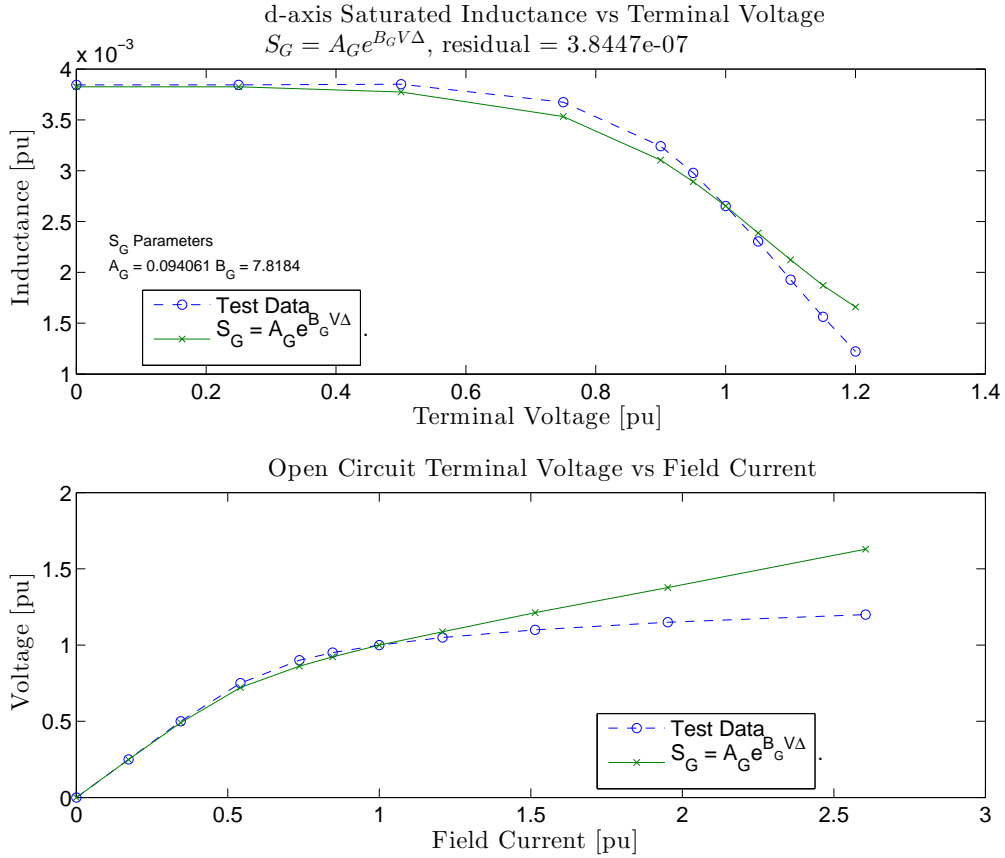
Figure 5.5: Comparing main generator d–axis inductance vs. open circuit voltage, and open circuit terminal voltage vs. field current when $S_G = A_G e^{B_G V \Delta}$.

urated inductance. Since there is an order of magnitude improvement in residual between the fifth ($r = 3.2e^{-9}$) and sixth ($r = 5.9e^{-10}$) order fit, the sixth order is selected to represent the generator saturation. A salient point here is that a generator saturation function expressing the departure from the air–gap line is *not* used for the simulations. Rather, the d axis saturated inductance is calculated directly based on circuit conditions.

An open circuit simulation was performed using the sixth order polynomial fit for d axis saturation in the Regal Beloit main generator HSG740066. Voltage set–points were altered, and the resulting field current plotted versus open circuit voltage. The results shown in Figure 5.9 demonstrate a good fit between the simulated and the design program data. Open circuit conditions are approximated by a high load impedance of $72 + j55.29$

38
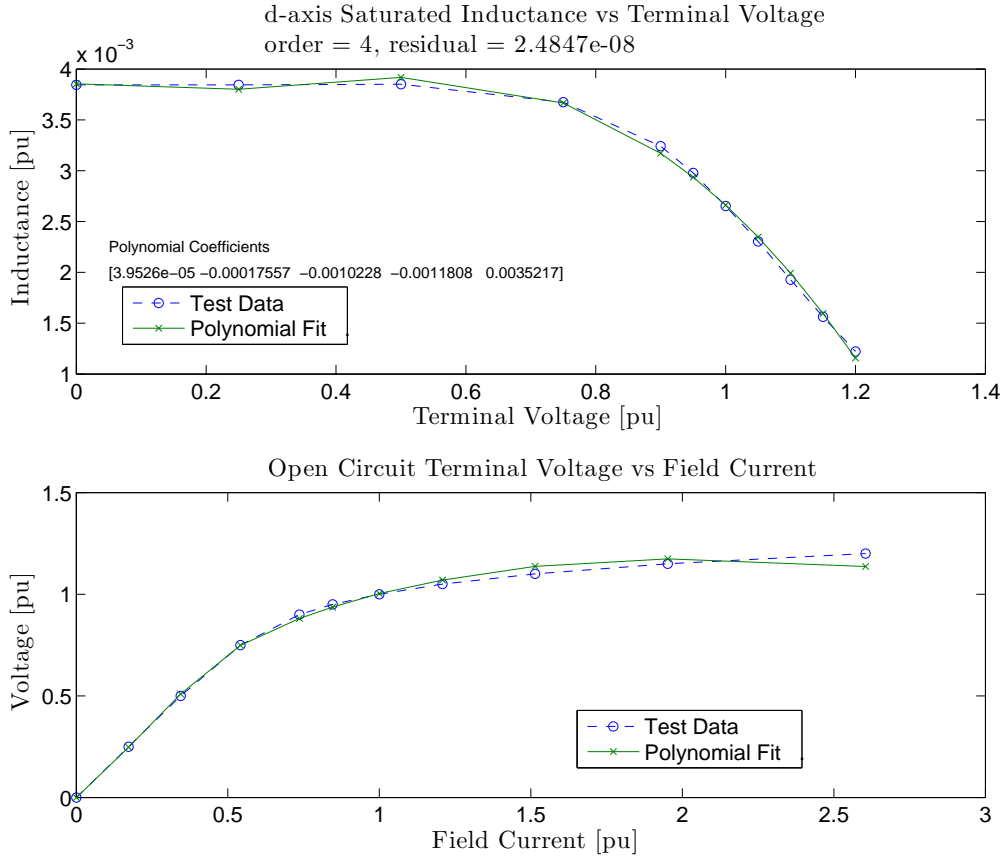
Figure 5.6: Comparing main generator d–axis inductance vs. open circuit voltage, and open circuit terminal voltage vs. field current using fourth order polynomial fit.

[Ω] in each leg of a wye connected three phase load.

5.3 Generator Excitation System Model

The generator voltage control loop is shown in Figure 5.10 on Page 43. In this representation, G_E represents the excitation system transfer function, G_P represents the main generator transfer function, and (5.24) and (5.25) are shown in the feedback loop. This section is dedicated to development of the non–linear first order differential equations describing G_E, H_{fb}, and the pseudo-rms calculation.

Using [4] as reference, the IEEE AC8B excitation system model is used for this disser-
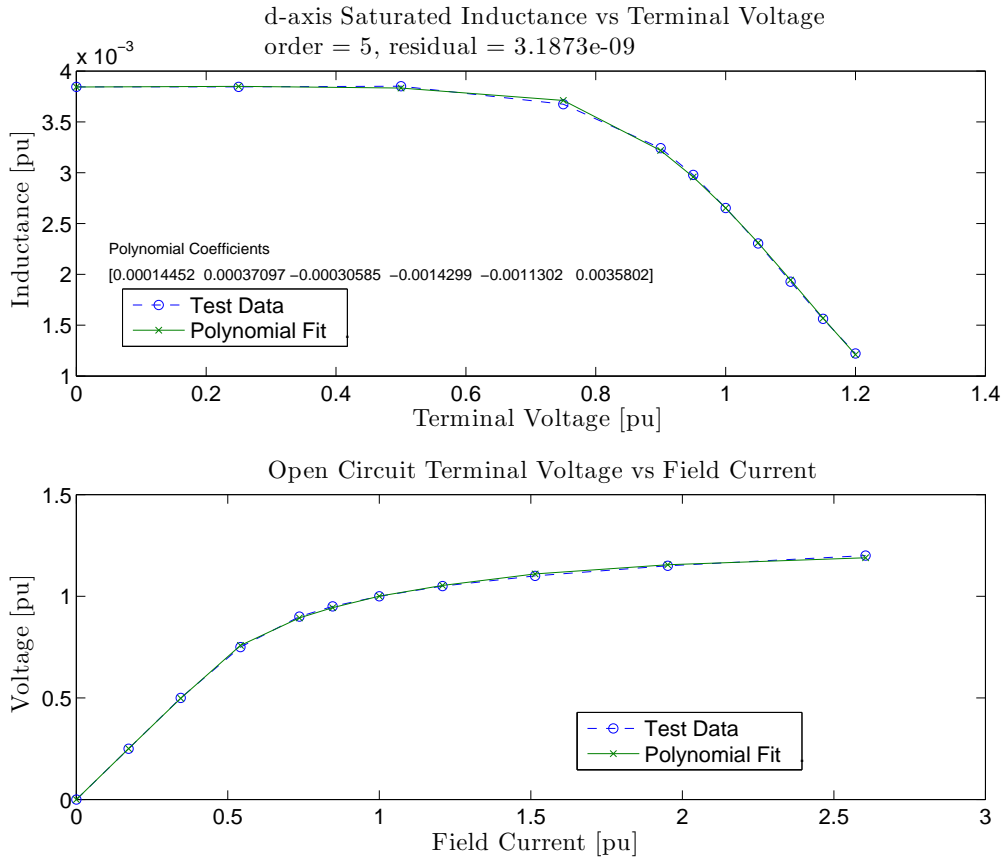
Figure 5.7: Comparing main generator d–axis inductance vs. open circuit voltage, and open circuit terminal voltage vs. field current using fifth order polynomial fit.

tation. The model block diagram is shown in Figure 5.12 on Page 46. Since there is no power system stabilizer in the control network, the input v_s is ignored. Generator terminal voltage stabilization is achieved using a PID controller in the abc reference frame.

A typical Regal Beloit generator is composed of three machines on a common shaft. Referring to Figure 5.11 on Page 43, the permanent magnetic generator and controlled rectifier produce a DC field current for the exciter module. The DC current is modulated in response to the $\mathbf{v}^*$ voltage command signal at the output of the PID controller as shown in Figure 5.12. In addition to representing the PID voltage control, the IEEE AC8B excitation system model is an attempt to model the Excitation System components shown in Figure 5.11, and capture the complex dynamic and steady state behavior exhibited by
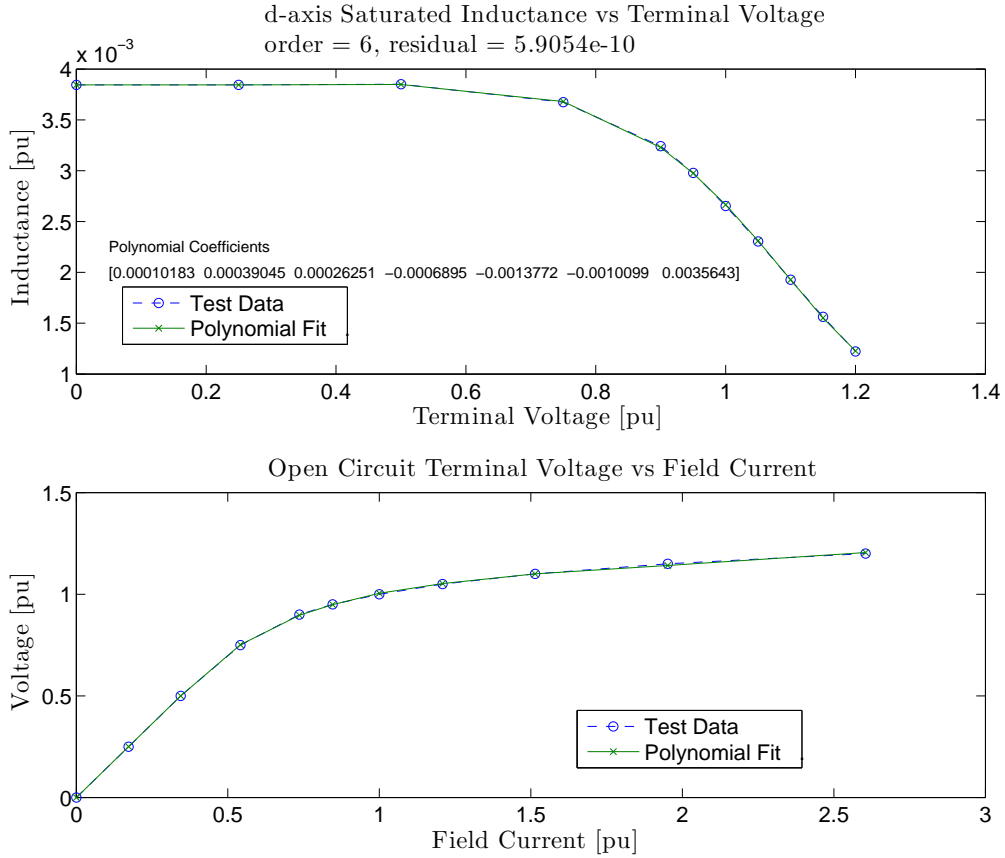
Figure 5.8: Comparing main generator d–axis inductance vs. open circuit voltage, and open circuit terminal voltage vs. field current using sixth order polynomial fit.

saturation in the permanent magnet machine and exciter modules, demagnetizing affects of field current, and the operation of the power electronic components as a function of current levels within the excitation system.

Since a voltage feedback signal v_{fb} is needed to close the control loop, development starts with the feedback gains. Using a root mean square value – one averaged over a half or full cycle – is not proposed. Rather, development of a pseudo–RMS voltage level is pursued.

The control vector for synchronous generator terminal voltage is field current which drives flux across the airgap. Zero sequence voltage is not produced as a result of flux crossing the air gap as evidenced by (5.6). Voltage control for generators is best accom-
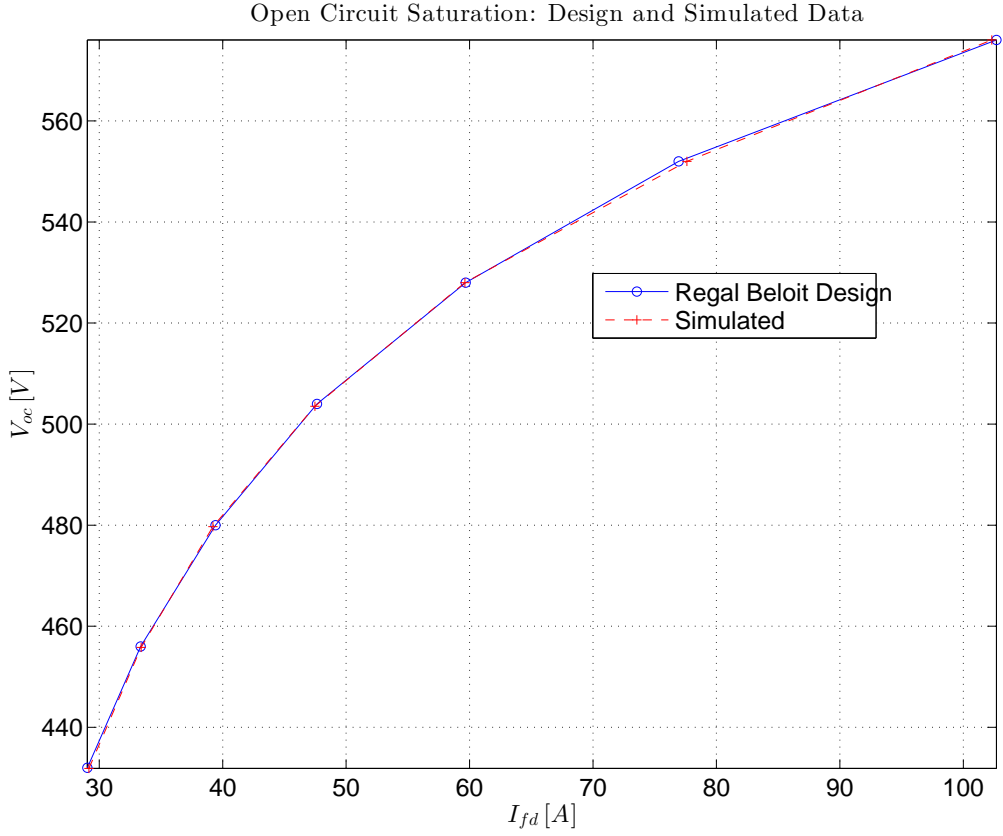
Figure 5.9: Comparing open circuit terminal voltage vs. field current for Regal Beloit design data against simulations using a sixth order polynomial approximation of d axis saturation.

plished using phase–to–phase voltage as the controlled variable and for feedback.

5.3.1 Voltage Feedback Signal

Given a set of three generator terminal phase–to–neutral voltages $\mathbf{v_{abcn}}$ – as shown in Figure 5.10 – equal in magnitude but displaced by 120°

$$
\begin{aligned}
v_{an} &= \sqrt{2}V_{rms}cos(\omega t + \alpha) \\
v_{bn} &= \sqrt{2}V_{rms}cos(\omega t + \alpha - 2\pi/3) \\
v_{cn} &= \sqrt{2}V_{rms}cos(\omega t + \alpha + 2\pi/3)
\end{aligned}
\tag{5.17}
$$
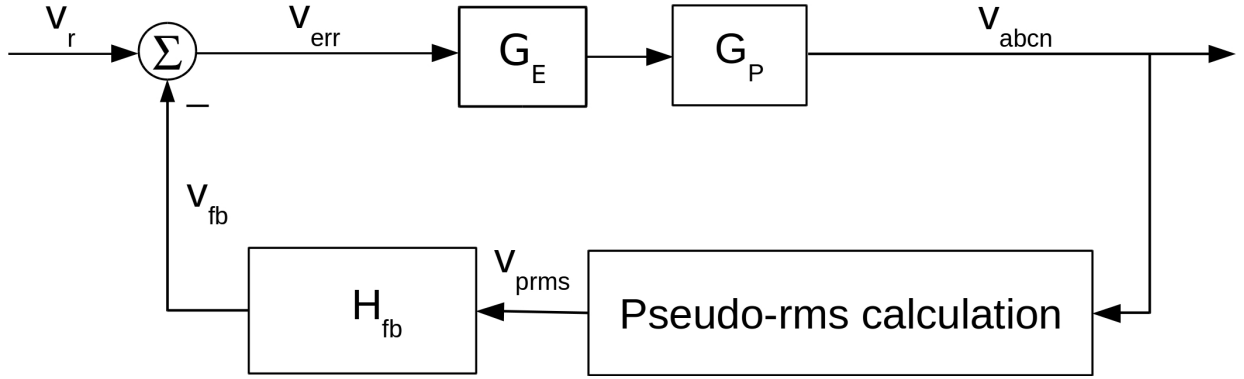
Figure 5.10: Control loop for the generator voltage control.
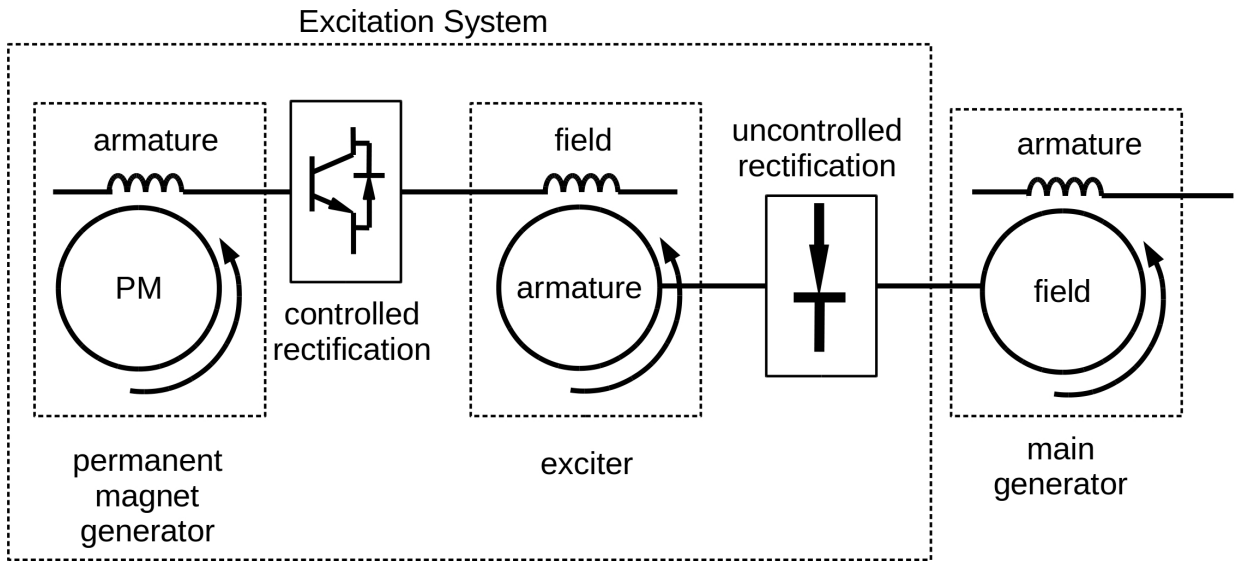
Figure 5.11: Typical common shaft three machine Regal Beloit generator.

Calculate the phase–to–phase voltages

$$v_{ab} = \sqrt{2}V_{rms}\big[cos(\omega t + \alpha) - cos(\omega t + \alpha - 2\pi/3)\big]$$

$$v_{bc} = \sqrt{2}V_{rms}\big[cos(\omega t + \alpha - 2\pi/3) - cos(\omega t + \alpha + 2\pi/3)\big] \qquad (5.18)$$

$$v_{ca} = \sqrt{2}V_{rms}\big[cos(\omega t + \alpha + 2\pi/3) - cos(\omega t + \alpha)\big]$$

43

Simplify (5.18)

$$v_{ab} = \sqrt{3}\sqrt{2}V_{rms}cos(\omega t + \alpha + \pi/6)$$

$$v_{bc} = \sqrt{3}\sqrt{2}V_{rms}cos(\omega t + \alpha - \pi/2) \tag{5.19}$$

$$v_{ca} = \sqrt{3}\sqrt{2}V_{rms}cos(\omega t + \alpha + 7\pi/6)$$

Start with a newly defined term v_{prms}, multiply it by $\sqrt{3}$ and set it equal to the square root sum of squares of terms in (5.19)

$$\sqrt{3}v_{prms} = \sqrt{3}\sqrt{2}V_{rms}[cos^2(\omega t + \alpha + \pi/6)$$
$$+cos^2(\omega t + \alpha - \pi/2) + cos^2(\omega t + \alpha + 7\pi/6)]^{1/2} \tag{5.20}$$

where v_{prms} is the pseudo root mean square voltage. Applying (A4) to bracketed terms in (5.20)

$$cos^2(\omega t + \alpha + \pi/6) = \frac{1}{4}\left(e^{j(\omega t+\alpha+\pi/6)} + e^{-j(\omega t+\alpha+\pi/6)}\right)^2$$
$$cos^2(\omega t + \alpha - \pi/2) = \frac{1}{4}\left(e^{j(\omega t+\alpha-\pi/2)} + e^{-j(\omega t+\alpha+\pi/2)}\right)^2 \tag{5.21}$$
$$cos^2(\omega t + \alpha + 7\pi/6) = \frac{1}{4}\left(e^{j(\omega t+\alpha+7\pi/6)} + e^{-j(\omega t+\alpha+7\pi/6)}\right)^2$$

Adding the right hand sides of the three lines of (5.21) together yields

$$\frac{1}{2}\{1 + cos[2(\omega t + \alpha + \pi/6)] + 1 + cos[2(\omega t + \alpha - \pi/2)] + 1 + cos[2(\omega t + \alpha + 7\pi/6)]\} \tag{5.22}$$

The cosinusoidal terms in (5.22) sum to zero (0) and (5.20) reduces to

$$v_{prms} = \sqrt{3}v_{rms} \tag{5.23}$$

which is the desired result. Writing (5.23) in terms of phase–to–neutral voltages

$$v_{prms} = \sqrt{[(v_{an} - v_{bn})^2 + (v_{bn} - v_{cn})^2 + (v_{cn} - v_{an})^2]/3} \tag{5.24}$$

44

Because the stated condition of perfectly balanced voltages does not exist, a 60 [Hz] $(377 \left[\frac{\text{rad}}{\text{s}} \right])$ signal will be present in v_{prms}. Judicious application of low pass filtering will smooth the ripple, but also slow the system response time. Ideally, the delay replicates that caused by calculation of RMS values in digital control systems. The first order low pass filter transfer function takes the form

$$H_{fb} = \frac{\omega_{co}}{s + \omega_{co}} \tag{5.25}$$

where

- H_{fb} is the unitless transfer function from the pseudo RMS voltage to the voltage that is fed back to the controller

- w_{co} is the cut–off frequency in $\left[\frac{\text{rad}}{\text{s}} \right]$, and

- s is the Laplace variable in the frequency domain with units of $\left[\frac{1}{\text{s}} \right]$.

The feedback gain may be written in first order nonlinear differential form by first recognizing

$$\dot{v}_{fb} = \omega_{co} \left(v_{prms} - v_{fb} \right) \tag{5.26}$$

then substituting (5.24) into (5.26) to yield

$$\dot{v}_{fb} = \omega_{co} \left\{ \sqrt{\left[(v_{an} - v_{bn})^2 + (v_{bn} - v_{cn})^2 + (v_{cn} - v_{an})^2 \right] / 3} - v_{fb} \right\} \tag{5.27}$$

5.3.2 Open Circuit Model Saturation versus Test Data

Exciter models were validated against data from testing performed at Regal Beloit Corporation. The exciter saturation function S_E characterizes the departure of the exciter machine output from the air gap line under open circuit conditions. The form of S_E is
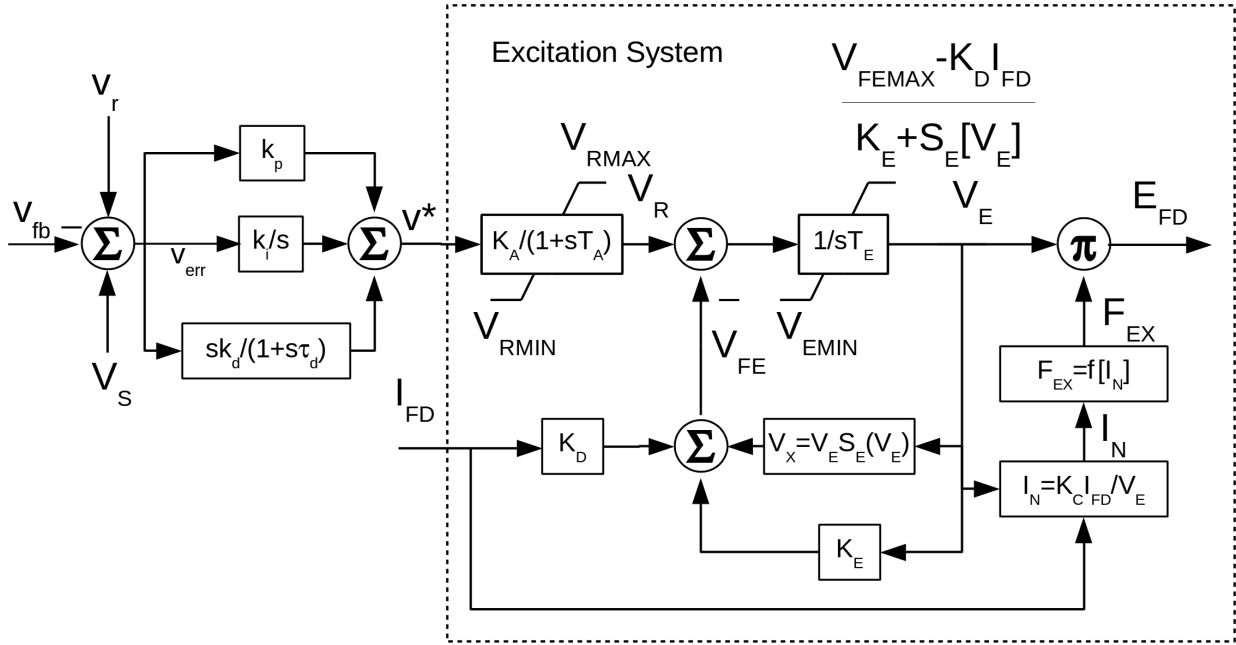
Figure 5.12: IEEE AC8B model for rotating rectifier excitation systems.

not defined in [4], it is considered part of the computer program used. In Figure 5.13 on Page 47, the air gap line, the open circuit armature voltage, the saturation function S_E, and the product of S_E and the open circuit voltage subtracted from the air gap line are plotted against field voltage. These values are all based on test data.

Two approaches are taken to conform the model to test data, the first uses the saturation function S_E defined in [6], and the second uses polynomial fits to approximate S_E. The components tested are shown in Figure 5.14 on Page 48. The machine on the test stand is an 8–pole device with the field winding located on the stator.

5.3.3 $S_E = A_{EX}e^{B_{EX}E_{FD}}$

Values for the exciter saturation function S_E are taken from *Calculation of AC8B Parameters* authored by D. Hyypio 07/22/2015 (internal Regal Beloit Company document). The system is simulated and armature voltage is compared with open circuit saturation test data for an exciter built using an H-ES00714 stator and H-ER00708 rotor (internal Regal Beloit Company reference numbers). Exciter test data is from the open circuit saturation

46
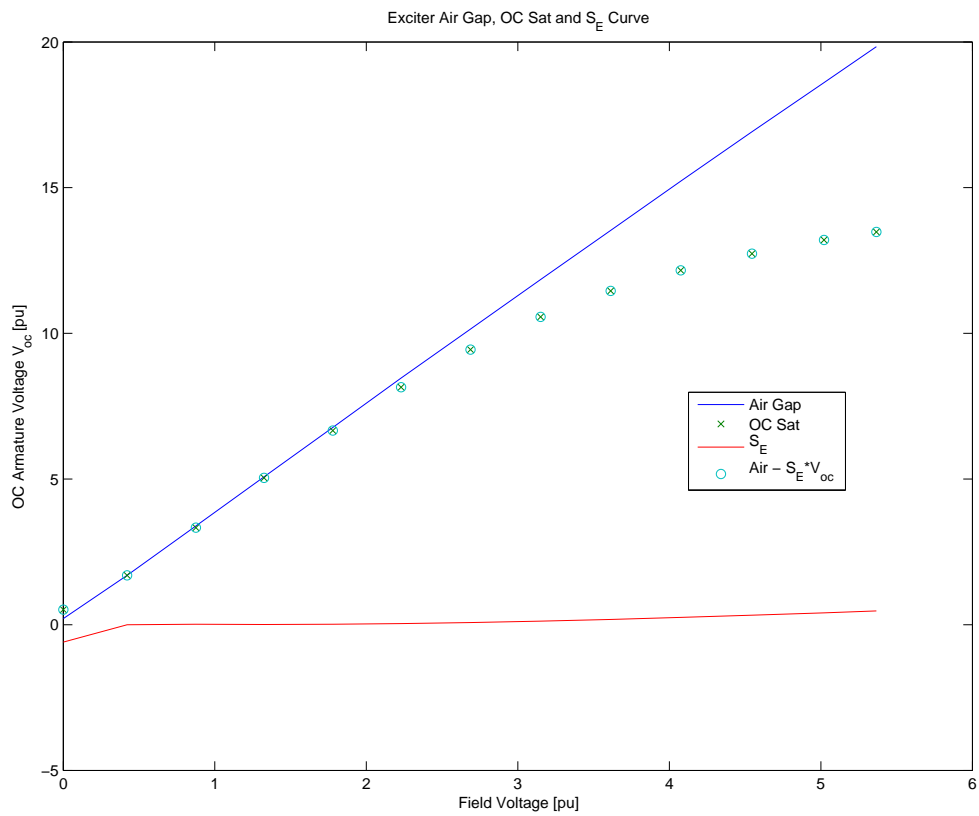
Figure 5.13: The exciter saturation function S_E characterizes the exciter departure from the air gap line.
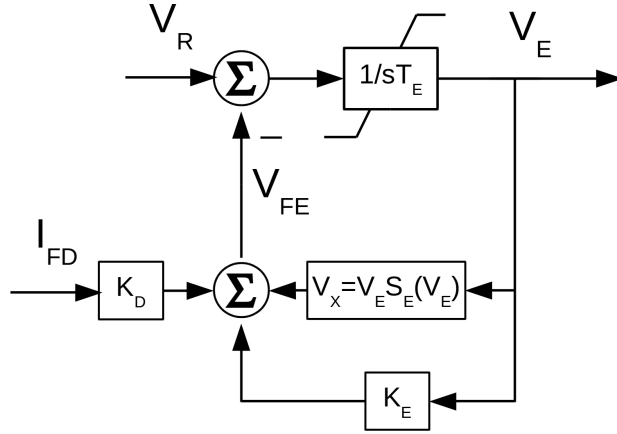
Figure 5.14: The IEEE AC8B exciter model components validated through testing.

testing by K. Felber 3/4/2015. K_E is set to zero per the AC8B parameter document, and T_E is set to 0.14 to accelerate settling time. More on the impact of T_E on rise time is covered in Section 5.3.5. Simulation results using the saturation function from [6] – $S_E = A_{EX}e^{B_{EX}E_{FD}}$ – are compared with test stand data in Figure 5.15 on Page 49.

5.3.4 Polynomial Fit for S_E

Polynomial fits for S_E are shown in Figures 5.19–5.22. Because there is nearly an order of magnitude improvement in fit between the fourth order (r = 0.142) and fifth order polynomial models (r = 0.025), and almost no change between the five and six (r = 0.025) order estimates, the fifth order fit is used. Simulations indicate a relatively good fit between model and test data under the assumption that $K_E = 0.3$. Increasing K_E has the effect of changing the slope, lowering the magnitude, and linearizing the response. Refer to Figures 5.16–5.18. In Figure 5.16, $K_E = 0$, in Figure 5.17, $K_E = 0.3$, and in Figure 5.17, $K_E = 0.6$.

5.3.5 Impact of T_E on Rise Time

Two brief simulations were executed to uncover the impact of T_E on the rise time for the exciter in response to step voltage changes. A value of 1.2 for T_E was provided verbally
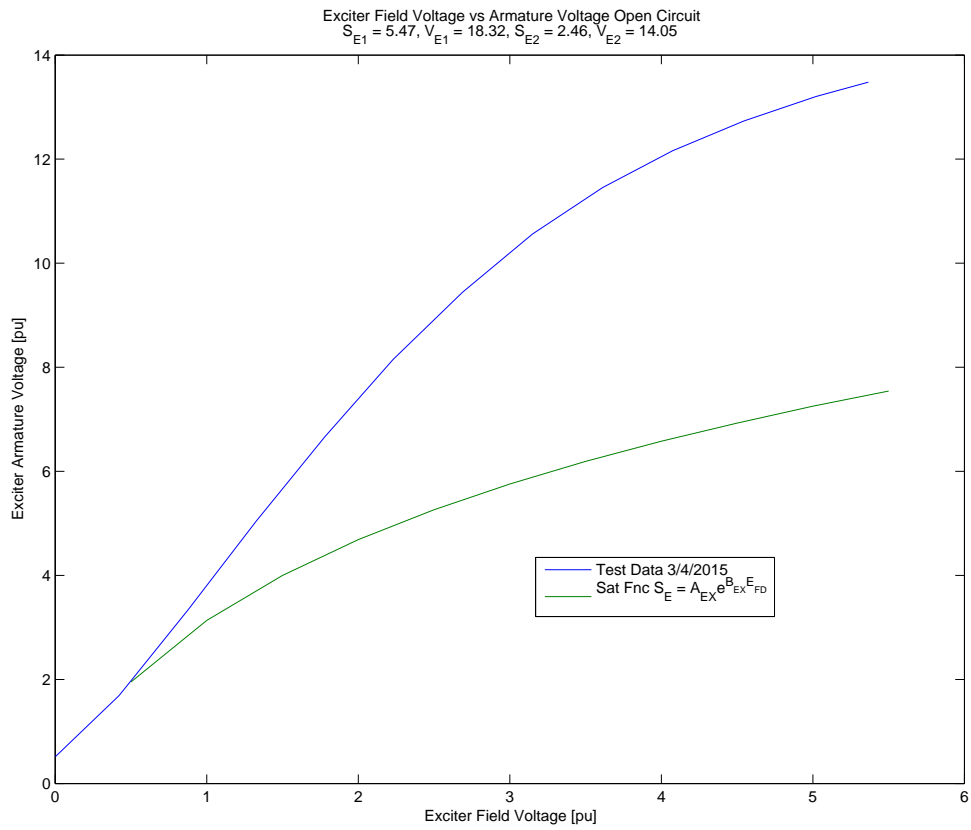
Figure 5.15: Comparing the AC8B model to test data using parameters from *Calculation of AC8B Parameters*, D. Hyypio 07/22/2015.
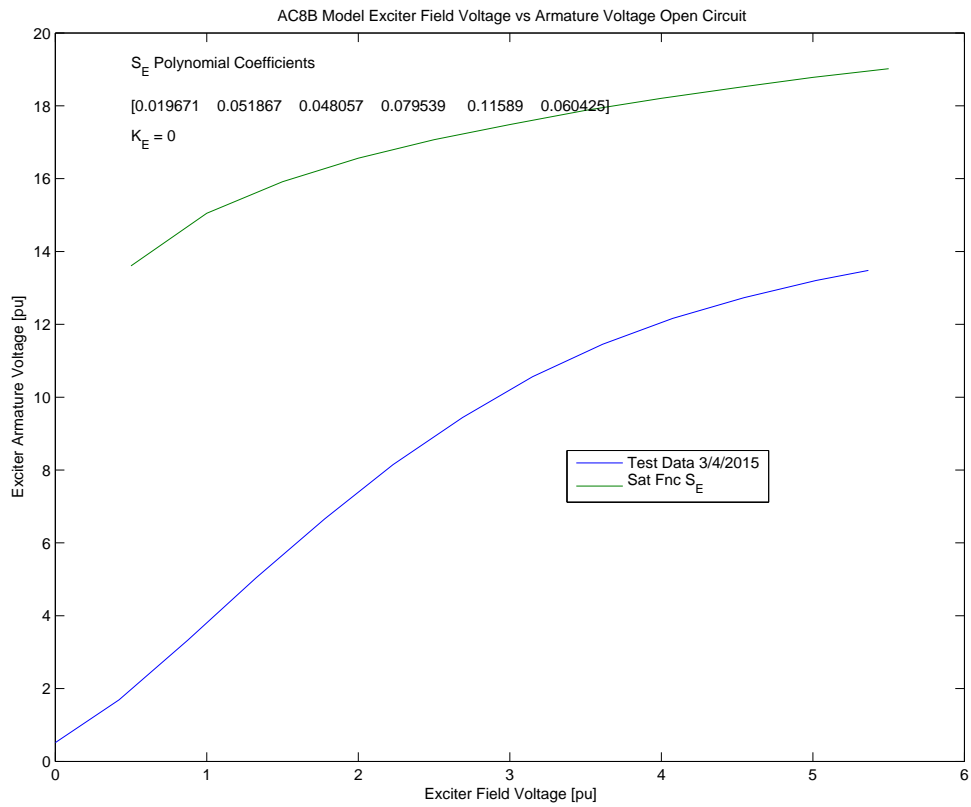
Figure 5.16: Simulation results versus test data using a fifth order polynomial expression for S_E and setting $K_E = 0$.
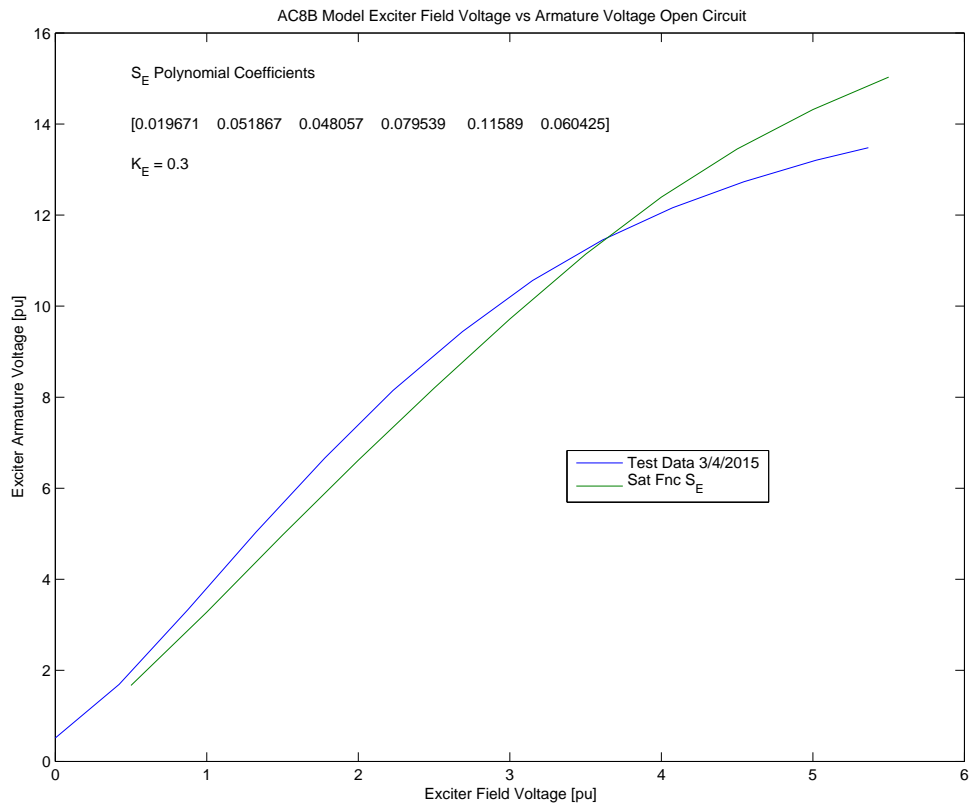
Figure 5.17: Simulation results versus test data using a fifth order polynomial expression for S_E and setting $K_E = 0.3$.
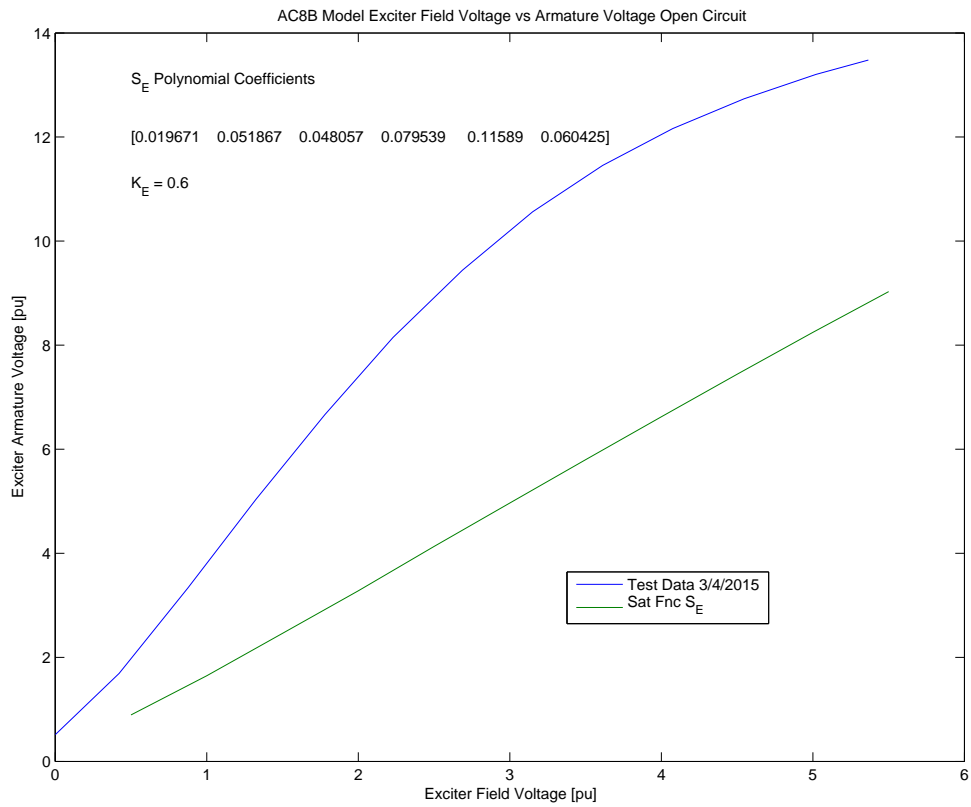
Figure 5.18: Simulation results versus test data using a fifth order polynomial expression for S_E and setting $K_E = 0.6$.
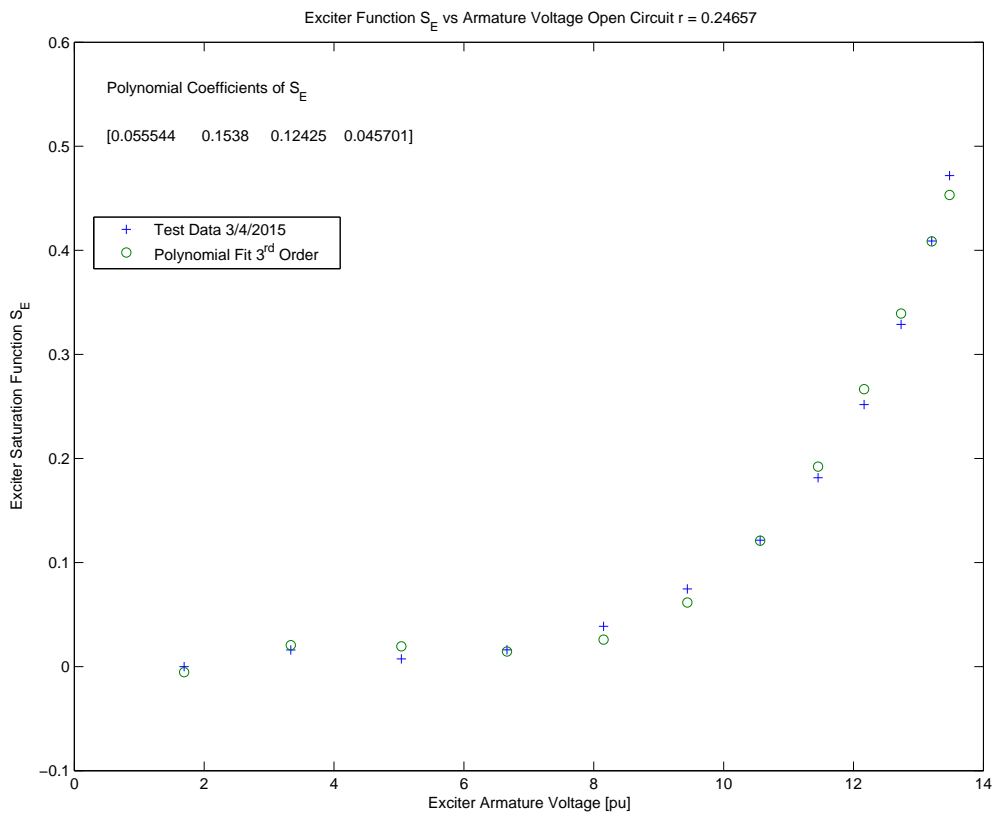
Figure 5.19: Third order polynomial fit for S_E.
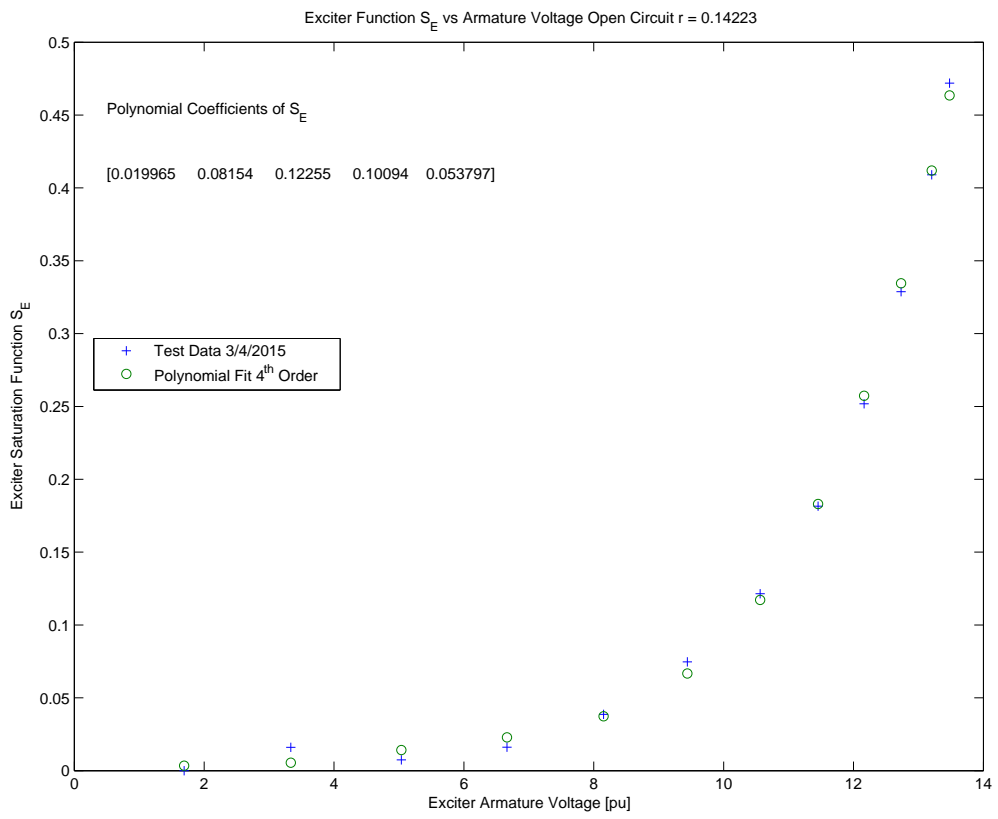
Figure 5.20: Fourth order polynomial fit for S_E.
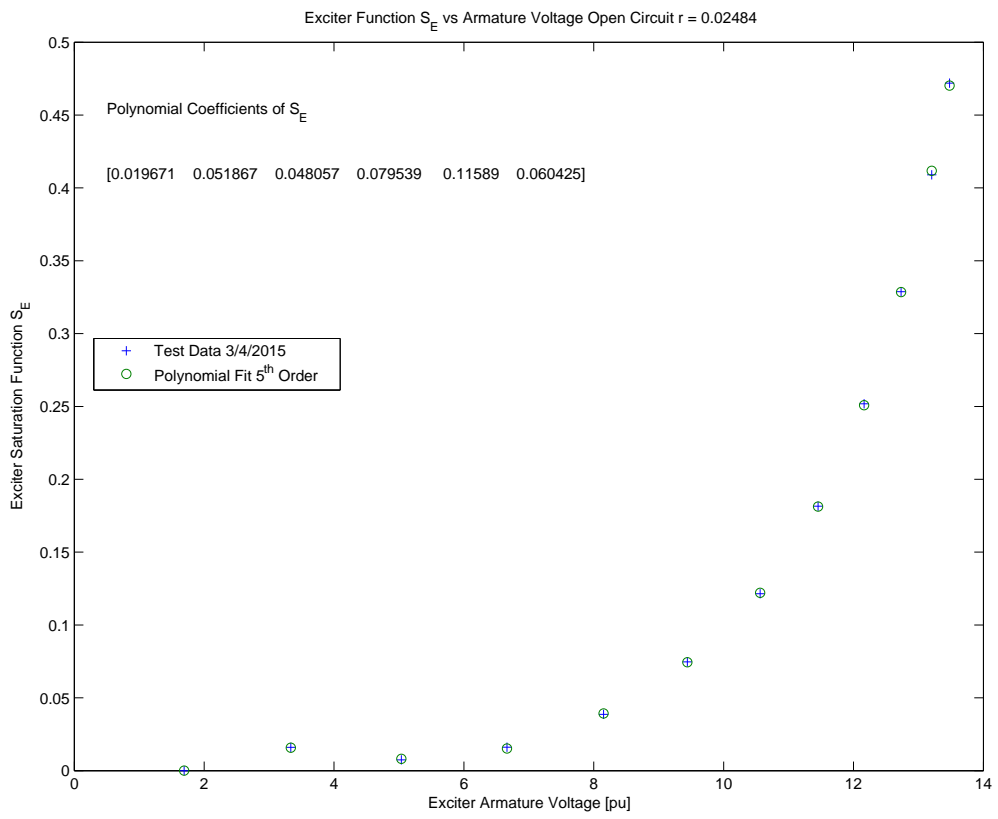
Figure 5.21: Fifth order polynomial fit for S_E.
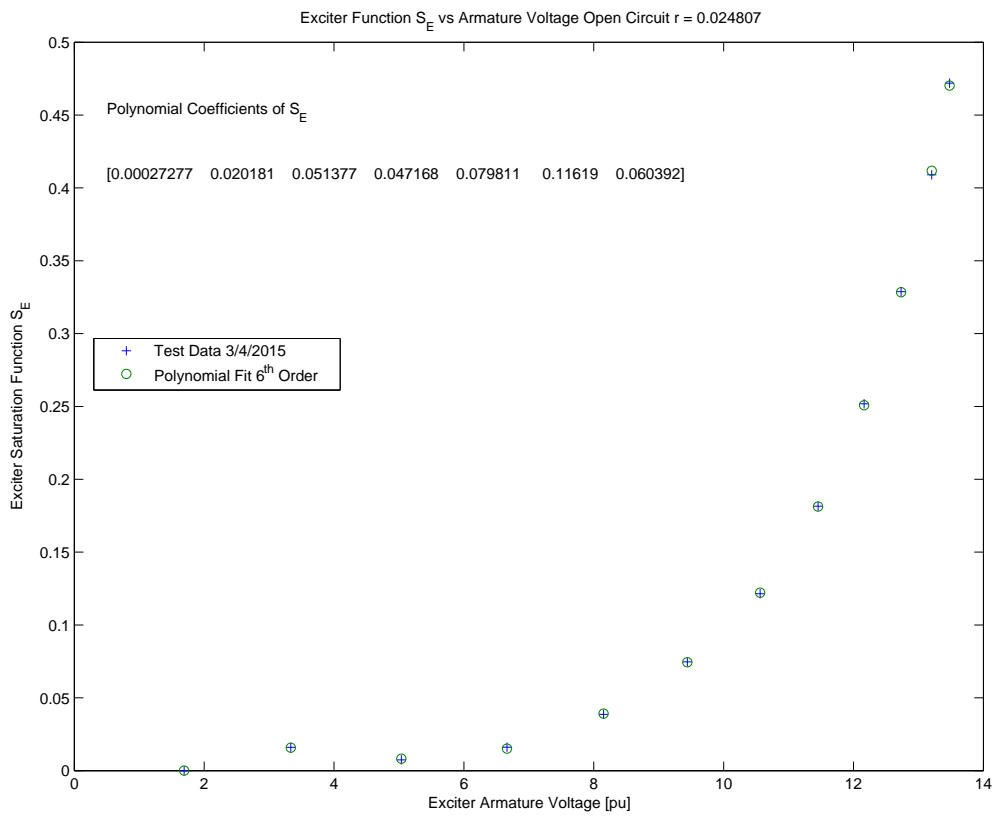
Figure 5.22: Sixth order polynomial fit for S_E.
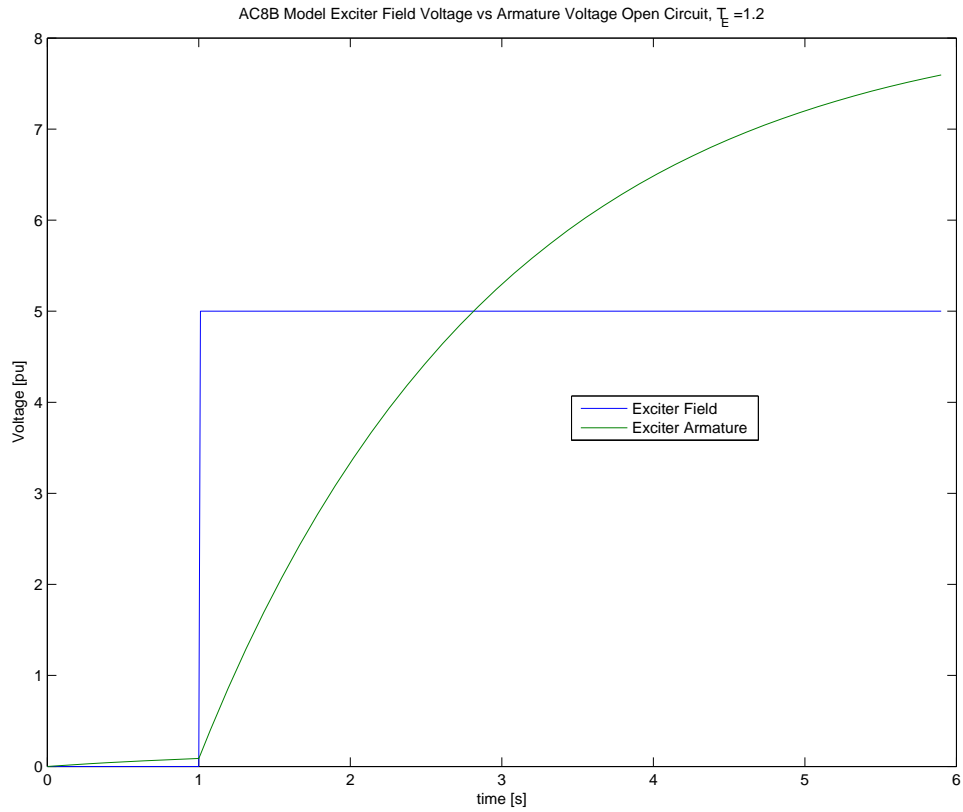
Figure 5.23: Rise time with T_E = 1.2.

by D. Hyypio 8/19/2015. Referring to Figure 5.23 on Page 57, using T_E = 1.2 results in a rise time in excess of 5 seconds, where T_E = 0.14 as in Figure 5.24 on Page 58 results in a much faster system. Load application and rejection tests on the 5 inch exciter using an H-ES00714 stator and H-ER00708 rotor indicate a rise time $t_{r_{10--90}}$ = 0.44 [s]. Refer to Figure 5.25 on Page 59.

5.3.6 PID Controller

To write the PID controller equations in first order nonlinear differential equation form requires the addition of one state for the integrator, and a second state for the differentiator. The proportional control is a linear function of existent states. Summing the three (3)
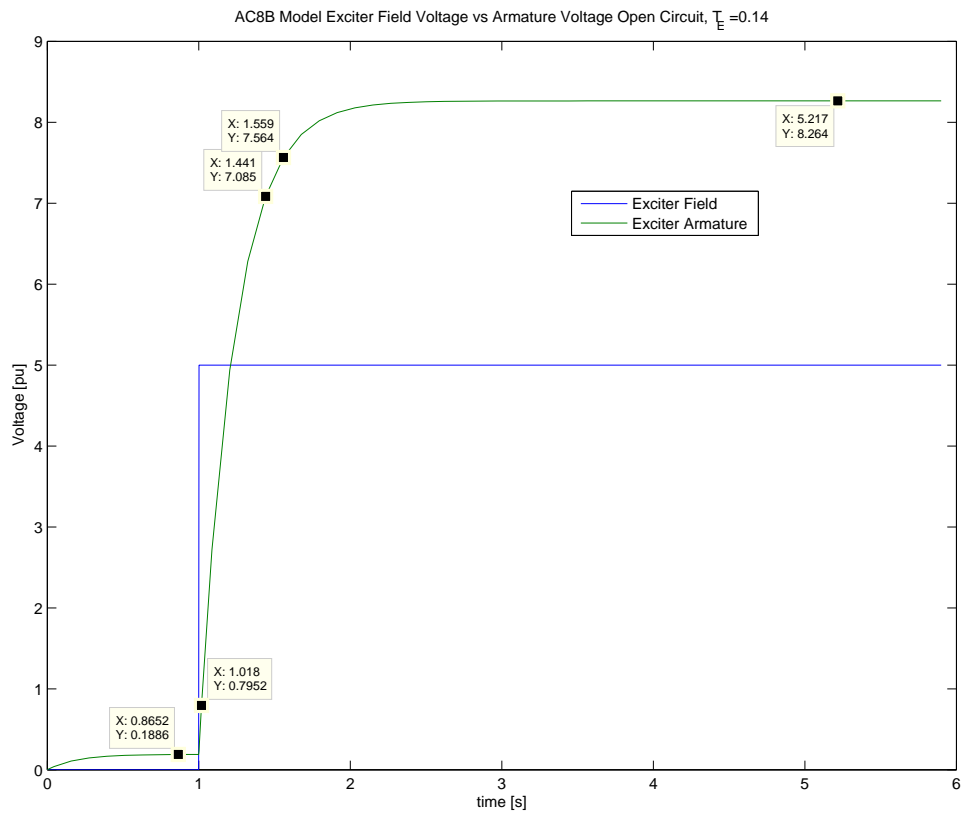
Figure 5.24: Rise time $t_{r_{10-90}}$ = 0.48 [s] with T_E = 0.14.
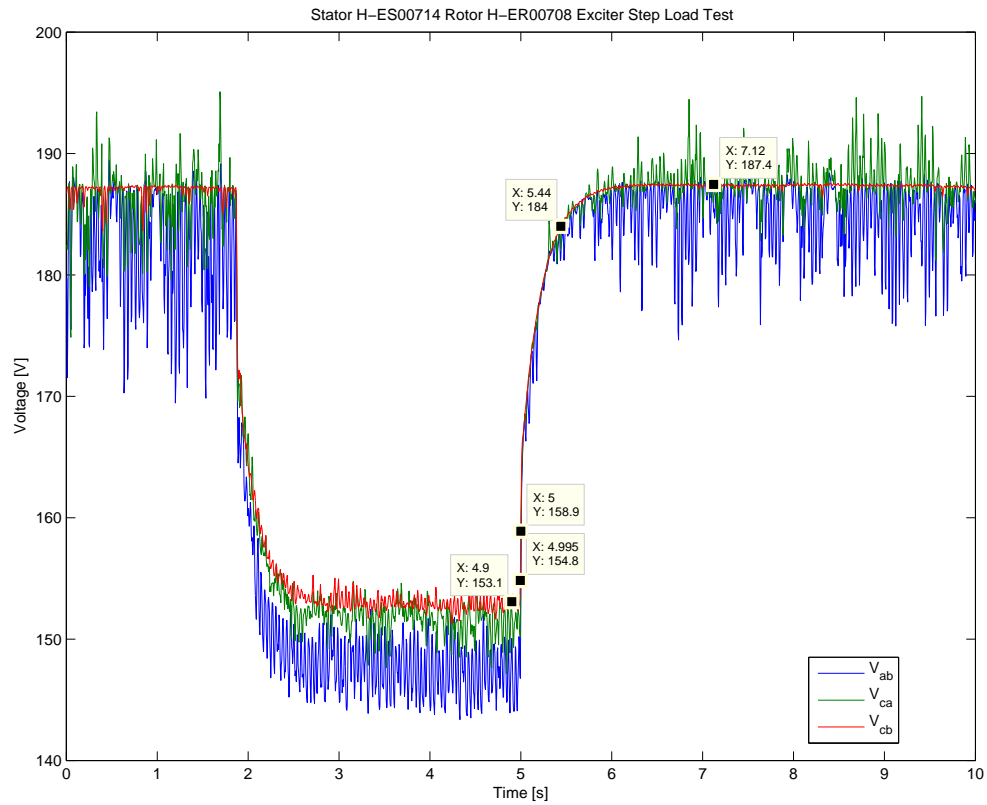
Figure 5.25: Load application and rejection tests performed on an exciter using an H-ES00714 stator and H-ER00708 rotor. The 10–90 rise time $t_{r_{10-90}} = 0.44$ [s].

outputs

$$v^* = v_i^* + v_p^* + v_d^* = \frac{k_i}{s}v_{err} + k_p v_{err} + \frac{k_d s}{1 + \tau_d s}v_{err} \tag{5.28}$$

Taking each term separately

$$\dot{v}_i^* = k_i v_{err} = k_i(v_r - v_{fb})$$

$$v_p^* = k_p v_{err} = k_p(v_r - v_{fb}) \tag{5.29}$$

$$\dot{v}_d^* = \frac{k_d}{\tau_d}(\dot{v}_{err}) - \frac{1}{\tau_d}v_d^* = \frac{k_d}{\tau_d}(\dot{v}_r - \dot{v}_{fb}) - \frac{1}{\tau_d}v_d^*$$

where

- $v_{err} = v_r + v_s - v_{fb}$, and

- $v_s = 0$ because there is no power system stabilizer input.

The first two elements in (5.29) are readily written into first order ordinary differential equation form. The third requires using outputs to augment the equations. For purposes of this dissertation, it is assumed that $\dot{v}_r = 0$, leaving

$$v_d^* = -\frac{k_d}{\tau_d}\dot{v}_{fb} - \frac{1}{\tau_d}v_d^* \tag{5.30}$$

Substituting (5.27) into (5.30) yields

$$v_d^* = -\frac{k_d}{\tau_d}\omega_{co}\left\{\sqrt{\left[(v_{an} - v_{bn})^2 + (v_{bn} - v_{cn})^2 + (v_{cn} - v_{an})^2\right]/3} - v_{fb}\right\} - \frac{1}{\tau_d}v_d^* \tag{5.31}$$

5.3.7 Amplifier Gain and Saturation Modeling

Two additional states are required to complete the AC8B model. The first comes from the amplifier time delay T_A. The amplifier represents the third machine on the generator shaft, a permanent magnet synchronous generator that provides field excitation voltage to

the exciter machine. Commence with the input–output relationship

$$V_R = V^* K_A / (1 + sT_A) \qquad (5.32)$$

where

- V_R [pu] is the amplifier output voltage,

- V^* [pu] is the sum of the PID controller outputs,

- K_A [·] is the amplifier gain, and

- T_A [s] is the amplifier time delay.

Written in first order equation form

$$\dot{V}_R = (K_A / T_A) V^* - (1/T_A) V_R \qquad (5.33)$$

To achieve non–linear saturation to limit V_R between V_{RMIN} and V_{RMAX}, set up a condition comparing the state V_R to the limits, and if the state V_R exceeds a limit, set a variable equal to the violated limit and use that variable in the differential equations for other states.

Start Example Code:

if y(24) $\leq$ V$_{RMIN}$

wye24 = V$_{RMIN}$

else if (y(24) > V$_{RMIN}$)&&(y(24) $\leq$ V$_{RMAX}$)

wye24 = y(24)

else

wye24 = V$_{RMAX}$

End Example Code.

The second state is due to the $1/sT_E$ term

$$V_E = (1/sT_E)(V_R - V_{FE}) \tag{5.34}$$

where

- V_E [pu] is the exciter output voltage,

- T_E [s] is the exciter time constant, integration rate associated with exciter control, and

- V_{FE} [pu] is a feedback signal defined in (5.36).

Written in first order form

$$\dot{V}_E = (1/T_E)V_R - (1/T_E)V_{FE} \tag{5.35}$$

V_{FE} is the sum of three signals

$$V_{FE} = K_C V_E + V_X + K_D I_{FD} \tag{5.36}$$

where

- K_C [·] is the rectifier loading factor proportional to commutating reactance,

- V_X [pu] is defined in (5.37),

- K_D [·] is the exciter demagnetizing factor, a function of exciter alternator reactances, and

- I_{FD} [pu] is the field current.

The first and third terms on the right hand side of (5.36) result in scaling feedback signals V_E and I_{FD} respectively. The second term is written as the product of V_E and S_E

$$V_X = V_E S_E(V_E) \tag{5.37}$$

Table 5.1: Calculating F_{EX} based on [4], Appendix D.

Condition	F_{EX}
$I_N \leq 0.433$	$1 - \frac{1}{\sqrt{3}} I_N$
$0.433 < I_N \leq 0.75$	$\sqrt{0.75 - I_N^2}$
$0.75 < I_N \leq 1.0$	$\sqrt{3}(1 - I_N)$
$1.0 < I_N$	0

where $S_E [\cdot]$ is the exciter saturation function defined by the fifth order polynomial expression shown in Figure 5.21.

5.3.8 Normalized Exciter Load Current and Rectifier Loading Factor

The normalized exciter current is calculated

$$I_N = K_C I_{FD}/V_E \tag{5.38}$$

where all terms have been previously defined. The rectifier loading factor F_{EX} is a function of the normalized exciter load current I_N [4]. The value is determined by the operating range of the exciter according to Table 5.1 on Page 63.

5.4 Generator Electrical and Mechanical Interface

The equation that models the machine motion, known as the swing equation may be written [6]

$$J\ddot{\Theta} = T_a \quad [N\,m] \tag{5.39}$$

where

- J $[\mathrm{kg\,m^2}]$ is the moment of inertia for all equipment on the generator shaft,

- Θ [rad] is the rotor angular position, and

- T_a [N m] is the accelerating torque.

The accelerating torque is the differential between the input mechanical input torque and the torque induced by electrical power output and electrical and mechanical losses in the generator

$$T_a = T_m - T_e - T_{fw} \quad [Nm] \tag{5.40}$$

where

- T_m is the mechanical torque impelling the shaft motion,

- T_e is the electromechanical torque resisting shaft motion, and

- T_{fw} is friction and windage torque resisting shaft motion.

Choosing a reference frame rotating with (nearly) constant velocity ω_m where the subscript m is for mechanical speed

$$\Theta = (\omega_m t + \alpha) = \delta_m \quad [rad] \tag{5.41}$$

Where

- δ_m is the mechanical torque angle, and

- α is $\pi/2$ based on the use of $\mathbf{P}$.

Replacing $\ddot{\Theta}$ with $\ddot{\delta}_m$ in (5.39)

$$J\ddot{\delta}_m = J\dot{\omega}_m = T_a \quad [Nm] \tag{5.42}$$

The friction term T_m is often written

$$T_m = D\omega_m \qquad (5.43)$$

The swing equation form used in this dissertation – written in terms of the shaft power P_e in watts is

$$J\omega_m\dot{\omega}_m = P_m - P_e - P_{fw} \quad [W] \qquad (5.44)$$

where

- P_m is the mechanical input power from the prime mover,

- P_e is the electrical power extracted from the generator shaft, and

- P_{fw} is power lost to friction and windage.

The term P_{fw} is

$$P_{fw} = D * \omega_m^2 \qquad (5.45)$$

Mechanical power P_m is an input to the generator shaft. In Section 5.5, the mechanical power becomes a state, with the input a power command in the control loop. The total three–phase power loading of a synchronous generator P_e is comparable to the shaft torque T_e, including mechanical and electrical losses, and may be expressed as

$$P_e = p_{out} + p_{loss} \quad \text{or}$$

$$p_{out} = P_e - p_{loss} \qquad (5.46)$$

Control systems normally use p_{out} since it is measurable and is calculated

$$p_{out} = v_a i_a + v_b i_b + v_c i_c = \boldsymbol{v_{abc}^T} \boldsymbol{i_{abc}} \quad [\text{pu}] \qquad (5.47)$$

Transforming to the dq0 frame, $v_{abc} = P^{-1}v_{0dq}$ and $i_{abc} = P^{-1}i_{0dq}$, and using the matrix identity $[AB]^T = A^T B^T$,

$$p_{out} = v_{0dq}^T (P^{-1})^T P^{-1} i_{0dq} \quad [\text{pu}] \tag{5.48}$$

Since P is orthogonal and power invariant, $(P^{-1})^T = P$ and

$$p_{out} = v_0 i_0 + v_d i_d + v_q i_q \tag{5.49}$$

The model for this dissertation includes generator current states in the 0dq reference frame, but terminal voltage states in the abc reference frame. Generator output power calculations shall include transformation of voltages from the abc reference frame to the 0dq frame. Combining (5.47) and (5.49)

$$p_{out} = \left[P \begin{bmatrix} v_a \\ v_b \\ v_c \end{bmatrix} \right]^T \begin{bmatrix} i_0 \\ i_d \\ i_q \end{bmatrix} \tag{5.50}$$

For implementing in ordinary differential equation solvers

$$
\begin{aligned}
v_0 &= \left(1/\sqrt{3} \right)(v_a + v_b + v_c) \\
v_d &= \left(\sqrt{2/3} \right)\left[v_a \cos(\theta_e) + v_b \cos(\theta_e - 2\pi/3) + v_c \cos(\theta_e + 2\pi/3) \right] \\
v_q &= \left(\sqrt{2/3} \right)\left[v_a \sin(\theta_e) + v_b \sin(\theta_e - 2\pi/3) + v_c \sin(\theta_e + 2\pi/3) \right]
\end{aligned}
\tag{5.51}
$$

where

$$\theta_e = \omega_e t + \delta_e + \pi/2 \tag{5.52}$$

The torque angle – equal to the electrical angle – compared to the rotor mechanical angle is

$$\delta_e = (p/2)\delta_m \tag{5.53}$$

and the electrical rotational frequency

$$\omega_e = (p/2)\omega_m \tag{5.54}$$

where p is the pole count. Substituting (5.53) and (5.54) into (5.52)

$$\theta_e = (p/2)(\omega_m t + \delta_m) + \pi/2 \tag{5.55}$$

Using (5.55) in (5.51)

$$
\begin{aligned}
v_0 &= \left(1/\sqrt{3}\right)(v_a + v_b + v_c) \\
v_d &= \left(\sqrt{2/3}\right)\{v_a \cos[(p/2)(\omega_m t + \delta_m) + \pi/2] \\
&\quad + v_b \cos[(p/2)(\omega_m t + \delta_m) - \pi/6] \\
&\quad + v_c \cos[(p/2)(\omega_m t + \delta_m) + 7\pi/6]\} \\
v_q &= \left(\sqrt{2/3}\right)\{v_a \sin[(p/2)(\omega_m t + \delta_m) + \pi/2] \\
&\quad + v_b \sin[(p/2)(\omega_m t + \delta_m) - \pi/6] \\
&\quad + v_c \sin[(p/2)(\omega_m t + \delta_m) + 7\pi/6]\}
\end{aligned} \tag{5.56}
$$

Rearranging (5.44) and using (5.56), the first order nonlinear differential equation for shaft motion becomes

$$
\begin{aligned}
\dot{\omega}_m = &-\left(1/\sqrt{3}\right)(v_a + v_b + v_c)\frac{i_0}{J\omega_m} \\
&-\left(\sqrt{2/3}\right)\{v_a \cos[(p/2)(\omega_m t + \delta_m) + \pi/2] \\
&\qquad +v_b \cos[(p/2)(\omega_m t + \delta_m) - \pi/6] \\
&\qquad +v_c \cos[(p/2)(\omega_m t + \delta_m) + 7\pi/6]\}\frac{i_d}{J\omega_m} \\
&-\left(\sqrt{2/3}\right)\{v_a \sin[(p/2)(\omega_m t + \delta_m) + \pi/2] \\
&\qquad +v_b \sin[(p/2)(\omega_m t + \delta_m) - \pi/6] \\
&\qquad +v_c \sin[(p/2)(\omega_m t + \delta_m) + 7\pi/6]\}\frac{i_q}{J\omega_m} \\
&+\frac{P_m}{J\omega_m}
\end{aligned}
\tag{5.57}
$$

The equation for the mechanical angle is

$$
\dot{\theta}_m = \omega_m
\tag{5.58}
$$

5.5   Prime Mover Model

The prime mover is a General Motors 4.3 liter Vortec V6 engine fueled with natural gas. Because the equipment provider has no model for the engine, a first order approximation of the combined fuel valve and combustion delays is used in this dissertation. Inertia of the engine is estimated to be 3 times the inertia of the alternator section of the generator. The governor model is based on IEEE models for gas turbines and is represented in Figure 5.26
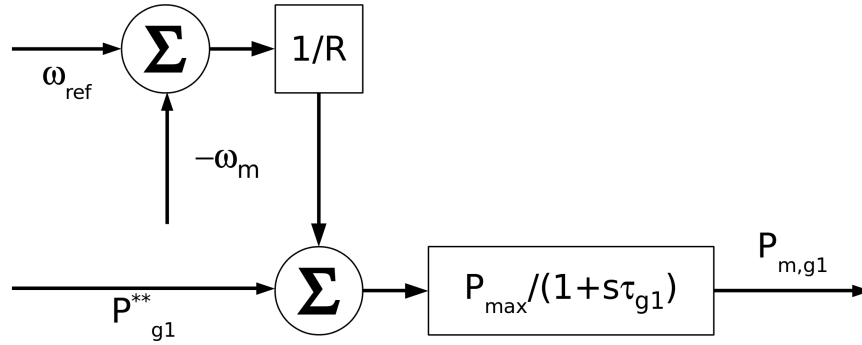
Figure 5.26: The internal combustion engine and governor model.

on Page 69 as $\frac{1}{R}$. Writing the equation for $P_{m,g1}$

$$P_{m,g1} = \frac{1}{1 + s\tau_{g1}} \left[P_{ref,g1} + \frac{1}{R} \left(\omega_{ref} - \omega_m \right) \right] \tag{5.59}$$

where

- $P_{ref,g1}$ is the desired power output of generator 1,

- $P_{m,g1}$ is the mechanical input to generator 1,

- τ_{g1} is the combined fuel valve and combustion delay for the internal combustion engine driving generator 1,

- ω_{ref} is the desired generator angular frequency, and

- ω_m is the measured generator angular frequency.

In first order form, (5.59) becomes

$$\dot{P}_{m,g1} = -\frac{1}{R\tau_{g1}} \omega_m - \frac{1}{\tau_{g1}} P_{m,g1} + \frac{1}{\tau_{g1}} P_{ref,g1} + \frac{1}{R\tau_{g1}} \omega_{ref} \tag{5.60}$$
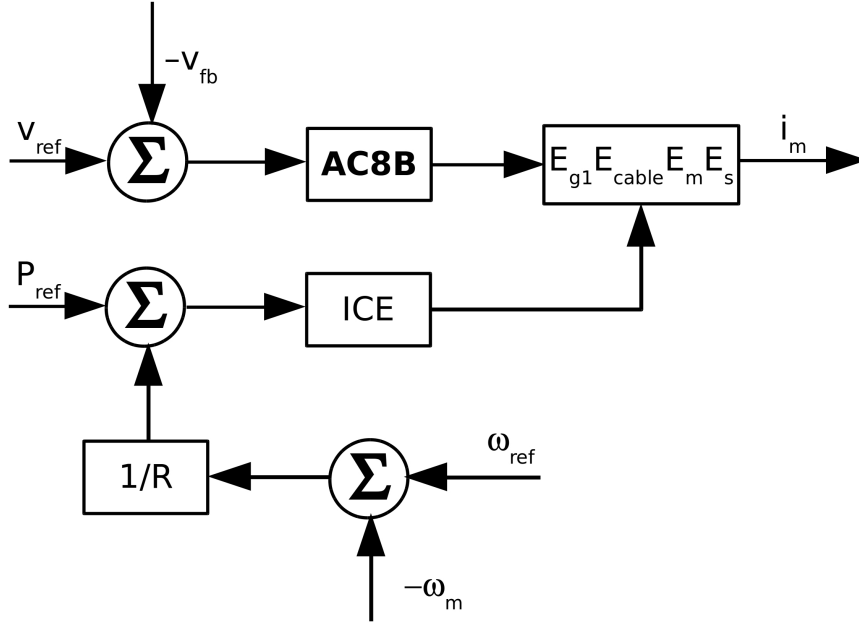
Figure 5.27: The system configuration used to tune the AC8B PID. E_{g1}, E_{cable}, E_m and E_s represent the equations describing the main generator, cable, micro–grid load, and electric power system respectively.

5.6   Tuning the AC8B PID Controller

The approach to tuning the AC8B exciter is to build and simulate the model in Simulnk©, extract linearized models, and plot pole–zero constellations at selected zero and gain values. This is a version of root locus, but in the closed loop. The chosen values are used to evaluate the system response, and adjustments made as needed. The system configuration is shown in Figure 5.27 on Page 70, and conditions for the initial selection are a lightly loaded system, power command to the generator is 0.1 [pu], the voltage reference is 1.0 [pu], and the generator system is connected to the grid.

Rather than assign proportional, derivative and integral gains, zeros are co–located on the real axis, and a gain is assigned. Equations for determining the proportional and integral gains given two zeros and a derivative gain start with the transfer function for a PID controller:

$$G_{PID} = \frac{k_d s^2 + k_p s + k_i}{s}. \tag{5.61}$$

70

The numerator may be written in terms of the zeros, and (5.61) becomes

$$G_{PID} = k_d \left[\frac{(s + z_1)(s + z_2)}{s} \right] = k_d \left[\frac{(s^2 + (z_1 + z_2)s + z_1 z_2)}{s} \right], \qquad (5.62)$$

and

$$k_p = k_d(z_1 + z_2) \qquad (5.63a)$$

$$k_i = k_d z_1 z_2. \qquad (5.63b)$$

The initial set of gains for k_d are selected over a wide range, and the same is true for the zeros. A nested do loop cycles through the various combinations and runs a series of simulations. From the simulated data the pole constellations were plotted to narrow in on an area of interest. A zero location and a new range of gains were selected and the process repeated. A final zero location and gain were selected, a simulation executed, and a review of voltage, power, current made. If the simulation did not meet expectations, the process was revisited to find better values.

For the Kohler generator, the process starts with 15 pole–zero constellations based on simulations performed using the following vectors for zeros and gains:

$$z_1 = z_2 = \begin{bmatrix} 10 & 100 & 1000 \end{bmatrix} \qquad (5.64a)$$

$$k_{dd} = \begin{bmatrix} 1 & 10 & 100 & 1000 & 2000 \end{bmatrix} \qquad (5.64b)$$

and the derivative gain is normalized so that $k_d = \frac{k_{dd}}{z_1 z_2}$.

Samples of the pole–zero constellations from preliminary runs are shown in Figures 5.28 and 5.29 on Pages 73 and 73. Based on the preliminary results, the zeros located at 100 and gains [80 90 100 110 120 130] were simulated. It was observed that as k_d was reduced, the right–most pole was gravitating leftward, and the next leftmost pole rightward. At $k_d = 0.001$, the poles become oscillatory at $-0.306 \pm j0.0331$, so that is the zero and gain

combination selected. In Figure 5.30 on Page 74, the a portion of the pole–zero constellation is shown for the system where the zeros are co–located at 100, and $k_d = 0.002$. The two rightmost poles are shown,and both are on the real axis. As k_d is reduced, the poles move closer together increasing the system speed. Referring to Figure 5.31 on Page 74, at $k_d = 0.001$, the poles have become oscillatory, and the system speed is nearly optimal.

Next, the power command to the generator is changed to 1.0 [pu], and the pole–zero constellation assessed for speed and stability. In this case, the generator is exporting full power of 39 [kW] to the grid. The rightmost poles are shown in Figure 5.32, and demonstrate the system remains stable, but has gotten a more oscillatory as the poles move away from the real axis and toward the quadrature axis. A final simulation is performed under the previously stated conditions with the addition of load on the micro–grid equal to the generator rating of 39 + j29 [kVA]. From the pole zero constellation is shown in Figure 5.33 on Page 75, the system is faster and has better damping due to the load addition.

Sample simulated data
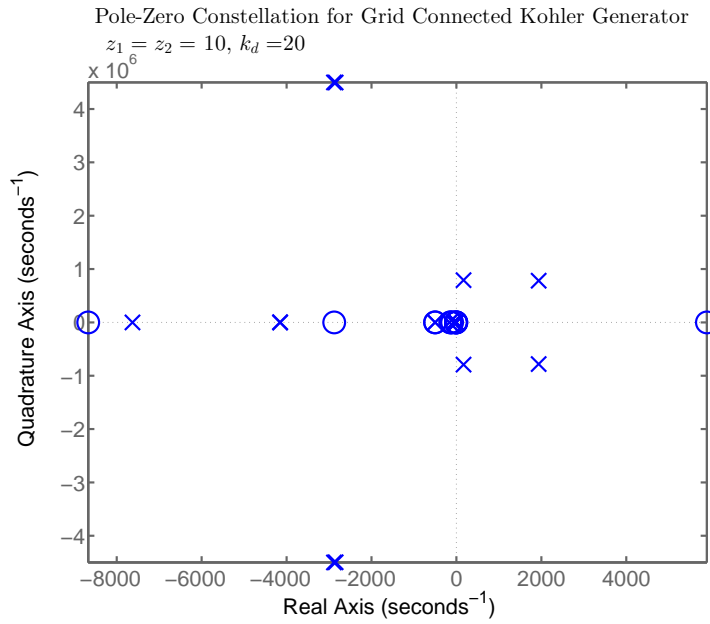
Figure 5.28: Preliminary PID tuning run for the Kohler AC8B regulator demonstrating an unstable pole constellation.
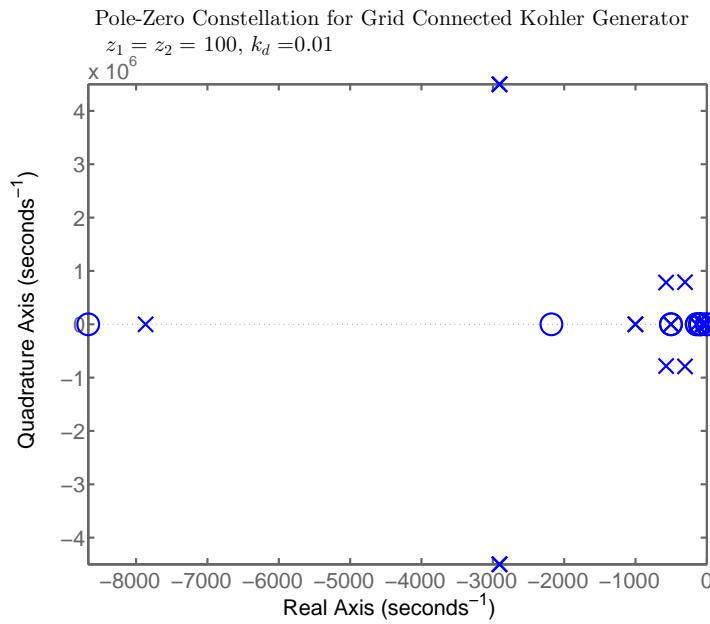
Figure 5.29: Preliminary PID tuning run for the Kohler AC8B regulator demonstrating a stable pole constellation.
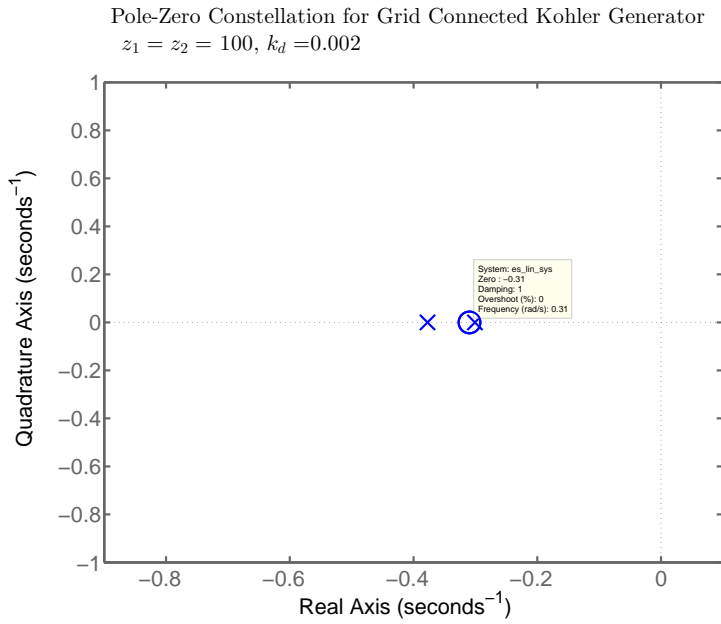
Figure 5.30: Secondary PID tuning run for the Kohler AC8B regulator showing the two rightmost poles with zeros placed at 100 and $k_d = 0.002$.
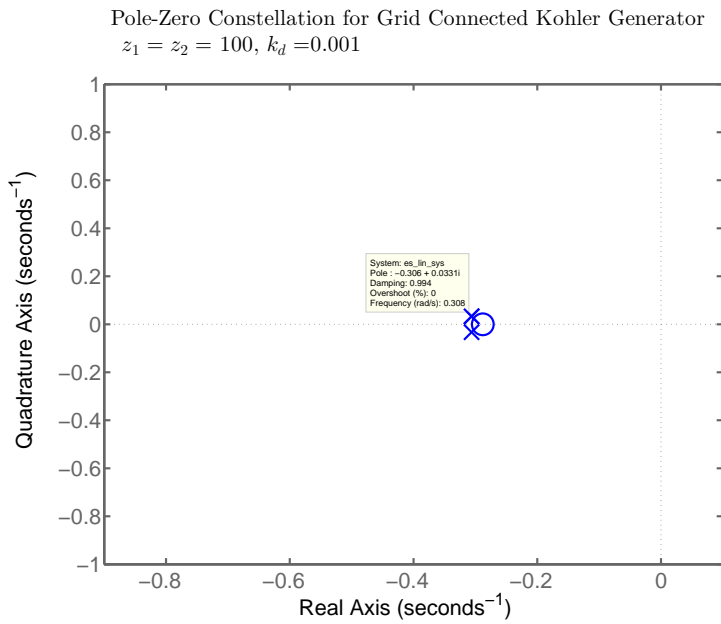
Figure 5.31: Secondary PID tuning run for the Kohler AC8B regulator showing the two rightmost poles with zeros placed at 100 and $k_d = 0.001$.
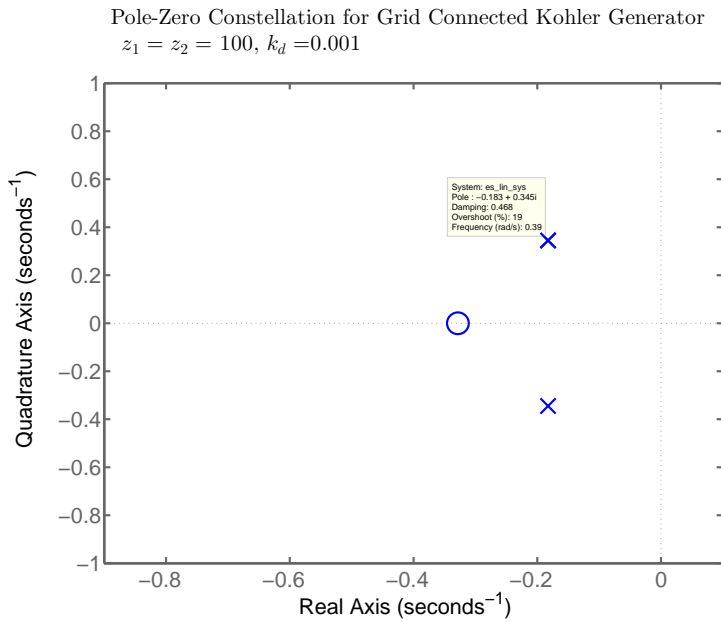
Figure 5.32: Secondary PID tuning run for the Kohler AC8B regulator showing the two rightmost poles with zeros placed at 100 and $k_d = 0.001$, the generator is now exporting 39 [kW] to the grid.
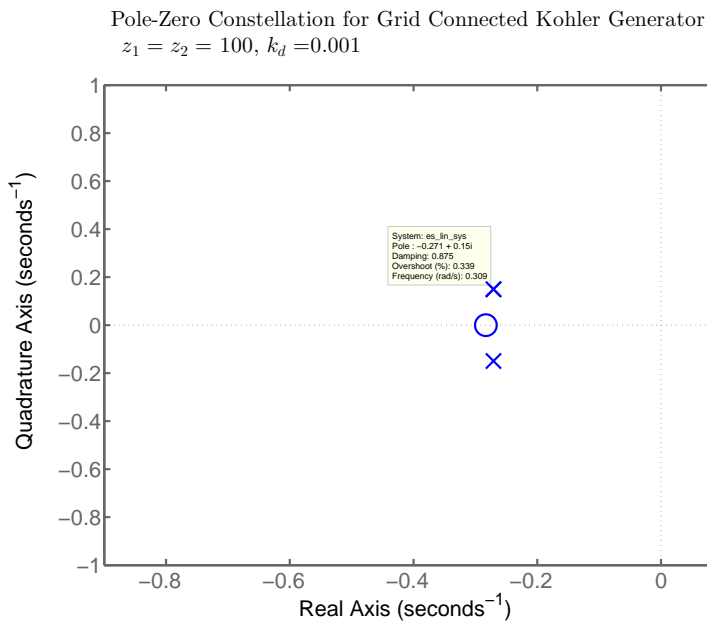
Figure 5.33: Secondary PID tuning run for the Kohler AC8B regulator showing the two rightmost poles with zeros placed at 100 and $k_d = 0.001$, the generator is at full power and the micro–grid load is $39 + j29$ [kVA].

Chapter 6

Energy Storage System Model

The energy storage system model is broken into the current carrying elements in Section 6.1, and the primary control elements in Section 6.2.

6.1 Battery, Inverter, LC Filter and Isolation Transformer

The energy storage system is built from second–use Odyne lithium–ion battery packs designed for vehicular use. The packs contain 25x512 [Wh], 14.6 [V] series connected cells. A battery management system controls cell level charging and discharging. The total power rating is 125 [kW], with an energy rating of 114 [kWh]. Output filtering uses 73 [μH] series line inductors and 230 [μF] capacitors in a Δ configuration. A 260 [kVA], 208 [V]–480 [V] 3.54%Z Δ–Δ transformer is connected to the output filter. The model assumes the isolation transformer 480 [V] terminals are directly connected to the micro–grid bus because the energy storage inverter is proximal.

While generator control is done in the abc stationary reference frame, inverter control is performed in the dq rotating reference frame. Transformation from the abc stationary reference frame to the 0dq rotating reference frame for inverter control uses transformation **P** in (5.4), assumes balanced three–phase conditions, and uses an average model for the inverter, and a basic battery model assuming linear behavior. The diagram for these components modeled in the dq reference frame is shown in Figure 6.1 on Page 77. It should be noted here that parasitic resistances associated with the filter inductor, the transformer, and cable capacitance are not shown.
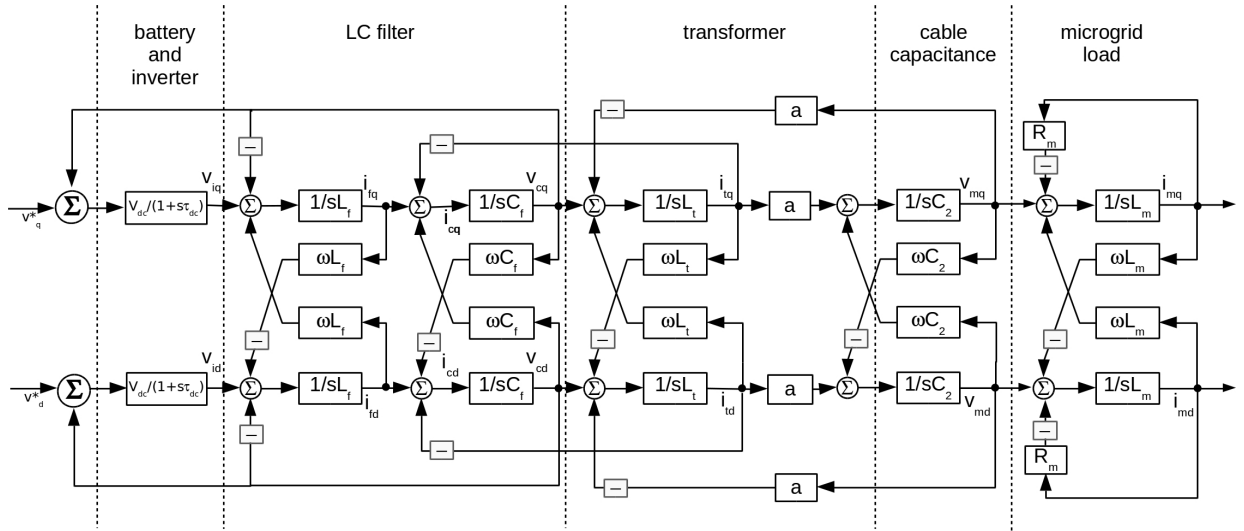
Figure 6.1: A qd reference frame model of the battery, inverter, LC filter, transformer, and micro–grid load. Parasitic resistances associated with the filter inductor, the transformer, and cable capacitance are not shown.

Starting with the energy storage system three–line diagram shown in Figure 6.2 on Page 80, the output LC filter and isolation transformer are converted to a single–phase equivalent circuit as shown in Figure 6.3 on Page 80. Writing the circuit equation for the inverter voltage in the abc fixed reference frame

$$\boldsymbol{v}_{i,abc} = \boldsymbol{v}_{c,abc} + R_f \boldsymbol{i}_{f,abc} + L_f \dot{\boldsymbol{i}}_{f,abc} \tag{6.1}$$

where

- $\boldsymbol{v}_{i,abc}$ is the filter input voltage vector in the abc reference frame [V],

- $\boldsymbol{v}_{c,abc}$ is the filter capacitor voltage vector in the abc reference frame [V],

- R_f is the filter inductor resistance [Ω],

- L_f is the filter inductance [H] and

- $\boldsymbol{i}_{l,abc}$ is the filter inductor current vector in the abc reference frame.

77

Applying the Park transform $\mathbf{P}$ to (6.1)

$$\boldsymbol{P}\boldsymbol{v}_{i,abc} = \boldsymbol{P}\boldsymbol{v}_{c,abc} + R_f\boldsymbol{P}\boldsymbol{i}_{f,abc} + L_f\boldsymbol{P}\dot{\boldsymbol{i}}_{f,abc} \tag{6.2}$$

It is the case that

$$\boldsymbol{P}\boldsymbol{v}_{i,abc} = \boldsymbol{v}_{i,0dq}$$

$$\boldsymbol{P}\boldsymbol{v}_{c,abc} = \boldsymbol{v}_{c,0dq} \tag{6.3}$$

$$\boldsymbol{P}\boldsymbol{i}_{f,abc} = \boldsymbol{i}_{f,0dq}$$

where

- $\boldsymbol{v}_{i,0dq}$ is the filter input voltage vector in the 0dq reference frame [V],

- $\boldsymbol{v}_{c,0dq}$ is the filter capacitor voltage vector in the 0dq reference frame [V] and

- $\boldsymbol{i}_{f,0dq}$ is the filter inductor current vector in the 0dq reference frame [A]

It is also true that

$$\dot{\boldsymbol{i}}_{l,0dq} = \boldsymbol{P}\dot{\boldsymbol{i}}_{l,abc} + \dot{\boldsymbol{P}}\boldsymbol{i}_{l,abc} \tag{6.4}$$

where $\boldsymbol{i}_{l,0dq}$ is the filter inductor current vector in the 0dq reference frame, and

$$\dot{\boldsymbol{P}}\boldsymbol{i}_{l,abc} = \dot{\boldsymbol{P}}\boldsymbol{P}^{-1}\boldsymbol{i}_{l,0dq} \tag{6.5}$$

Substituting (6.5) and (6.4) into (6.2) and rearranging terms

$$\dot{\boldsymbol{i}}_{f,0dq} = \frac{1}{L_f}\boldsymbol{v}_{i,0dq} - \frac{1}{L_f}\boldsymbol{v}_{c,0dq} - \frac{R_m}{L_m}\boldsymbol{i}_{f,0dq} + \dot{\boldsymbol{P}}\boldsymbol{P}^{-1}\boldsymbol{i}_{f,0dq} \tag{6.6}$$

Invoking A13, the matrix form of 6.6 is

$$
\begin{bmatrix} \dot{i}_{f0} \\ i_{fd} \\ i_{fq} \end{bmatrix} = \frac{1}{L_f} \begin{bmatrix} v_{i0} \\ v_{id} \\ v_{iq} \end{bmatrix} - \frac{1}{L_f} \begin{bmatrix} v_{c0} \\ v_{cd} \\ v_{cq} \end{bmatrix} - \frac{R_m}{L_m} \begin{bmatrix} i_{f0} \\ i_{fd} \\ i_{fq} \end{bmatrix} + \begin{bmatrix} 0 & 0 & 0 \\ 0 & 0 & -\omega \\ 0 & \omega & 0 \end{bmatrix} \begin{bmatrix} i_{f0} \\ i_{fd} \\ i_{fq} \end{bmatrix}
\tag{6.7}
$$

Under balanced conditions, i_{l0} is superfluous leaving equations for i_{ld} and i_{lq}

$$
\begin{bmatrix} \dot{i}_{fd} \\ i_{fq} \end{bmatrix} = \frac{1}{L_f} \begin{bmatrix} v_{id} \\ v_{iq} \end{bmatrix} - \frac{1}{L_f} \begin{bmatrix} v_{cd} \\ v_{cq} \end{bmatrix} + \begin{bmatrix} -\frac{R_m}{L_m} & -\omega \\ \omega & -\frac{R_m}{L_m} \end{bmatrix} \begin{bmatrix} i_{fd} \\ i_{fq} \end{bmatrix}
\tag{6.8}
$$

Writing out the filter inductor currents on the d (6.9a) and q (6.9b) axes,

$$
\dot{i}_{fd} = \frac{1}{L_f} \left[v_{id} - v_{cd} - R_f i_{fd} - \omega L_f i_{fq} \right]
\tag{6.9a}
$$

$$
\dot{i}_{fq} = \frac{1}{L_f} \left[v_{iq} - v_{cq} - R_f i_{fq} + \omega L_f i_{fd} \right].
\tag{6.9b}
$$

To write the equations for the capacitor voltage terms under the assumption of balanced conditions, start by converting the delta connected capacitor bank into an equivalent wye configuration. Then

$$
\boldsymbol{i}_{c,abc} = 3C_{ll}\dot{\boldsymbol{v}}_{c,abcf}
\tag{6.10}
$$

Where

- $\boldsymbol{i}_{c,abc}$ represents the line current flowing into the filter capacitor

- C_{ll} is the capacitance connected line–to–line

- $\boldsymbol{v}_{c,abcf}$ represents the capacitor line–to–wye floating point voltages

Transforming (6.10) to the rotating 0dq reference frame

$$
\boldsymbol{P}\boldsymbol{i}_{c,abc} = 3C_{ll}\boldsymbol{P}\dot{\boldsymbol{v}}_{c,abcf}
\tag{6.11}
$$

79
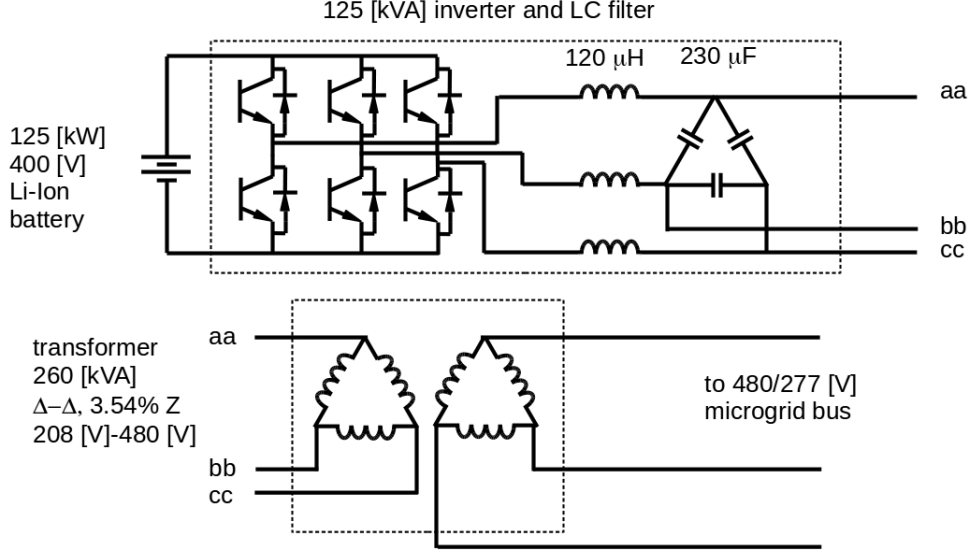
Figure 6.2: The energy storage device schematic diagram.
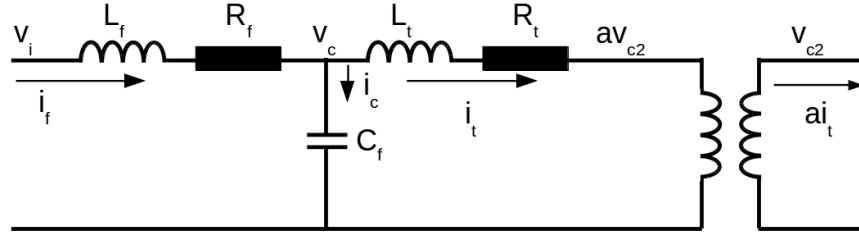
Figure 6.3: The energy storage device LC filter and isolation transformer circuit diagram.

Since $\boldsymbol{P}\boldsymbol{i}_{c,abc} = \boldsymbol{i}_{c,0dq}$ and $\boldsymbol{P}\dot{\boldsymbol{v}}_{c,abcf} = \dot{\boldsymbol{v}}_{c,0dq} - \dot{\boldsymbol{P}}\boldsymbol{P}\dot{\boldsymbol{v}}_{c,0dq}$, (6.11) may be written

$$\boldsymbol{i}_{c,0dq} = 3C_{ll}\left[\dot{\boldsymbol{v}}_{c,0dq} - \dot{\boldsymbol{P}}\boldsymbol{P}\dot{\boldsymbol{v}}_{c,0dq}\right] \tag{6.12}$$

In matrix form, (6.12) becomes

$$\begin{bmatrix} i_{c0} \\ i_{cd} \\ i_{cq} \end{bmatrix} = 3C_{ll}\begin{bmatrix} \dot{v}_{c0} \\ \dot{v}_{cd} \\ \dot{v}_{cq} \end{bmatrix} - 3C_{ll}\begin{bmatrix} 0 & 0 & 0 \\ 0 & 0 & -\omega \\ 0 & \omega & 0 \end{bmatrix}\begin{bmatrix} v_{c0} \\ v_{cd} \\ v_{cq} \end{bmatrix} \tag{6.13}$$

Rearranging (6.13) and eliminating the zero sequence term to avoid singularity, the non–

linear first order differential equations become

$$\begin{bmatrix} \dot{v}_{cd} \\ v_{cq} \end{bmatrix} = \frac{1}{3C_{ll}} \begin{bmatrix} i_{cd} \\ i_{cq} \end{bmatrix} + \begin{bmatrix} -\omega v_{cq} \\ \omega v_{cd} \end{bmatrix} \tag{6.14}$$

Writing (6.14) in terms of states defined in the non–linear differential equations

$$\begin{bmatrix} \dot{v}_{cd} \\ v_{cq} \end{bmatrix} = \frac{1}{3C_{ll}} \begin{bmatrix} i_{fd} \\ i_{fq} \end{bmatrix} - \frac{1}{3C_{ll}} \begin{bmatrix} i_{td} \\ i_{tq} \end{bmatrix} + \begin{bmatrix} 0 & -\omega \\ \omega & 0 \end{bmatrix} \begin{bmatrix} v_{cd} \\ v_{cq} \end{bmatrix} \tag{6.15}$$

Where as shown in Figure 6.3 on Page 80

- $\boldsymbol{i}_{c,dg} = \boldsymbol{i}_{l,dg} - \boldsymbol{i}_{t,dg}$,

- i_{fd} and i_{fq} are the filter inductor d and q axis currents respectively, and

- i_{td} and i_{tq} are the transformer d and q axis currents respectively.

Setting $C_f = 3C_{ll}$ and writing the equations for $\dot{\boldsymbol{v}}_{c,dq}$ on the d (6.16a) and q (6.16b) axes,

$$\dot{v}_{cd} = \frac{1}{C_f} \left[i_{fd} - i_{td} - \omega C_f v_{cq} \right] \tag{6.16a}$$

$$\dot{v}_{cq} = \frac{1}{C_f} \left[i_{fq} - i_{tq} + \omega C_f v_{cd} \right]. \tag{6.16b}$$

Transformer current equations are of the same form as (6.8)

$$\begin{bmatrix} \dot{i}_{td} \\ i_{tq} \end{bmatrix} = \frac{1}{L_t} \begin{bmatrix} v_{cd} \\ v_{cq} \end{bmatrix} - \frac{208}{480L_t} \begin{bmatrix} v_{c2d} \\ v_{c2q} \end{bmatrix} + \begin{bmatrix} -\frac{R_t}{L_t} & -\omega \\ \omega & -\frac{R_t}{L_t} \end{bmatrix} \begin{bmatrix} i_{td} \\ i_{tq} \end{bmatrix} \tag{6.17}$$

Writing the equations for transformer currents on the d (6.18a) and q (6.18b) axes,

$$\dot{i}_{td} = \frac{1}{L_t} \left[v_{cd} - a v_{c2d} - R_t i_{td} - \omega L_t i_{tq} \right] \tag{6.18a}$$

$$\dot{i}_{tq} = \frac{1}{L_t} \left[v_{cq} - a v_{c2q} - R_t i_{tq} + \omega L_t i_{td} \right]. \tag{6.18b}$$

81

Note that C_2 voltage terms are scaled by the isolation transformer ratio. Since the transformer connections are Δ–Δ, there is no phase shift to model.

To transition from a 3 wire rotating dq reference frame to a 4 wire stationary abc reference frame at this location, write the equations for v_{c2d} and v_{c2q} based on the v_{abcn} values

$$
\begin{bmatrix} v_{c2d} \\ v_{c2q} \end{bmatrix} = \sqrt{\frac{2}{3}} \begin{bmatrix} \cos\left(\theta_{mb} + \frac{\pi}{2}\right) & \cos\left(\theta_{mb} - \frac{\pi}{6}\right) & \cos\left(\theta_{mb} + \frac{7\pi}{6}\right) \\ \sin\left(\theta_{mb} + \frac{\pi}{2}\right) & \sin\left(\theta_{mb} - \frac{\pi}{6}\right) & \sin\left(\theta_{mb} + \frac{7\pi}{6}\right) \end{bmatrix} \begin{bmatrix} v_{c2a} \\ v_{c2b} \\ v_{c2c} \end{bmatrix} \tag{6.19}
$$

Where θ_{mb} is the reference angle at the micro–grid bus as defined by (6.20) and (6.22)–(6.24) for the phase–locked–loop (PLL). Letting

$$
\boldsymbol{P}_{2:3,1:3} = \sqrt{\frac{2}{3}} \begin{bmatrix} \cos\left(\theta_{mb} + \frac{\pi}{2}\right) & \cos\left(\theta_{mb} - \frac{\pi}{6}\right) & \cos\left(\theta_{mb} + \frac{7\pi}{6}\right) \\ \sin\left(\theta_{mb} + \frac{\pi}{2}\right) & \sin\left(\theta_{mb} - \frac{\pi}{6}\right) & \sin\left(\theta_{mb} + \frac{7\pi}{6}\right) \end{bmatrix} \tag{6.20}
$$

Substituting (6.20) and (6.19) into (6.17)

$$
\begin{bmatrix} \dot{i}_{td} \\ \dot{i}_{tq} \end{bmatrix} = \frac{1}{L_t} \begin{bmatrix} v_{cd} \\ v_{cq} \end{bmatrix} - \frac{208}{480L_t} \boldsymbol{P}_{2:3,1:3} \begin{bmatrix} v_{c2a} \\ v_{c2b} \\ v_{c2c} \end{bmatrix} + \begin{bmatrix} 0 & -\omega \\ \omega & 0 \end{bmatrix} \begin{bmatrix} i_{td} \\ i_{tq} \end{bmatrix} \tag{6.21}
$$

Referring to Figure 6.4 on Page 83, a PLL is modeled to estimate the angle θ_{mb} at the micro–grid bus. Within the PLL structure, the resultant angle is used in calculation of v_{c2d} and v_{c2q} relevant to (6.17). Because micro–grid frequency is needed at the secondary control level, a frequency estimate ω_{mb} is extracted and ported into a low–pass filter to yield $\omega_{lpf,mb}$.

Since the PLL is connected to the 480/277 [V] system, v_{c2d} is defined by (6.20). Writing v_{c2di} in first order form

$$
\dot{v}_{c2di} = K_{ipll}\left(v_{c2d}\right) \tag{6.22}
$$
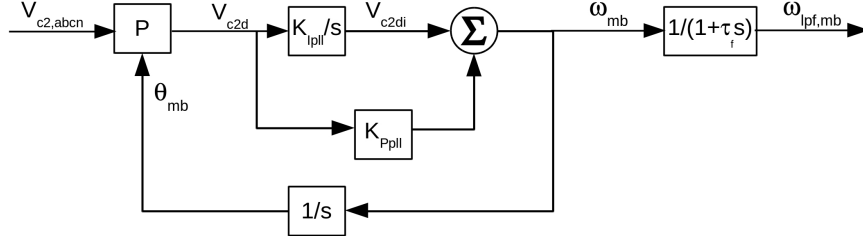
Figure 6.4: The phase–locked–loop (PLL) block diagram for extracting estimates of the micro–grid bus phase angle and frequency.

The estimated micro–grid bus voltage angle θ_{mb} first order equation is

$$\dot{\theta}_{mb} = v_{c2di} + K_{Ppll}\left(v_{c2d}\right) \tag{6.23}$$

The equation for the micro–grid bus filtered frequency signal $\omega_{lpf,mb}$ is

$$\dot{\omega}_{lpf,mb} = \frac{1}{\tau_f} v_{c2di} + \frac{K_{Ppll}}{\tau_f}\left(v_{c2d}\right) - \frac{1}{\tau_f}\left(\omega_{lpf,mb}\right) \tag{6.24}$$

6.2 Battery, Inverter and Energy Storage Device Primary Control Models

The energy storage battery, inverter, and primary control model block diagram is shown in Figure 6.6 on Page 87. In this section, model equations are presented, and the primary control is tuned.

Primary control for the energy storage device consists of an inner current feedback loop and an outer voltage feedback loop. The essence of the primary control strategy is to drive the filter capacitor q axis voltage magnitude to 1 [pu], and drive the d axis to 0 [V]. This is the equivalent of placing the energy storage voltage phasor $\mathbf{V_c}$ on the q axis as shown in Figure 6.5 on Page 84. Conceptually, the q axis is used to control voltage magnitude,
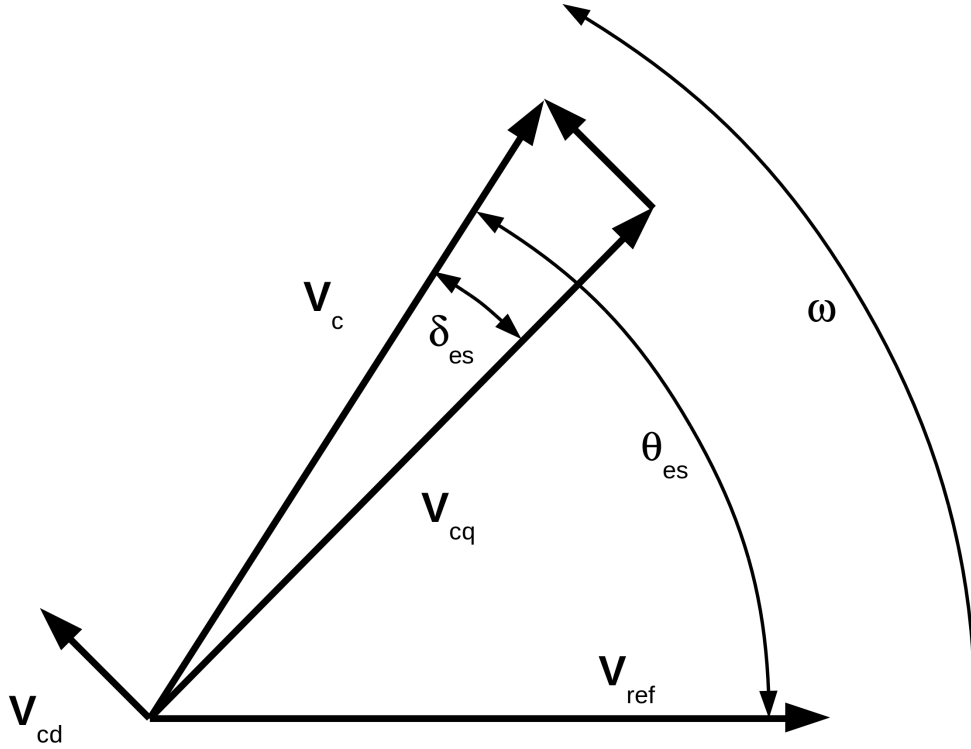
Figure 6.5: Energy storage filter capacitor voltage phasors and angular relationships. Primary control drives δ_{es} to zero so $|\boldsymbol{V_{cq}}| = |\boldsymbol{V_c}|$ and $|\boldsymbol{V_{cd}}| = \delta_{es}$

.

and the d axis is used to control the power angle across the energy storage filter inductor.

When δ_{es} is near to zero

$$\boldsymbol{V_{cq}} = \boldsymbol{V_c} \tag{6.25a}$$

$$|\boldsymbol{V_{cd}}| = \tan^{-1} \frac{|\boldsymbol{V_{cd}}|}{|\boldsymbol{V_{cq}}|} = \delta_{es}. \tag{6.25b}$$

6.2.1　Battery and Inverter

Writing the equations for inverter voltage on the d (6.26a) and q (6.26b) axes,

$$\dot{v}_{id} = \frac{v_{dc}}{\tau_{dc}} \left[v_{cd} + v_d^* - \frac{1}{v_{dc}} v_{id} \right] \tag{6.26a}$$

$$\dot{v}_{iq} = \frac{v_{dc}}{\tau_{dc}} \left[v_{cq} + v_q^* - \frac{1}{v_{dc}} v_{iq} \right]. \tag{6.26b}$$

6.2.2　Inner Current Feedback Loop

Describing the voltage commands for d (6.27a) and q (6.27b) axes,

$$v_d^* = k_{p3} i_{derr} + i_{derri} + i_{derrd} \tag{6.27a}$$

$$v_q^* = k_{p3} i_{qerr} + i_{qerri} + i_{qerrd}. \tag{6.27b}$$

The i_{derr} and i_{qerr} terms in (6.27) represent the d and q axes errors between current commands i_d^* and i_q^* and filter inductor currents i_{fd} and i_{fq} in the feedback loop:

$$i_{derr} = i_d^* - i_{fd} \tag{6.28a}$$

$$i_{qerr} = i_q^* - i_{fq}. \tag{6.28b}$$

Current commands i_d^* and i_q^* are defined in Section 6.2.3. The first right–hand terms in (6.27) are linearly dependent on other system states. The second right–hand terms in (6.27) represent integrator functions and may be written:

$$\dot{i}_{derri} = k_{i3} \left[i_d^* - i_{fd} \right] \tag{6.29a}$$

$$\dot{i}_{qerri} = k_{i3} \left[i_q^* - i_{fq} \right]. \tag{6.29b}$$

The third right–hand terms in (6.27) represent derivative functions and the equations are written:

$$\dot{i}_{derrd} = \frac{k_{d3}}{\tau_{d3}} \left[\dot{i}_{derr} - \frac{1}{\tau_{d3}} i_{derrd} \right] \tag{6.30a}$$

$$\dot{i}_{qerrd} = \frac{k_{d3}}{\tau_{d3}} \left[\dot{i}_{qerr} - \frac{1}{\tau_{d3}} i_{qerrd} \right]. \tag{6.30b}$$

6.2.3 Outer Voltage Feedback Loop

The equations for command values i_d^* and i_q^* for d (6.31a) and q (6.31b) axes are:

$$i_d^* = k_{p2} v_{derr} + v_{derri} + v_{derrd} \tag{6.31a}$$

$$i_q^* = k_{p2} v_{qerr} + v_{qerri} + v_{qerrd}. \tag{6.31b}$$

The v_{derr} and v_{qerr} terms in (6.31) represent the d and q axes errors between voltage commands v_d^{**} and v_q^{**} and filter capacitor voltages v_{cd} and v_{cq} in the feedback loop:

$$v_{derr} = v_d^{**} - v_{cd} \tag{6.32a}$$

$$v_{qerr} = v_q^{**} - v_{cq}. \tag{6.32b}$$

Voltage commands v_d^{**} and v_q^{**} are defined in Section 7.2. The first right–hand terms in (6.31) are linearly dependent on other system states. The second right–hand terms in (6.31) represent integrator functions and may be written:

$$\dot{v}_{derri} = k_{i2} \left[v_d^{**} - v_{cd} \right] \tag{6.33a}$$

$$\dot{v}_{qerri} = k_{i2} \left[v_q^{**} - v_{cq} \right]. \tag{6.33b}$$

86
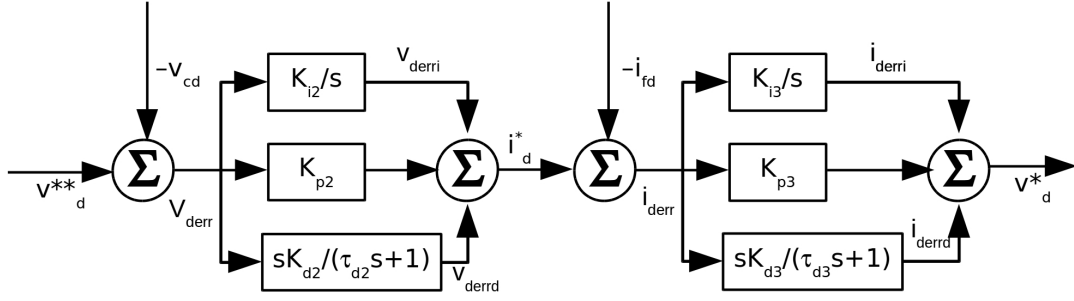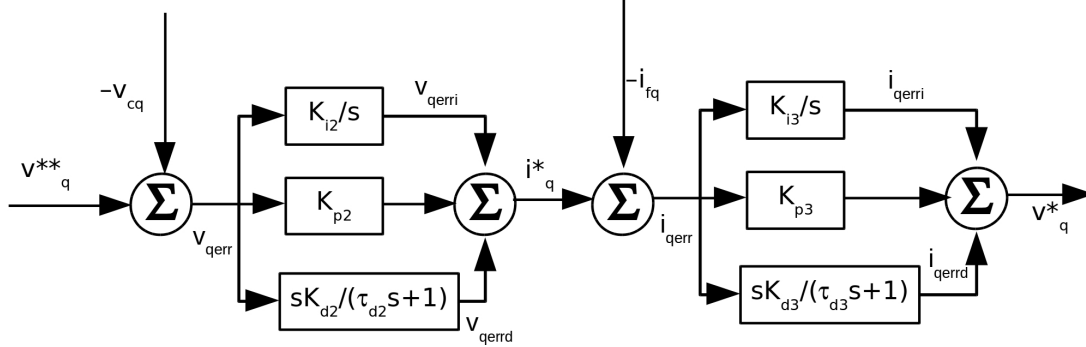
Figure 6.6: The energy storage device primary control block diagram.

The third right–hand terms in (6.31) represent derivative functions and the equations are written:

$$\dot{v}_{derrd} = \frac{k_{d2}}{\tau_{d2}} \left[\dot{v}_{derr} - \frac{1}{\tau_{d2}} v_{derrd} \right] \tag{6.34a}$$

$$\dot{v}_{derrd} = \frac{k_{d2}}{\tau_{d2}} \left[\dot{i}_{derr} - \frac{1}{\tau_{d2}} v_{qerrd} \right]. \tag{6.34b}$$

6.2.4   Controller Tuning

The primary control tuning was performed under the assumption that frequency remains stable and fixed at 1 [pu]. The approach taken is to tune each controller in succession, starting with the inner current feedback loop, and moving to the outer voltage feedback
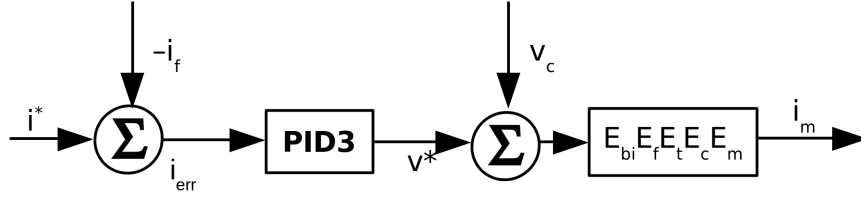
Figure 6.7: Inner current feedback loop simplified diagram for tuning PID3. E_{bi}, E_f, E_t, E_c, and E_m, represent the battery and inverter, LC filter, transformer, cable capacitor, and micro–grid RL load equations.

loop. Referring to Figure 6.7 on Page 88, the system model includes equations for the battery and inverter, LC filter, transformer, cable capacitance, and micro–grid RL load.

PID3 Tuning

In the same technique used in Section 5.6, an initial set of gains and co–located zeros were used to narrow the selection. Tuning was performed under full load conditions where $S_m = 100 + j75$ [kVA], then tested at light load. In the initial runs, zeros and poles were iterated through the following values:

$$z_{31} = z_{32} = \begin{bmatrix} 10 & 100 & 1000 & 10,000 \end{bmatrix}$$
$$kdd = \begin{bmatrix} 1000 & 2000 & 3000 \end{bmatrix}.$$

After careful inspection of the pole–zero constellations, the ranges were narrowed:

$$z_{31} = z_{32} = \begin{bmatrix} 1000 & 2000 & 3000 & 4000 & 5000 \end{bmatrix}$$
$$kdd3 = \begin{bmatrix} 5000 & 6000 & 7000 \end{bmatrix}$$

and more simulations performed. Based on the pole–zero constellations, and some iterations with PID2 tuning, the selected zero locations are at 3000, and k_{dd3} is chosen to be 7000.
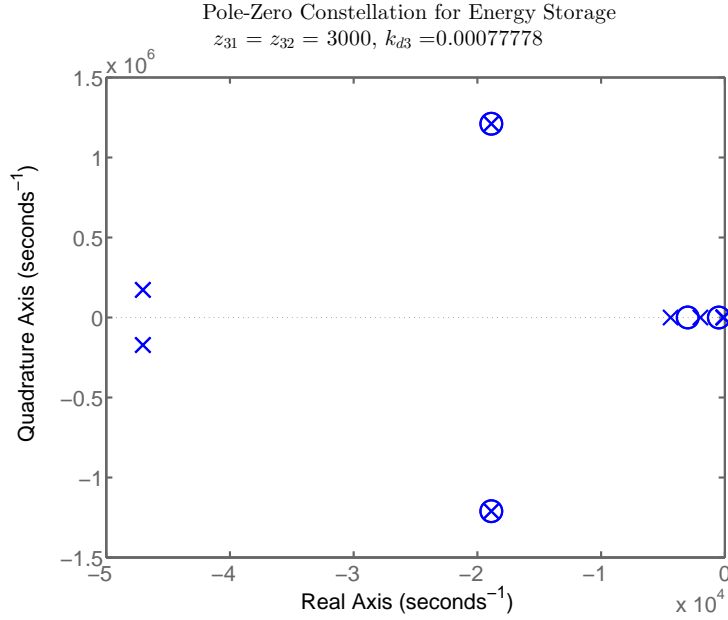
Figure 6.8: Pole–zero constellation for the system shown in Figure 6.7 at full load using gains specified in (6.35).

That translates to

$$k_{d3} = \frac{k_{dd3}}{z_{31}z_{32}} = \frac{7000}{3000^2} = 7.78 \times 10^{-6} \tag{6.35a}$$

$$k_{p3} = (z_{31} + z_{32})k_{d3} = 4.67 \tag{6.35b}$$

$$k_{i3} = z_{31}z_{32}k_{d3} = 7000. \tag{6.35c}$$

A wide view of the pole–zero constellation for full load conditions is shown in Figure 6.8 Page 89, and a view of the poles nearest the quadrature axis in Figure 6.9 on Page 90.

A light load condition where $S_m = 4 + j3$ [kVA] was also simulated with the resulting pole–zero constellation shown in Figure 6.10 on Page 91. Only the poles nearest the quadrature axis are shown. Notice the improvement in damping over the full–load case. In the full load case, the dominant poles are located at $-112 \pm j1630 \left[\frac{rad}{s}\right]$, indicate a damping ratio of 0.07, with overshoot at 81%. In the light–load case the poles move to $-237 \pm j274 \left[\frac{rad}{s}\right]$, the damping ratio is 0.65, and overshoot at 6.7%. With the additional of the next stage
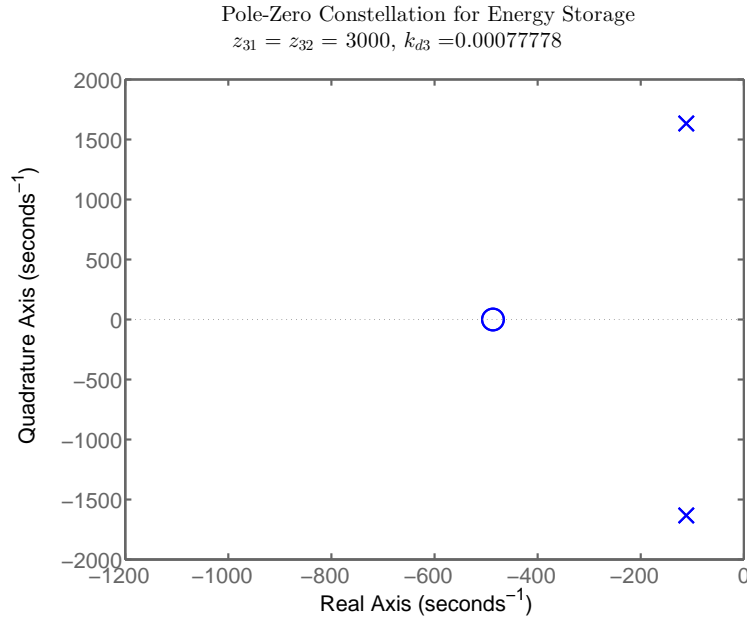
Figure 6.9: A view of the poles nearest to the quadrature axis for the pole–zero constellation for the system shown in Figure 6.7 at full load using gains specified in (6.35). The dominant poles are located at $-112 \pm j1630 \left[\frac{rad}{s} \right]$

PID controller, the control performance improves for both conditions.

PID2 Tuning

The tuning for PID2 as shown in Figure 6.11 on Page 91uses values for the PID3 gains specified in (6.35). For the voltage feedback outer loop, a set of zeros and gains were selected:

$$z_{21} = z_{22} = \begin{bmatrix} 3000 & 4000 & 5000 & 6000 & 7000 \end{bmatrix}$$

$$kdd2 = \begin{bmatrix} 5000 & 6000 & 7000 & 8000 \end{bmatrix}$$
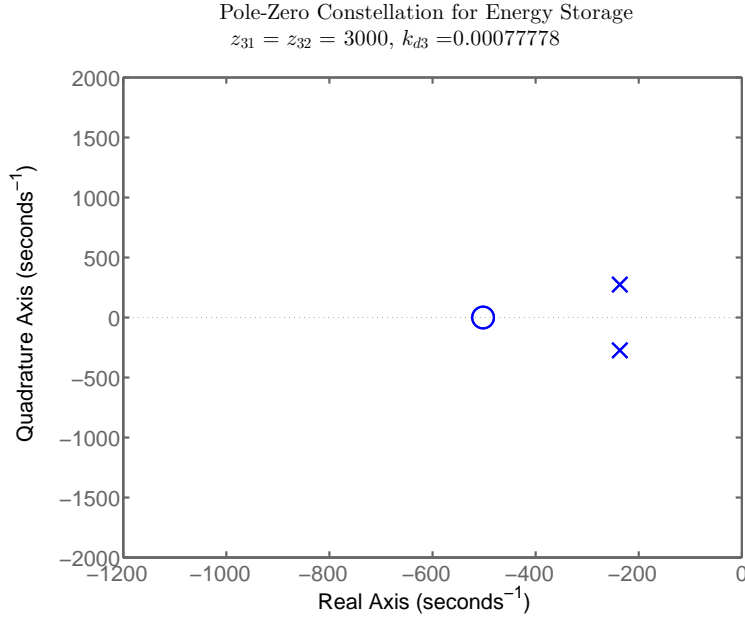
Figure 6.10: A view of the poles nearest to the quadrature axis for the pole–zero constellation for the system shown in Figure 6.7 at light load using gains specified in (6.35). Rightmost poles are located at $-237 \pm j274 \left[\frac{rad}{s}\right]$
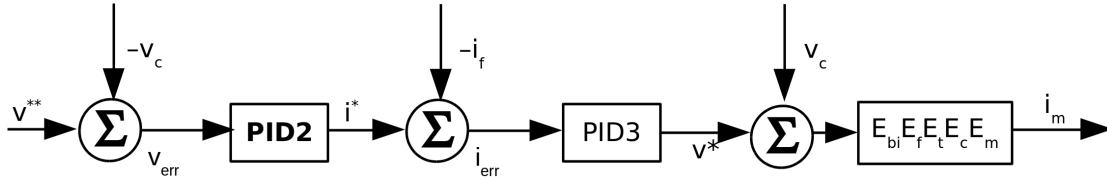
Figure 6.11: Outer voltage feedback loop simplified diagram for tuning PID2. E_{bi}, E_f, E_t, E_c, and E_m, represent the battery and inverter, LC filter, transformer, cable capacitor, and micro–grid RL load equations.

and simulations run to extract the pole–zero constellations. Careful examination of the data led to a tighter search window:

$$z_{21} = z_{22} = \begin{bmatrix} 2800 & 2900 & 3000 & 3100 & 3200 \end{bmatrix}$$

$$kdd2 = \begin{bmatrix} 6900 & 7000 & 7100 \end{bmatrix}.$$
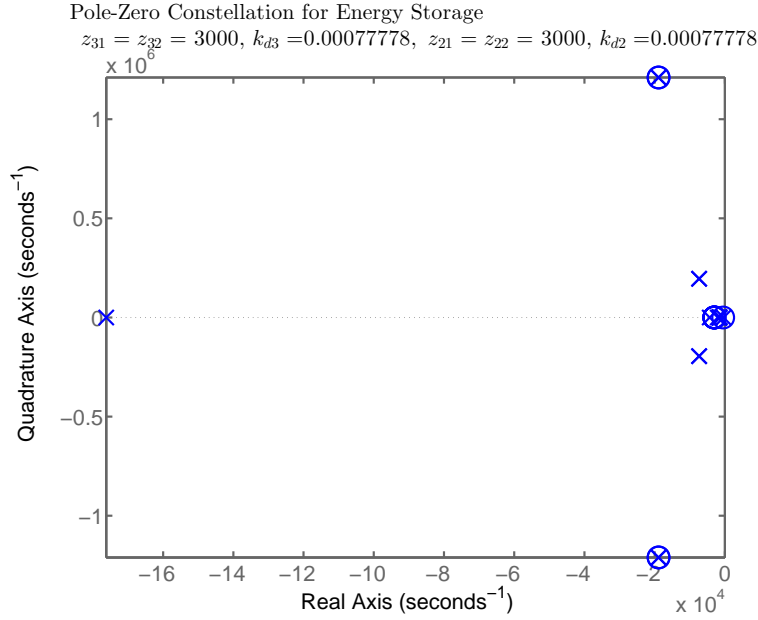
Figure 6.12: Pole–zero constellation for the system shown in Figure 6.11 at full load using gains specified in (6.36) and (6.35).

Based on the pole–zero constellations, the selected zero locations are at 3000, and k_{dd2} is chosen to be 7000. That translates to

$$k_{d2} = \frac{k_{dd2}}{z_{21}z_{22}} = \frac{7000}{3000^2} = 7.78 \times 10^{-6} \tag{6.36a}$$

$$k_{p2} = (z_{21} + z_{22})k_{d2} = 4.67 \tag{6.36b}$$

$$k_{i2} = z_{21}z_{22}k_{d2} = 7000. \tag{6.36c}$$

The pole–zero constellation for the gains specified in (6.35) and (6.36) under full load conditions where $S_m = 100 + j75$ [kVA] is shown in Figure 6.12 on Page 92. A closer lok at the poles nearest the quadrature axis is shown in Figure 6.13 on Page 93. The dominant pole location is on the real axis at $-369 \left[\frac{rad}{s}\right]$, has a damping ratio of 1 with 0% overshoot.

A light load condition where $S_m = 4 + j3$ [kVA] was also simulated with the resulting pole–zero constellation shown in Figure 6.14 on Page 94. Only the poles nearest the quadra- ture axis are shown. The dominant pole location is again on the real axis at $-495 \left[\frac{rad}{s}\right]$,
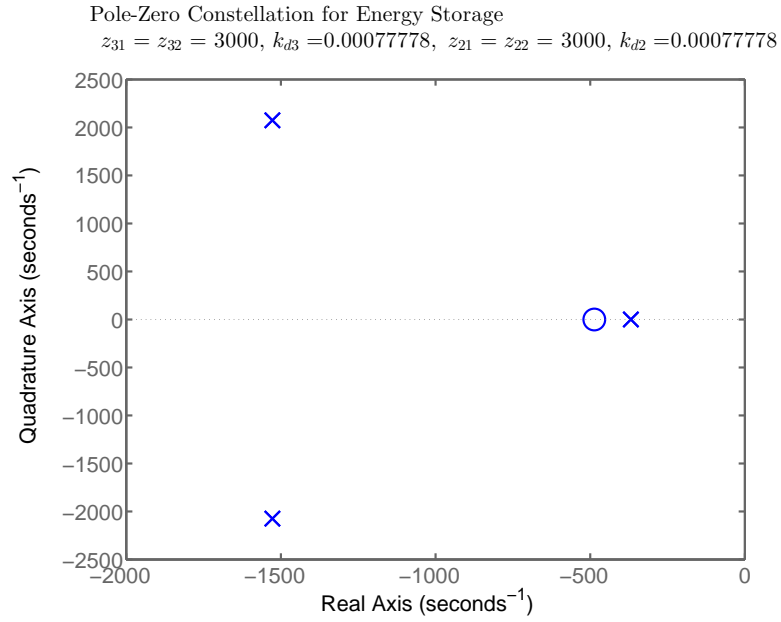
Figure 6.13: A view of the poles nearest to the quadrature axis for the pole–zero constellation for the system shown in Figure 6.11 at full load using gains specified in (6.36) and (6.35). The rightmost pole locations $-369 \pm j0.0 \left[\frac{rad}{s}\right]$

has a damping ratio of 1 with 0% overshoot.
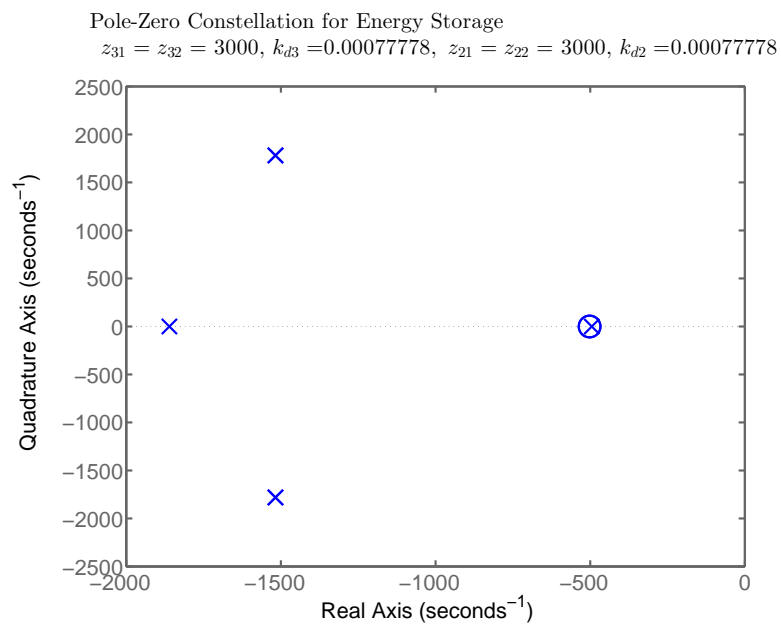
Figure 6.14: A view of the poles nearest to the quadrature axis for the pole–zero constellation for the system shown in Figure 6.11 at light load using gains specified in (6.36) and (6.35). The dominant pole location is on the real axis at $-495 \left[\frac{rad}{s} \right]$

Chapter 7

Formulation of Voltage and Frequency Control

Secondary control for the synchronous machine and energy storage device has four competing objectives: active power, frequency, reactive power, and voltage. The high level system block diagram is shown in Figure 7.3 on Page 99. Primary control comes with the equipment, but the secondary control would come in the form of external architecture and sensing equipment. The theory of operation is that an error between micro–grid active power and active power set–points will bias the frequency command signals sent to the generator and energy storage device primary control system in a manner to compensate for the error. The active power error is weighted relative to the frequency control signal.

Similarly an error between micro–grid reactive power and reactive power set–points will bias the voltage command signals sent to the generator and energy storage device primary control system in a manner to compensate for the error. The reactive power error is weighted relative to the voltage control signal.

Because the model equations are written in the rotating dq reference frame, there is a need to extract a frequency signal based on the changing angular relationship between the d and q axis voltage vectors. In the design of the primary controls for the energy storage device in Section 6.2, phasors for the energy storage filter capacitor voltage are shown in Figure 6.5 on Page 84. The angle θ_{es} represents the instantaneous value of the voltage angle. Using the filter capacitor voltage as an example, but without loss of application to other locations, the equation form for θ_{es} is

$$\theta_{es} = \int_0^T \omega dt + \delta_{es}. \tag{7.1}$$

Taking the derivative of both sides in (7.1) yields

$$\frac{d\theta_{es}}{dt} = \omega + \frac{d\delta_{es}}{dt}. \tag{7.2}$$

Recognizing that $\delta_{es} = \tan^{-1} \frac{v_{cd}}{v_{cq}}$ and under the presumption the command frequency for the energy storage device is 1 [pu], (7.2) may be written

$$\omega_{es} = 1 + \frac{1}{2\pi f} \frac{d\left(\tan^{-1} \frac{v_{cd}}{v_{cq}}\right)}{dt}. \tag{7.3}$$

The proposed implementation for the derivative term in this dissertation is a band–pass filter realization. A transfer function of the form

$$H_d(s) = \frac{s}{0.01s + 1} \tag{7.4}$$

is combined with a low pass filter

$$H_{lp}(s) = \frac{1}{0.05s + 1} \tag{7.5}$$

to form the composite transfer function

$$H_c(s) = \frac{s}{0.0005s^2 + 0.06s + 1}. \tag{7.6}$$

The Bode plot for the composite is shown in Figure 7.1 on Page 97, and a simulation of the response to a ramp input shown in Figure 7.2 on Page 98.

A representation of the generator system is shown in Figure 7.4 on Page 100, and shows equations used to model the generator and secondary control system. For more detail on the generator matrices see Section 5.1. The AC8B regulator equations are not listed explicitly, please refer to Section 5.3.

Similarly, the energy storage device is illustrated in Figure 7.5 on Page 101. In the dia-
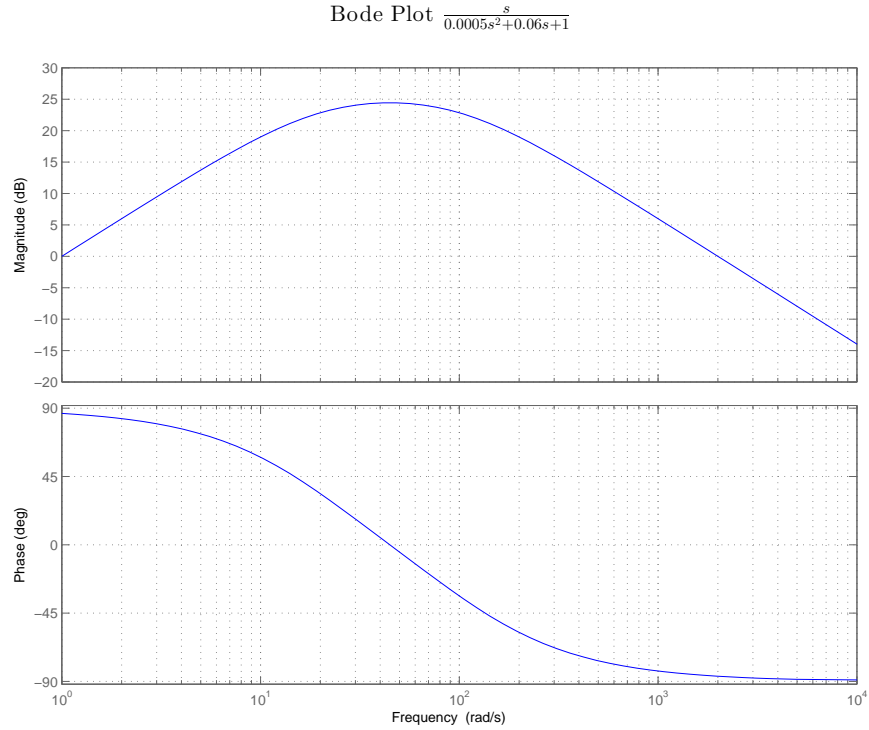
Figure 7.1: Bode plot for the derivative function described by (7.6).

grams for both systems, frequency domain representations are used for the PID controllers.

The secondary control block diagrams for the generator are shown in Figure 7.6 on Page 102, and the energy storage in Figure 7.7 on Page 103. For active and reactive power control vectors, the devices are assigned user selected participation factors as defined in Table 8.6. The participation factor compensates for differences between power commands and loads, adding or subtracting from the device power set–points. Each device responds to active and reactive power deviations according to the relative magnitude of its participation and weighting factors.

Referring to Figure 7.7 on Page 103, $f_{p,es}$ represents the energy storage device participation factor for active power and $f_{p,tot}$ represents the sum of all active power participation factors for power sources presently on line. $P_{ref,tot}$ is the sum of active power reference points for power sources, and P_{tot} is the sum of active power being delivered by all power

97
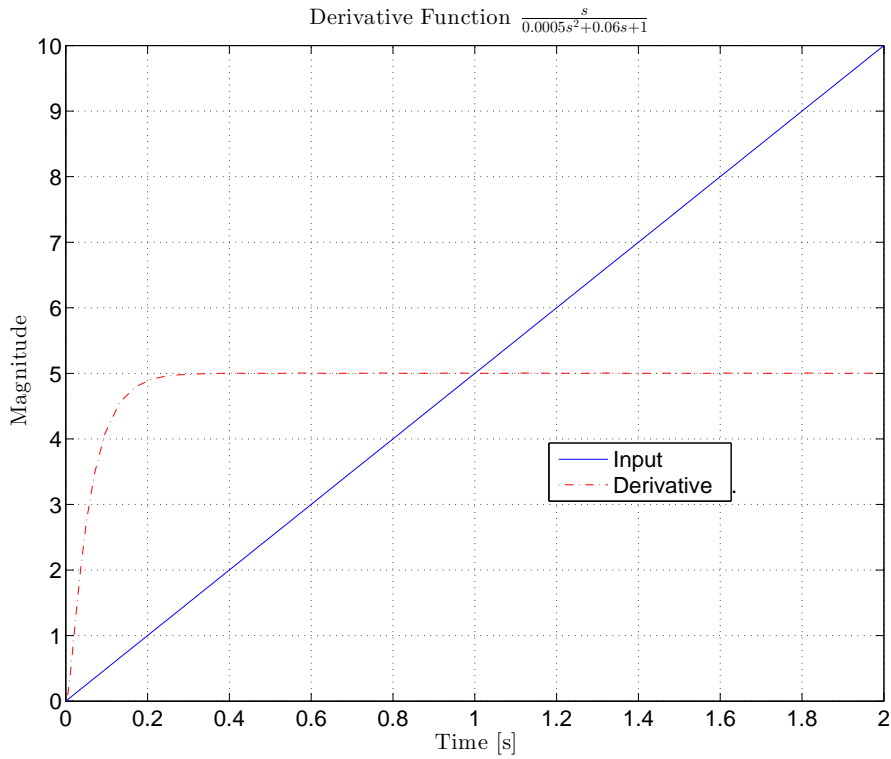
Figure 7.2: A simulation of the response to a ramp input for the derivative function described by (7.6).

sources. $P_{ref,es}$ is the active power reference for the energy storage device, and P_{es} is the active power supplied by the energy storage device. Similarly, in Figure 7.6 on Page 102, $f_{p,g1}$ represents the generator participation factor for active power, $P_{ref,g1}$ is the active power reference for the generator, and P_{g1} is the active power supplied by the generator. P_{tot}, $P_{ref,tot}$, and $f_{tot,p}$ are defined above. For example, say the following conditions exist on the micro–grid with an energy storage device and a generator on line:

- $f_{p,es}$ = 100

- $f_{p,g1}$ = 50

- $P_{ref,es}$ = 50 [kW]

- $P_{ref,g1}$ = 10 [kW]

98
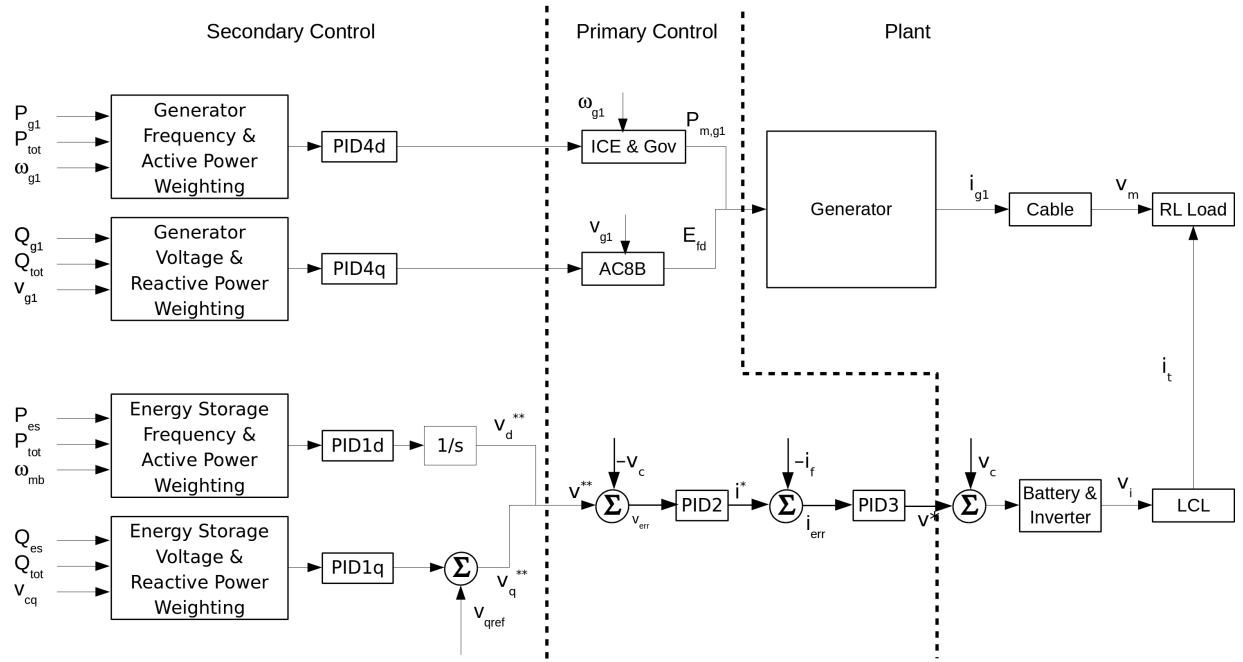
Figure 7.3: High level system diagram showing the demarcations between secondary and primary control stages, and between primary control and plant.

- P_{es} = 70 [kW]

- P_{g1} = 14 [kW]

Then

- $f_{p,tot}$ = 150

- $P_{ref,tot}$ = 50 + 10 = 60 [kW]

- P_{tot} = 70 + 14 = 84 [kW]

- $P_{err,tot}$ = 60 − 84 = −24 [kW]

- $P_{comp,es}$ = −24 * $\frac{100}{150}$ = −16 [kW]

- $P_{comp,g1}$ = −24 * $\frac{50}{150}$ = −8 [kW]

- P_{es}^{*} = 50 − 70 − (−16) = −4 [kW]

- P_{g1}^{*} = 10 − 14 − (−8) = 4 [kW]

99
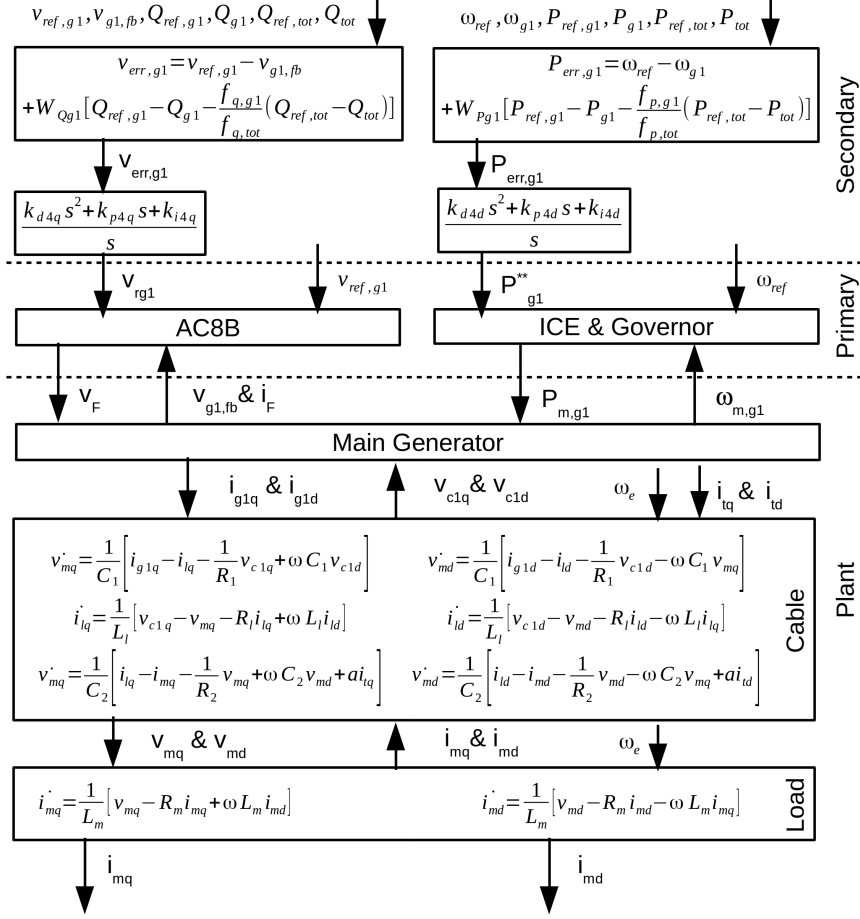
Figure 7.4: Generator plant and control systems block diagram showing model equations. For more on the generator matrices see Section 5.1, for the AC8B regulator equations see Section 5.3.

suggesting the energy storage device should decrease active power output by 4 [kW] and the generator should increase active power output by 4 [kW].

Tertiary control is anticipated using economic commitment and dispatch, but is out of scope for this dissertation.

7.1 Synchronous Machine

Equations for the synchronous machine secondary control are developed, and the controller is tuned in this section.

$v_{ref,es}, v_{mq}, Q_{ref,es}, Q_{es}, Q_{ref,tot}, Q_{tot}$

$$Q_{err,es} = v_{ref,es} - v_{mq}$$
$$+ W_{Qes}\left[Q_{ref,es} - Q_{es} - \frac{f_{q,es}}{f_{q,tot}}\left(Q_{ref,tot} - Q_{tot}\right)\right]$$

$\omega_{ref}, \omega_{mb}, P_{ref,es}, P_{es}, P_{ref,tot}, P_{tot}$

$$P_{err,es} = \omega_{ref} - \omega_{mb}$$
$$+ W_{Pes}\left[P_{ref,es} - P_{es} - \frac{f_{p,es}}{f_{p,tot}}\left(P_{ref,tot} - P_{tot}\right)\right]$$

$Q_{err,es}$: $\dfrac{k_{d1q}s^2 + k_{p1q}s + k_{i1q}}{s}$

$P_{err,es}$, dv_d^{**} : $\dfrac{k_{d1d}s^2 + k_{p1d}s + k_{i1d}}{s}$ $\rightarrow$ $v_d^{**} = dv_d^{**}$

Secondary

Q_{adj} , $v_{ref,es}, v_{cq}$: $\dfrac{k_{d2}s^2 + k_{p2}s + k_{i2}}{s}$

v_d^{**} , v_{cd} : $\dfrac{k_{d2}s^2 + k_{p2}s + k_{i2}}{s}$

Primary

i_q^* , i_{fq} : $\dfrac{k_{d3}s^2 + k_{p3}s + k_{i3}}{s}$

i_{fd} , i_d^* : $\dfrac{k_{d3}s^2 + k_{p3}s + k_{i3}}{s}$

v_q^* , v_d^*

$$\dot{v}_{iq} = \frac{v_{dc}}{\tau_{dc}}\left[v_{cq} + v_q^* - \frac{1}{v_{dc}}v_{iq}\right]$$

$$\dot{v}_{id} = \frac{v_{dc}}{\tau_{dc}}\left[v_{cd} + v_d^* - \frac{1}{v_{dc}}v_{id}\right]$$

Battery & Inverter

V_{iq} , V_{cq} , V_{id} , V_{cd}

$$\dot{i}_{fq} = \frac{1}{L_f}\left[v_{iq} - a v_{mq} - R_t i_{tq} + \omega L_t i_{td}\right]$$
$$\dot{v}_{cq} = \frac{1}{C_f}\left[i_{fq} - i_{tq} + \omega C_f v_{cd}\right]$$
$$\dot{i}_{tq} = \frac{1}{L_t}\left[v_{cq} - a v_{mq} - R_t i_{tq} + \omega L_t i_{td}\right]$$

$$\dot{i}_{fd} = \frac{1}{L_f}\left[v_{id} - a v_{md} - R_t i_{td} - \omega L_t i_{tq}\right]$$
$$\dot{v}_{cd} = \frac{1}{C_f}\left[i_{fd} - i_{td} - \omega C_f v_{cq}\right]$$
$$\dot{i}_{td} = \frac{1}{L_t}\left[v_{cd} - a v_{md} - R_t i_{td} - \omega L_t i_{tq}\right]$$

Plant — LC Filter & Transformer

i_{tq} , v_{mq} , i_{td} , v_{md}

Figure 7.5: Energy storage system plant and control systems model equations.

7.1.1 Equation Development

Referring to Figure 7.6 on Page 102, the equations for active power P_{g1}^{**} and voltage $v_{r,g1}$ command values for the generator are

$$P_{g1}^{**} = k_{p4}P_{err,g1} + P_{erri,g1} + P_{errd,g1} \tag{7.7a}$$

$$v_{r,g1} = k_{p4}v_{err,g1} + v_{erri,g1} + v_{errd,g1}. \tag{7.7b}$$
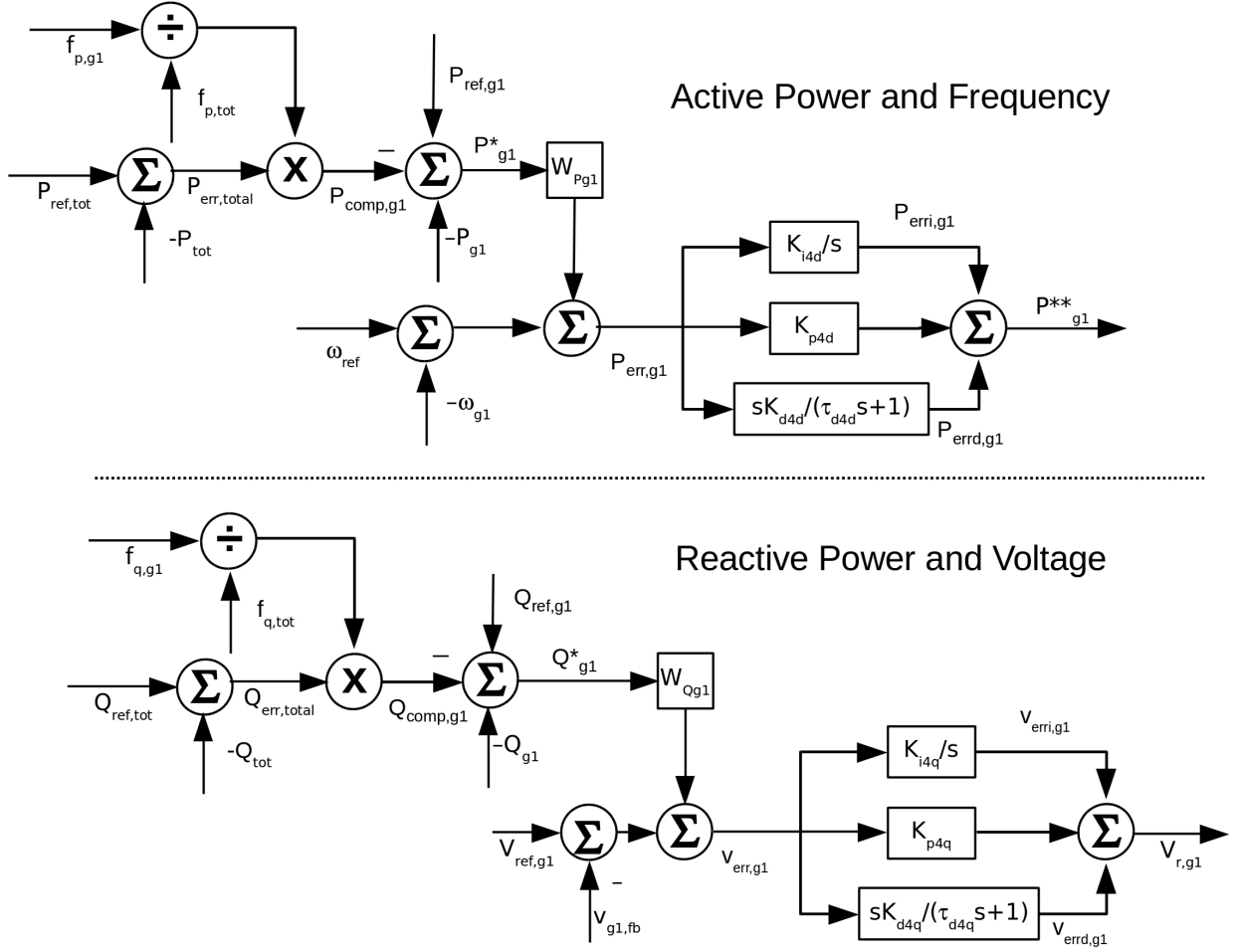
Figure 7.6: The generator secondary control block diagram.

The $P_{err,g1}$ and $v_{err,g1}$ terms in (7.7) represent the power and voltage errors and are written:

$$P_{err,g1} = \omega_{ref} - \omega_{g1}$$
$$+ W_{Pg1}\left[P_{ref,g1} - P_{g1} - \frac{f_{p,g1}}{f_{p,tot}}\left(P_{ref,tot} - P_{tot} \right) \right] \tag{7.8a}$$

$$v_{err,g1} = v_{ref,g1} - v_{g1,fb}$$
$$+ W_{Qg1}\left[Q_{ref,g1} - Q_{g1} - \frac{f_{q,g1}}{f_{q,tot}}\left(Q_{ref,tot} - Q_{tot} \right) \right] \tag{7.8b}$$

where

- ω_{ref} is the reference frequency,
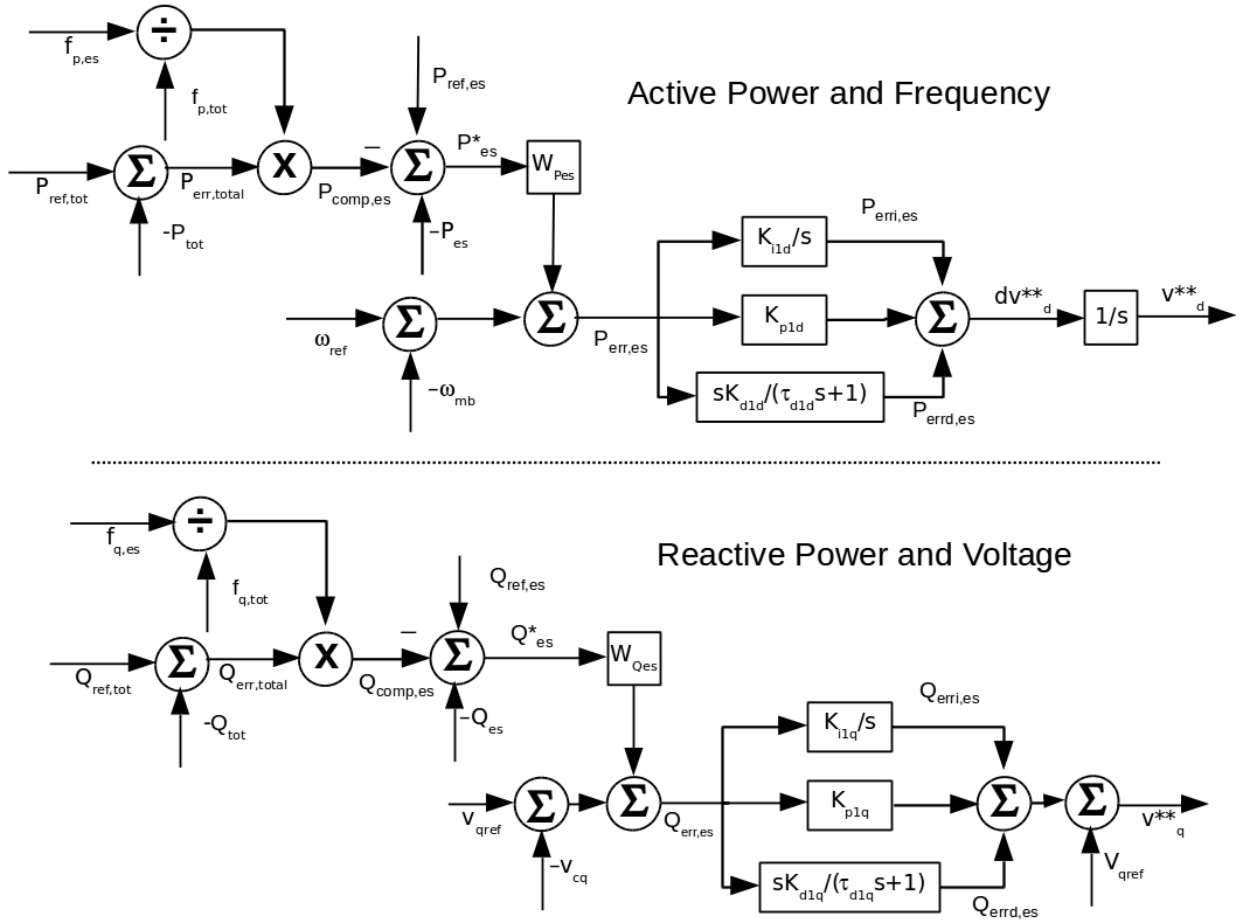
Figure 7.7: The energy storage device secondary control block diagram.

- ω_{g1} is generator 1 angular velocity,

- $P_{ref,g1}$ is the reference active power for generator 1,

- P_{g1} is measured generator active power,

- $P_{ref,tot}$ is the sum of active power references for all dispatchable devices,

- P_{tot} is the measured active power for the load,

- v_{ref} is generator 1 reference voltage,

- $v_{g1,fb}$ is the measured generator terminal voltage,

- $Q_{ref,g1}$ is the reference reactive power for generator 1,

103

- Q_{g1} is measured generator reactive power,

- $Q_{ref,tot}$ is the sum of reactive power references for all dispatchable devices, and

- Q_{tot} is the measured reactive power for the load.

The first right–hand terms in (7.8) are linearly dependent on other system states. The second right–hand terms in (7.8) represent integrator functions and may be written:

$$\dot{P}_{erri,g1} = k_{i4} P_{err,g1} \tag{7.9a}$$

$$\dot{v}_{erri,g1} = k_{i4} v_{err,g1}. \tag{7.9b}$$

The third right–hand terms in (7.8) represent derivative functions and the equations are written:

$$\dot{P}_{errd} = \frac{k_{d4}}{\tau_{d4}} \left[\dot{P}_{err} - \frac{1}{\tau_{d4}} P_{errd} \right] \tag{7.10a}$$

$$\dot{v}_{errd} = \frac{k_{d4}}{\tau_{d4}} \left[\dot{v}_{err} - \frac{1}{\tau_{d4}} v_{errd} \right]. \tag{7.10b}$$

7.1.2 PID4 Tuning

For micro–grid applications, the energy storage device is paired with a Kohler REZG40 generator set with parameters listed in Table A3 on Page 152. The generator is connected to the micro–grid bus using 150 [feet] of #2 [AWG] cable with parameters listed in Table A5 on Page 153. It is notable that for this cable, the ratio X/R = 0.167, implying that AC power flow is driven less by angular difference and more by voltage difference than is normally assumed for AC systems.

Tuning the generator secondary control picks up from the end of Section 5.6. A similar approach is taken: given the AC8B parameters determined in Section 5.6, three zero locations and five values for k_d are used in simulations for the secondary control PID gains.

Pole–zero constellations are examined and zero locations selected. The gain is tuned, and the system simulated. This process is iterated until system performance is satisfactory.

Of note is there are separate zeros and gains for the q and d axes leading to distinct sets of proportional, integral and derivative gains for each axis. From the iterative process, gains for the q axis are

$$k_{d4q} = 0.2,$$

$$k_{p4q} = 4.0, \quad \text{and}$$

$$k_{i4q} = 20,$$

and for the d axis

$$k_{d4d} = 1.0,$$

$$k_{p4d} = 20., \quad \text{and}$$

$$k_{i4d} = 100.$$

The pole–zero constellation using the selected gains is shown in Figures 7.8 and 7.9 on Pages 106 and 107. Figure 7.9 shows the three right–most poles illustrated in Figure 7.8.

To validate the selection, a simulation is performed where the load is initially very light, and then a step load change occurs. Sample simulation data are shown in Figures 7.10 and 7.11 on Pages 108 and 109. Figure 7.10 indicates the generator terminal voltage and power response to a change in load occurring at t = 25 [s]. The initial loading is 1.6 + j1.2 [kVA], stepped to 39 + j29 [kVA]. The settling time is dictated by the rightmost pole located at $-0.692 \left[\frac{rad}{s} \right]$, corresponding to a frequency of about 0.11 [Hz]. This response is attributed to the field winding which has a high inductance but low resistance, resulting in a large $\frac{L}{R}$ time constant. In Figure 7.11, the voltage on the q axis is shown with a time scale from 24.9999 [s] to 25.0002 [s] to illustrate ringing near 125 [kHz]. The poles responsible for this

Pole-Zero Constellation for Grid Connected Kohler Generator Plus Secondary Contr

$z_{41d} = z_{42d} = 10,\ k_{d4d} = 1,\ z_{41q} = z_{42q} = 10,\ k_{d4q} = 0.2$
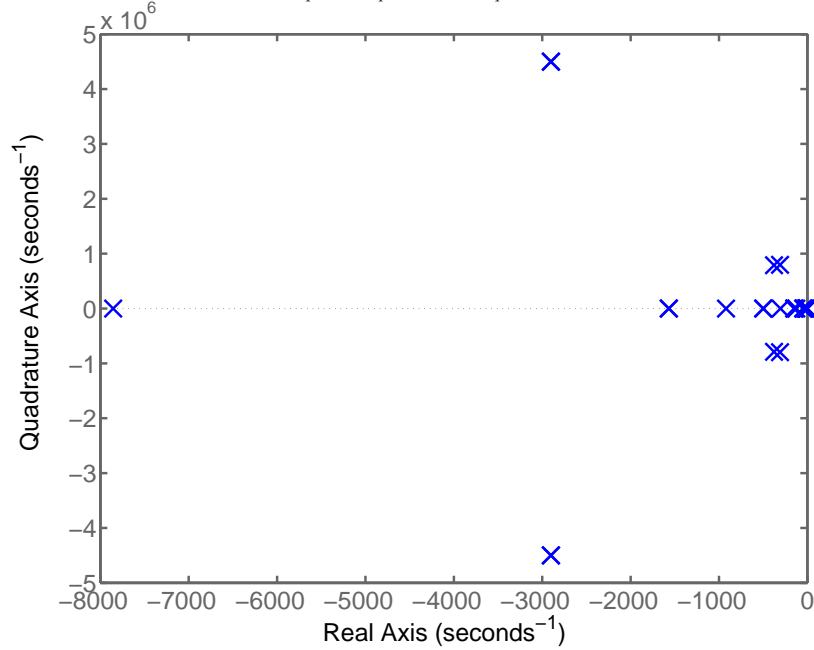
Figure 7.8: Final PID tuning run for the generator secondary control – complete constellation.

ringing are shown in Figure 7.12 on Page 110, the ringing frequency being

$$f_r = \frac{7.89 \times 10^5 \left[\frac{rad}{s}\right]}{2\pi} = 126\,[kHz].$$

7.2 Energy Storage

The equations for the energy storage device secondary control are developed and PID tuning is outlined in this section.
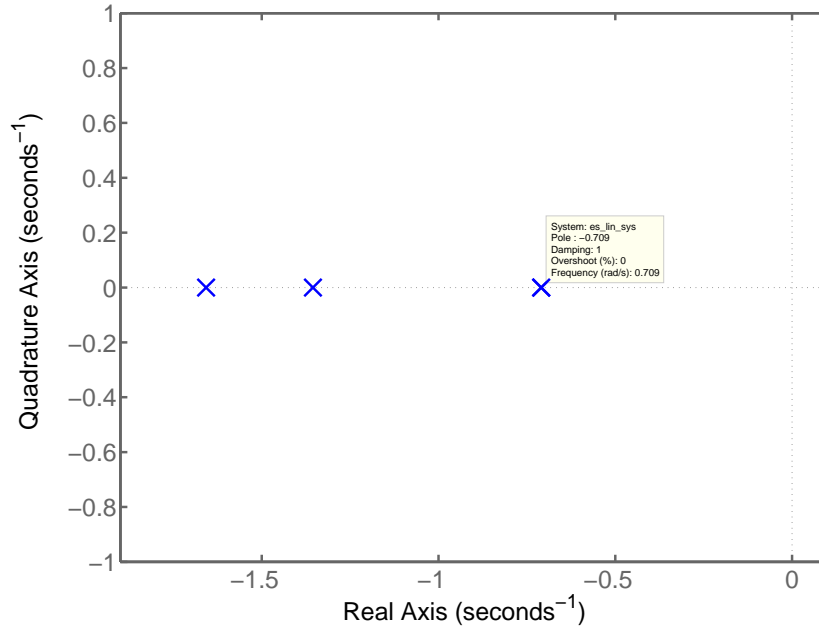
Figure 7.9: Final PID tuning run for the generator secondary control – rightmost poles only.

7.2.1 Equation Development

The equations for d axis $\dot{v}_d^{**}$ and q axis v_q^{**} voltage command values for the energy storage device are:

$$\dot{v}_d^{**} = k_{p1d}P_{err,es} + P_{erri,es} + P_{errd,es} \tag{7.11a}$$

$$v_q^{**} = k_{p1q}Q_{err,es} + Q_{erri,es} + Q_{errd,es}. \tag{7.11b}$$
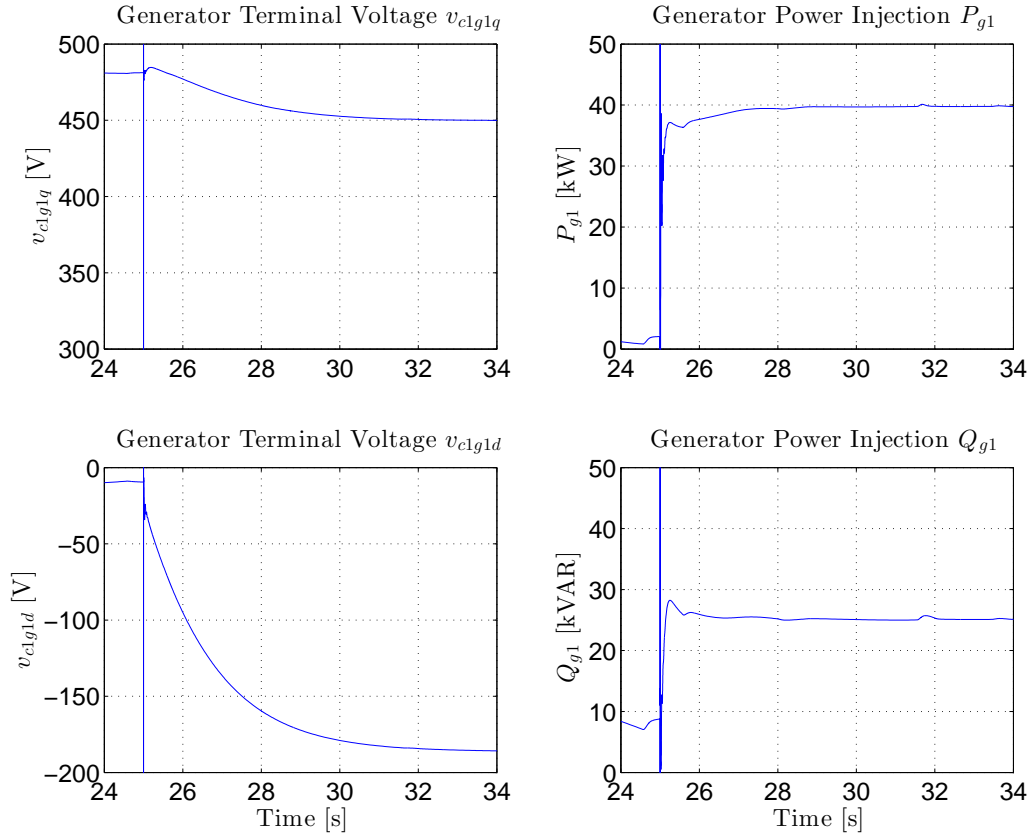
Figure 7.10: Simulation data for Kohler generator with grid connection. A step change in load is initiated at t = 25 [s].

The $P_{err,es}$ and $Q_{err,es}$ terms in (7.11) represent the power and voltage errors and are written:

$$P_{err,es} = \omega_{ref} - \omega_{mb}$$
$$+ W_{Pes} \left[P_{ref,es} - P_{es} - \frac{f_{p,es}}{f_{p,tot}} \left(P_{ref,tot} - P_{tot} \right) \right] \tag{7.12a}$$

$$Q_{err,es} = v_{qref,es} - v_{cq}$$
$$+ W_{Qes} \left[Q_{ref,es} - Q_{es} - \frac{f_{q,es}}{f_{q,tot}} \left(Q_{ref,tot} - Q_{tot} \right) \right] \tag{7.12b}$$

where

- ω_{ref} is the reference frequency,

108
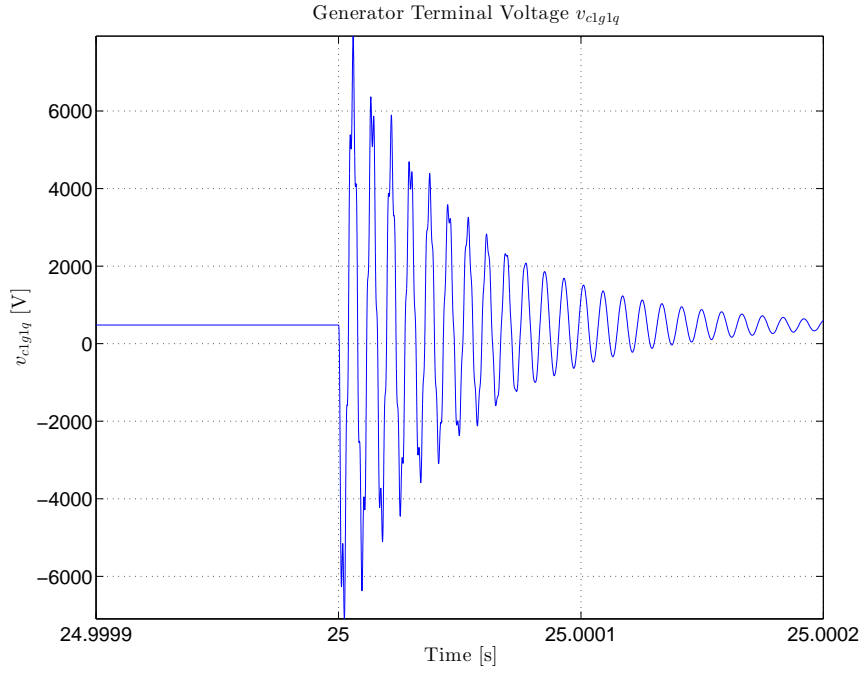
Figure 7.11: High frequency due to lumped parameter π cable model. Despite low cable $\frac{X}{R}$ ratio, the cable end capacitors resonate with generator and transformer inductances.

- ω_{mb} is the measured frequency at the micro–grid bus,

- $P_{ref,es}$ is the reference active power for the energy storage device,

- P_{es} is measured energy storage device active power,

- $P_{ref,tot}$ is the sum of active power references for all dispatchable devices,

- P_{tot} is the measured active power for the load,

- v_{qref} is energy storage device reference voltage,

- v_{cq} is the q axis filter capacitor terminal voltage,

- $Q_{ref,es}$ is the reference reactive power for the energy storage device,

- Q_{es} is measured the energy storage device reactive power,

- $Q_{ref,tot}$ is the sum of reactive power references for all dispatchable devices, and

109
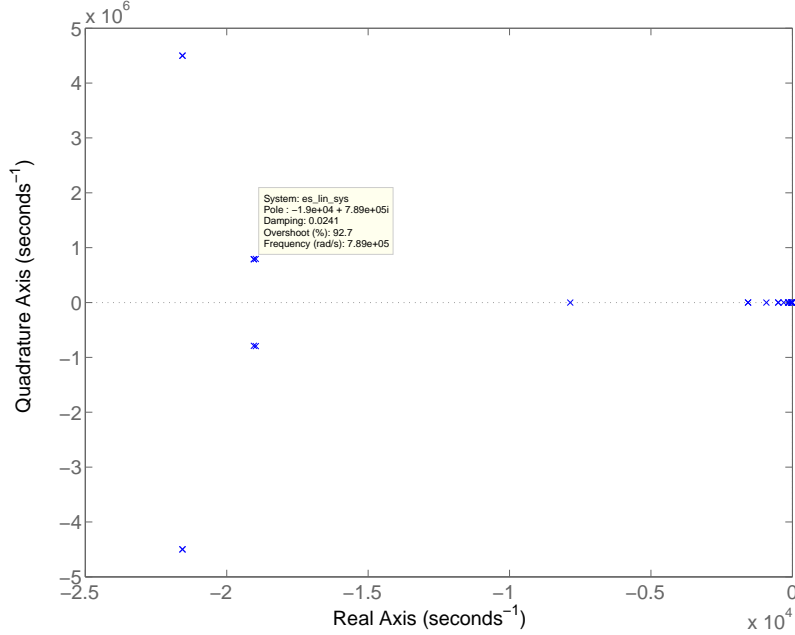
Figure 7.12: High frequency due to lumped parameter π cable model. Despite low cable $\frac{X}{R}$ ratio, the cable end capacitors resonate with generator and transformer inductances.

- Q_{tot} is the measured reactive power for the load.

The first right–hand terms in (7.11) are linearly dependent on other system states. The second right–hand terms in (7.11) represent integrator functions and may be written:

$$\dot{P}_{erri,es} = k_{i1d}P_{err,es} \tag{7.13a}$$

$$\dot{Q}_{erri,es} = k_{i1q}Q_{err,es}. \tag{7.13b}$$

The third right–hand terms in (7.11) represent derivative functions and the equations are written:

$$\dot{P}_{errd,es} = \frac{k_{d1d}}{\tau_{d1d}}\left[\dot{P}_{err,es} - \frac{1}{\tau_{d1d}}P_{errd,es}\right] \tag{7.14a}$$

$$\dot{Q}_{errd,es} = \frac{k_{d1q}}{\tau_{d1q}}\left[\dot{Q}_{err,es} - \frac{1}{\tau_{d1q}}Q_{errd,es}\right]. \tag{7.14b}$$

The command $P_{es}*$ ($Q_{es}*$) from the first stage described above amplified is by a relative weight W_{Pes} (W_{Qes}) and added to the frequency (voltage) error to produce a command $P_{err,es}$ ($Q_{err,es}$). $P_{err,es}$ is amplified by proportion and integral control gains to produce the derivative of the d axis voltage reference dv_d**. A pure integrator produces the d axis voltage command v_d**. For implementation, the firing angle for the PWM or vector control scheme would include the reference frequency ω_{ref} as an input to the final integrator.

$Q_{err,es}$ is amplified by proportional and integral control gains then added to the energy storage q axis voltage reference (v_{qref}) to arrive at a voltage command v_q**.

The d and q axis voltage commands v_d** and v_q** are fed directly to the inverter primary control as set points. The control block diagrams are shown in Figure 7.7 on Page 103.

Secondary generator control is accomplished in a manner similar to secondary energy storage control. Referring to Figure 7.6 on Page 102, $P*_{g1}$ ($Q*_{g1}$) is amplified by a weighting factor W_{Pg1} (W_{Qg1}) and added to the frequency (voltage) error to generate a signal $P_{err,g1}$ ($v_{err,g1}$). Proportional and integral control gains are applied to $P_{err,g1}$ and $v_{err,g1}$ to arrive at the prime mover control input command for active power $P_{g1}**$ and generator primary control input command for voltage $v_{r,g1}$.

Picking up the first order non–linear equation development for the energy storage device from the end of Section 6.2, assuming one generator, one energy storage device, and a collection of loads, the equation for dv_d** is written

$$\dot{v}_d^{**} = P_{erri,es} + K_{P1} \left\{ (\omega_{ref} - \omega_{lpf,mb}) + W_{Pes} \left[P_{ref,es} - P_{es} - \frac{f_{p,es}}{f_{tot}} (P_{ref,tot} - P_{tot}) \right] \right\} \quad (7.15)$$

where

- ω_{ref} is the reference frequency,

- $P_{erri,es}$ is the integrated value of $P_{err,es}$ described above,

- P_{es} is the active power output of the energy storage device,

111

- $f_{p,es}$ is the energy storage device active power participation factor,

- $f_{p,tot}$ is the sum of $f_{p,es}$ and $f_{p,g1}$,

- $f_{p,g1}$ is the generator active power participation factor, and

- $W_{p,es}$ is the energy storage device active power weighting factor.

7.2.2 PID1 Tuning

As in Section 7.1.2, PID1 has separate gains for the q and d axes. Tuning PID1 was performed while the energy storage device was interconnected with the generator and other micro–grid components. After some unstable initial attempts, the set of zeros and gains attempted for this stage were

$$z_{11q} = z_{12q} = z_{11d} = z_{12d} = \begin{bmatrix} 100 & 200 \end{bmatrix}$$

$$kdd1q = \begin{bmatrix} 0.5 & 1.0 & 1.5 & 2.0 \end{bmatrix}$$

$$kdd1d = \begin{bmatrix} 5 & 10 & 15 & 20 \end{bmatrix}.$$

Final values selected are $z_{11q} = z_{12q} = z_{11d} = z_{12d} = 200 \left[\frac{rad}{s} \right]$, $kdd1q = 1$, and $kdd1d = 10$. Or

$$k_{d1q} = \frac{k_{dd1q}}{z_{11q}z_{12q}} = \frac{1}{200^2} = 25 \times 10^{-6} \tag{7.16a}$$

$$k_{d1d} = \frac{k_{dd1d}}{z_{11d}z_{12d}} = \frac{10}{200^2} = 250 \times 10^{-6} \tag{7.16b}$$

$$k_{p1q} = (z_{11q} + z_{12q})k_{d1q} = 10 \times 10^{-3} \tag{7.16c}$$

$$k_{p1d} = (z_{11d} + z_{12d})k_{d1d} = 100 \times 10^{-3} \tag{7.16d}$$

$$k_{i1q} = z_{11q}z_{12q}k_{d1q} = 1.0 \tag{7.16e}$$

$$k_{i1d} = z_{11d}z_{12d}k_{d1d} = 10. \tag{7.16f}$$

Pole–zero constellations for the full load case are shown in Figures 7.13 and 7.14 on
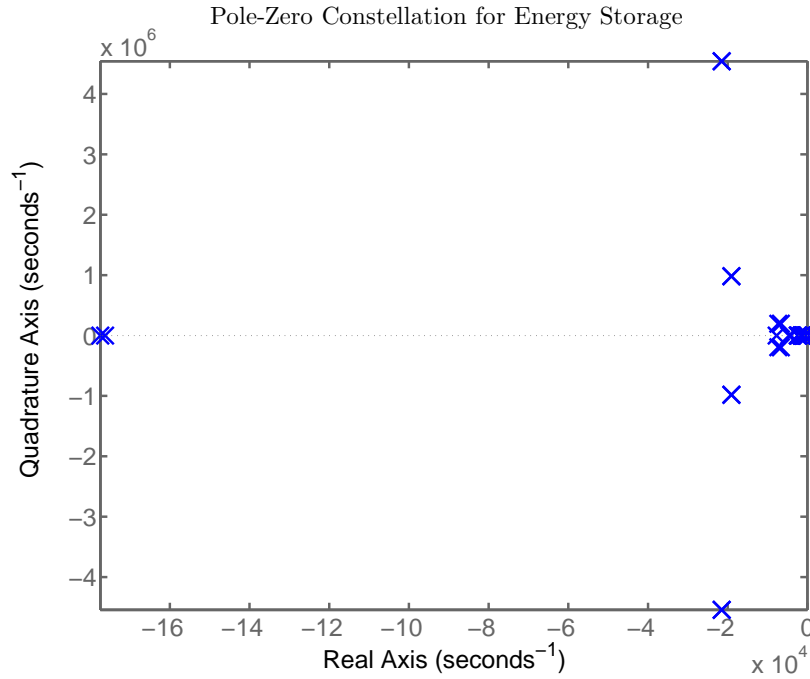
Figure 7.13: Final PID tuning run for the energy storage secondary control – full load conditions and full constellation. $z_{1q} = z_{2q} = 200$, $k_{d1q} = 25 \times 10^{-6}$, $z_{1q} = z_{2q} = 200$, $k_{d1d} = 250 \times 10^{-4}$, $z_{31} = z_{32} = 3000$, $k_{d3} = 7.778 \times 10^{-4}$, $z_{21} = z_{22} = 3000$, $k_{d2} = 7.778 \times 10^{-4}$.

Pages 113 and 114. Figure 7.13 is the full view of the constellation, and Figure 7.14 shows the poles nearest the quadrature axis. Figure 7.15 on Page 115 is the comparable constellation for the light load case. The pole locations indicate an extremely slow response time from the dominant pole location near to the quadrature axis – at −0.112 for the light load case – and the potential for high frequency ringing due to the poorly damped poles at several locations: near $(-2 \pm j450) \times 10^4 \left[\frac{rad}{s}\right]$ and $(-2 \pm j100) \times 10^4 \left[\frac{rad}{s}\right]$.
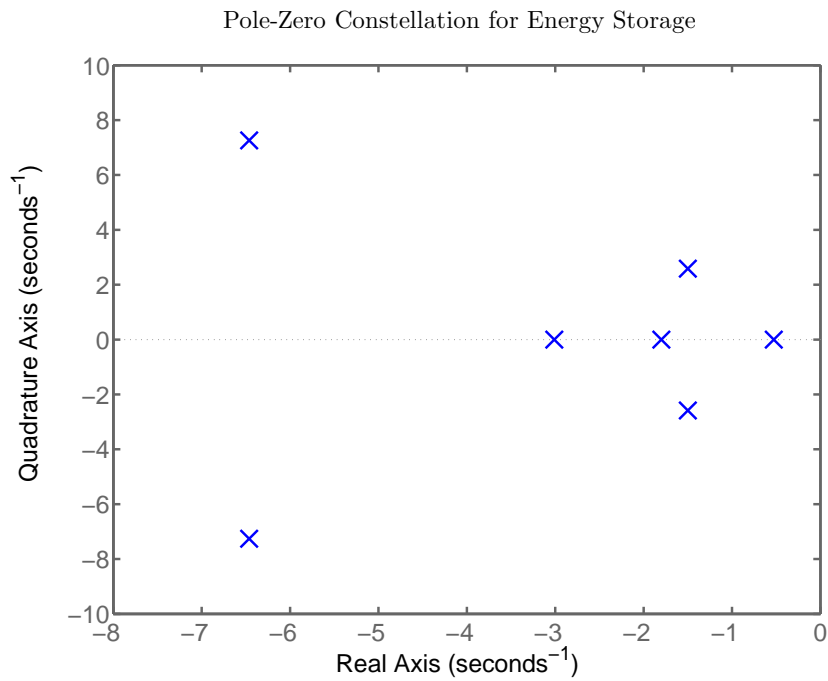
Figure 7.14: Final PID tuning run for the energy storage secondary control – full load conditions showing rightmost poles, the slowest at -0.527 $\left[\frac{rad}{s}\right]$. $z_{1q} = z_{2q} = 200$, $k_{d1q} = 25 \times 10^{-6}$, $z_{1q} = z_{2q} = 200$, $k_{d1d} = 250 \times 10^{-4}$, $z_{31} = z_{32} = 3000$, $k_{d3} = 7.778 \times 10^{-4}$, $z_{21} = z_{22} = 3000$, $k_{d2} = 7.778 \times 10^{-4}$.

Pole-Zero Constellation for Energy Storage
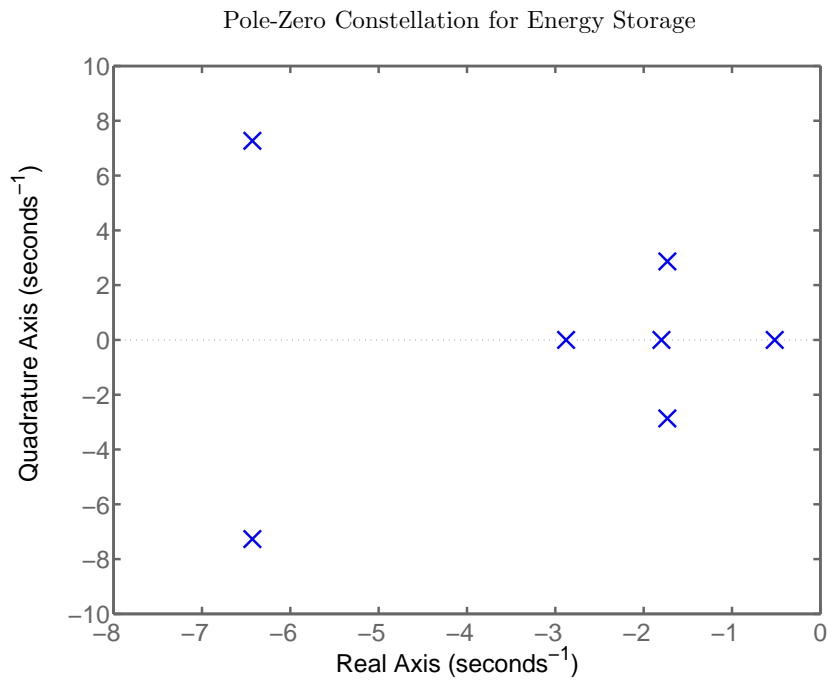
Figure 7.15: Final PID tuning run for the energy storage secondary control – light load conditions showing rightmost polesthe slowest at -0.517 $\left[\frac{rad}{s}\right]$. $z_{1q} = z_{2q} = 200$, $k_{d1q} = 25{\times}10^{-6}$, $z_{1q} = z_{2q} = 200$, $k_{d1d} = 250 \times 10^{-4}$, $z_{31} = z_{32} = 3000$, $k_{d3} = 7.778 \times 10^{-4}$, $z_{21} = z_{22} = 3000$, $k_{d2} = 7.778 \times 10^{-4}$.

Chapter 8

Simulations

This chapter is dedicated to two distinct simulation scenarios. The first revolves around the fault current magnitude experienced by a synchronous generator when exposed to phase–to–neutral faults using the four wire system model developed in earlier sections. The second relates to the stability of an isolated micro–grid using the models and tuning parameters developed in previous sections.

8.1 Four Wire with Generator and Grid – Nonlinear Model Using Matlab

The main reason for this inquiry is to investigate the level of fault current flowing during a phase to ground fault. Statements in [23, 37, 2] motivated the investigation. Due to pressing commercial demands, testing the subject Regal Beloit generating equipment was not feasible. To establish some level of confidence in the proposed model, simulations using generator parameters described in [16] Chapter 3 are compared with results published in [36].

8.1.1 Model Implementation

A one line representation of the simulated system is shown in Figure 8.1. A generator connects through a 1 foot section of cable to a micro–grid bus. A net load represented by series resistance and inductance is place on the bus. The bus is also supplied through a Δ– Grounded Wye transformer from an external electric power system. To impose a phase–to–ground fault, the "a" phase–to–neutral load impedances on the micro–grid bus

are set to small values.

The model is written in first order non–linear differential equations of the form

$$\dot{\boldsymbol{x}} = f(x, u, t). \tag{8.1}$$

Writing (8.1) in matrix form – noting many equations are non–linear – yields

$$
\begin{bmatrix} \dot{\boldsymbol{x}_G} \\ \boldsymbol{x}_E \\ \boldsymbol{x}_A \end{bmatrix}
= \begin{bmatrix} \boldsymbol{GG} \end{bmatrix}
\begin{bmatrix} \boldsymbol{x}_G \\ \boldsymbol{x}_E \\ \boldsymbol{x}_A \end{bmatrix}
+ \begin{bmatrix} \boldsymbol{GB} \end{bmatrix} \begin{bmatrix} \boldsymbol{u}_G \end{bmatrix},
\tag{8.2}
$$

where

$$\boldsymbol{x}_G = \begin{bmatrix} i_{g10} & i_{g1d} & i_{g1q} & i_{g1F} & i_{g1D} & i_{g1Q} & \omega_{g1m} & \Theta_{g1m} \end{bmatrix}^T, \tag{8.3}$$

$$\boldsymbol{x}_E = \begin{bmatrix} v_{c1a} & v_{c1b} & v_{c1c} & i_{ln1a} & i_{ln1b} & i_{ln1c} & v_{c2a} & v_{c2b} & v_{c2c} & i_{lda} & i_{ldb} & i_{ldc} \end{bmatrix}^T, \tag{8.4}$$

$$\boldsymbol{x}_A = \begin{bmatrix} v_{g1fb} & v^*_{g1i} & v^*_{g1d} & v_{g1R} & v_{g1E} & \hat{\omega}_i & \hat{\Theta} & \hat{\omega}_{lpf} & P_{mechg1} & i_{sa} & i_{sb} & i_{sc} \end{bmatrix}^T, \tag{8.5}$$

the states being defined in Table 8.1.1 on Page 118

$$\boldsymbol{GG(1:6)} = \begin{bmatrix} & \begin{smallmatrix} 0 & 0 \\ 0 & 0 \\ 0 & 0 \\ 0 & 0 \\ 0 & 0 \\ 0 & 0 \end{smallmatrix} & \begin{smallmatrix} -\boldsymbol{B_1P} \\ \\ -\boldsymbol{B_2P} \end{smallmatrix} & \begin{smallmatrix} 0\,0\,0\,0\,0\,0\,0\,0\,0\,0\,0\,0\,0\,0\,0\,0\,0\,0\,0\,0\,0\,0\,0\,0 \\ 0\,0\,0\,0\,0\,0\,0\,0\,0\,0\,0\,0\,0\,0\,0\,0\,0\,0\,0\,0\,0\,0\,0\,0 \\ 0\,0\,0\,0\,0\,0\,0\,0\,0\,0\,0\,0\,0\,0\,0\,0\,0\,0\,0\,0\,0\,0\,0\,0 \\ 0\,0\,0\,0\,0\,0\,0\,0\,0\,0\,0\,0\,0\,0\,0\,0\,0\,0\,0\,0\,0\,0\,0\,0 \\ 0\,0\,0\,0\,0\,0\,0\,0\,0\,0\,0\,0\,0\,0\,0\,0\,0\,0\,0\,0\,0\,0\,0\,0 \\ 0\,0\,0\,0\,0\,0\,0\,0\,0\,0\,0\,0\,0\,0\,0\,0\,0\,0\,0\,0\,0\,0\,0\,0 \end{smallmatrix} \end{bmatrix}, \tag{8.6}$$

with $-r\boldsymbol{L}^{-1}$ in the left block.

and **r** and **L** are defined in Section 5.1, $\boldsymbol{B}_1 = \boldsymbol{L}^{-1}(1:3, 1:3)$, $\boldsymbol{B}_2 = \boldsymbol{L}^{-1}(1:3, 4:6)$, and **P** is defined in (5.4). Continuing

$$\boldsymbol{GG(7:8)} = \begin{bmatrix} g71 & g72 & g73 & 0\,0\,0 & -Dx(7) & 0\,0\,0\,0\,0\,0\,0\,0\,0\,0\,0\,0\,0\,0\,0\,0\,0\,0\,0\,0\,0\,0\,0\,0 & 1/(Jx(7)) & 0\,0\,0 \\ 0 & 0 & 0 & 0\,0\,0 & 1 & 0\,0\,0\,0\,0\,0\,0\,0\,0\,0\,0\,0\,0\,0\,0\,0\,0\,0\,0\,0\,0\,0\,0\,0 & 0 & 0\,0\,0 \end{bmatrix}, \tag{8.7}$$

where

$$g71 = \frac{-1}{\sqrt{3}Jx(7)}[x(9) + x(10) + x(11)] \tag{8.8}$$

117

Table 8.1: Symbol definitions for states used to describe the generator and electric power system components in first order differential form.

State #s	Symbol	Description	Units
1	i_{g10}	Generator 1 zero sequence current	[A]
2	i_{g1d}	Generator 1 d axis current	[A]
3	i_{g1q}	Generator 1 q axis current	[A]
4	i_{g1F}	Generator 1 field current	[A]
5	i_{g1D}	Generator 1 d axis damper winding current	[A]
6	i_{g1Q}	Generator 1 q axis damper winding current	[A]
7	ω_{g1m}	Generator 1 mechanical speed	$\left[\frac{rad}{s}\right]$
8	Θ_{g1m}	Generator 1 mechanical angle	[rad]
9–11	v_{c1abc}	Cable charging capacitor 1 a,b,c phase voltages	[V]
12–14	i_{lnabc}	Cable a,b,c phase current	[A]
15–17	v_{c2abc}	Cable charging capacitor 2 a,b,c phase voltages	[V]
18–20	i_{ldabc}	Micro–grid load a,b,c phase current	[A]
21	v_{g1fb}	Generator 1 pseudo–rms terminal voltage	[V]
22	v_{g1i}^*	Generator 1 terminal voltage integrated error	[pu]
23	v_{g1d}^*	Generator 1 terminal voltage derivative error	[pu]
24	v_{g1R}	Voltage regulator output	[pu]
25	v_{g1E}	Exciter voltage behind commutating reactance	[pu]
26	$\hat{\omega}_i$	Integrator state for PLL	$\left[\frac{rad}{s}\right]$
27	$\hat{\Theta}$	Estimated micro–grid electrical angle	[rad]
28	$\hat{\omega}_{lpf}$	Estimated micro–grid electrical frequency	$\left[\frac{rad}{s}\right]$
29	P_{mechg1}	Internal combustion engine output power	[W]
30–32	i_{sabc}	Electric power system a,b,c phase current	[A]

$$g72 = \frac{-\sqrt{2}}{\sqrt{3}Jx(7)}\{x(9)\cos[p/2 \times x(8) + \pi/2]$$

$$+ x(10)\cos[p/2 \times x(8) - \pi/6] + x(11)\cos[p/2 \times x(8) + 7\pi/6]\} \tag{8.9}$$

$$g73 = \frac{-\sqrt{2}}{\sqrt{3}Jx(7)}\{x(9)\sin[p/2 \times x(8) + \pi/2]$$

$$+ x(10)\sin[p/2 \times x(8) - \pi/6] + x(11)\sin[p/2 \times x(8) + 7\pi/6]\}, \tag{8.10}$$

and D and J are defined in Section 5.4.

$$GG(9:11) = \left[c^{-1}P^{-1} \quad zed35 \quad -c^{-1}g \quad -c^{-1} \quad zed318\right], \tag{8.11}$$

where $\mathbf{c}$ and $\mathbf{g}$ are defined in Section 3.2, $\mathbf{zed35}$ is a 3x5 matrix of zeros, and $\mathbf{zed318}$ is a 3x18 matrix of zeros. Next

$$GG(12:14) = \left[zed38 \quad L_{ln}^{-1} \quad -L_{ln}^{-1}r_{ln} \quad -L_{ln}^{-1} \quad zed315\right], \tag{8.12}$$

where $\mathbf{r}_{\mathrm{ln}}$ and $\mathbf{L}_{\mathrm{ln}}$ are defined in Section 3.1, $\mathbf{zed38}$ is a 3x8 matrix of zeros, and $\mathbf{zed315}$ is a 3x15 matrix of zeros. Then

$$GG(15:17) = \left[zed311 \quad c^{-1} \quad -c^{-1}g \quad -c^{-1} \quad zed39 \quad c^{-1}\right], \tag{8.13}$$

where $\mathbf{zed311}$ is a 3x11 matrix of zeros, and $\mathbf{zed312}$ is a 3x12 matrix of zeros. Rows 18–20 are

$$GG(18:20) = \left[zed314 \quad L_{ld}^{-1} \quad -L_{ld}^{-1}r_{ld} \quad -c^{-1} \quad zed312\right], \tag{8.14}$$

where $\mathbf{r}_{\mathrm{ld}}$ and $\mathbf{L}_{\mathrm{ld}}$ are defined in Section 3.3, $\mathbf{zed314}$ is a 3x14 matrix of zeros and $\mathbf{zed312}$

is a 3x12 matrix of zeros. Rows 21–25 are

$GG(21:25)$ =

$$
\begin{bmatrix}
0\,0\,0 & 0 & 0\,0\,0\,0\,0\,0\,0\,0\,0\,0\,0\,0\,0\,0\,0\,0 & 0 & 0 & 0 & 0\,0\,0\,0\,0\,0\,0\,0\,0 \\
0\,0\,0 & 0 & 0\,0\,0\,0\,0\,0\,0\,0\,0\,0\,0\,0\,0\,0\,0\,0 & -k_i & 0 & 0 & 0\,0\,0\,0\,0\,0\,0\,0\,0 \\
0\,0\,0 & 0 & 0\,0\,0\,0\,0\,0\,0\,0\,0\,0\,0\,0\,0\,0\,0\,0 & 0 & 0 & -1/\tau_d & 0\,0\,0\,0\,0\,0\,0\,0\,0 \\
0\,0\,0 & 0 & 0\,0\,0\,0\,0\,0\,0\,0\,0\,0\,0\,0\,0\,0\,0\,0 & -k_p K_A x(7)/T_A & K_A x(7)/T_A & K_A x(7)/T_A & 0\,0\,0\,0\,0\,0\,0\,0\,0 \\
0\,0\,0 & -K_D/(T_E I_{rb}) & 0\,0\,0\,0\,0\,0\,0\,0\,0\,0\,0\,0\,0\,0\,0\,0 & 0 & 0 & 0 & 0\,0\,0\,0\,0\,0\,0\,0\,0
\end{bmatrix},
$$

(8.15)

where terms are defined in Section 5.3. Rows 26–29 are

$GG(26:29)$ =

$$
\begin{bmatrix}
0\,0\,0\,0\,0\,0 & 0 & 0\,0\,0\,0\,0\,0\,0\,0\,0\,0\,g2617\;g2618\;g2619\;0\,0\,0\,0\,0\,0 & 0 & 0 & 0 & 0 & 0\,0\,0 \\
0\,0\,0\,0\,0\,0 & 0 & 0\,0\,0\,0\,0\,0\,0\,0\,0\,0\,g2717\;g2718\;g2719\;0\,0\,0\,0\,0\,0 & 1 & 0 & 0 & 0 & 0\,0\,0 \\
0\,0\,0\,0\,0\,0 & 0 & 0\,0\,0\,0\,0\,0\,0\,0\,0\,0\,g2817\;g2818\;g2819\;0\,0\,0\,0\,0\,0 & 1/\tau f & 0 & -1/\tau f & 0 & 0\,0\,0 \\
0\,0\,0\,0\,0\,0 & -P_{max}/(377R\tau_{g1}) & 0\,0\,0\,0\,0\,0\,0\,0\,0\;0\quad0\quad0\quad0\,0\,0\,0\,0\,0 & 0 & 0 & 0 & -1/\tau g1 & 0\,0\,0
\end{bmatrix},
$$

(8.16)

where

$$g2617 = k_{ipll}\sqrt{2/3}\cos[x(27) + \pi/2],$$

$$g2618 = k_{ipll}\sqrt{2/3}\cos[x(27) - \pi/6],$$

$$g2619 = k_{ipll}\sqrt{2/3}\cos[x(27) + 7\pi/6],$$

$$g2717 = k_{ppll}\sqrt{2/3}\cos[x(27) + \pi/2],$$

$$g2718 = k_{ppll}\sqrt{2/3}\cos[x(27) - \pi/6],$$

$$g2719 = k_{ppll}\sqrt{2/3}\cos[x(27) + 7\pi/6],$$

$$g2817 = \frac{k_{ppll}}{\tau_f}\sqrt{2/3}\cos[x(27) + \pi/2],$$

$$g2818 = \frac{k_{ppll}}{\tau_f}\sqrt{2/3}\cos[x(27) - \pi/6],$$

$$g2819 = \frac{k_{ppll}}{\tau_f}\sqrt{2/3}\cos[x(27) + 7\pi/6],$$

where terms relating to the phase–locked–loop in rows 26–28 are defined in Section 6.1,

and those relating to the internal combustion engine in row 29 are defined in Section 5.5. Rows 30–32 are

$$GG(30:32) = \begin{bmatrix} \boldsymbol{zed314} & \boldsymbol{L}_t^{-1} & \boldsymbol{zed312} & -\boldsymbol{L}_t^{-1}\boldsymbol{r}_t \end{bmatrix}, \tag{8.17}$$

where $\mathbf{r}_t$ and $\mathbf{L}_t$ are the total system impedances defined in Section 4.2, **zed314** is a 3x14 matrix of zeros and **zed312** is a 3x12 matrix of zeros.

The "input" vector is defined as

$$\boldsymbol{u} =$$

$$\begin{bmatrix} 0\ 0\ 0\ x25F_{EX}V_{rb}\ 0\ 0\ 0\ 1\ 1\ v_r\ P_{refg1}\ 1\ 480\sqrt{2/3}\{[cos(\omega t+\theta)\ cos(\omega t+\theta-2pi/3)\ cos(\omega t+\theta+2pi/3)]\}\ x24\ x25 \end{bmatrix}^T,$$

$$\tag{8.18}$$

where terms x24 and x25 are lower and upper bound versions of states 24 and 25 respectively as defined by the example code in Section 5.3.7, F_{EX} is also defined in Section 5.3.7, v_r is the generator 1 voltage setpoint in [pu], P_{refg1} is the generator 1 power setpoint in [pu], the three cosinusoidal terms represent the grid input voltage in [V], ω is the electrical frequency in $[\frac{rad}{s}]$, and θ is the synchronizing angle in [rad].

The terms in rows 1–6 in **GB** are

$$GB(1:6) = \begin{bmatrix} \boldsymbol{L}^{-1} & \boldsymbol{zed611} \end{bmatrix}, \tag{8.19}$$

where **zed611** is a 6x11 matrix of zeros. Rows 7–20 are

$$GB(7:20) = \begin{bmatrix} \boldsymbol{zed1417} \end{bmatrix}, \tag{8.20}$$

where **zed1417** is a 14x17 matrix of zeros. Row 21 is

$$
\begin{aligned}
&\mathbf{GB(21)} = \\
&\Big[\; \mathbf{zed18} \;\; w_{co}\Big(\sqrt{\{[y(9)-y(10)]^2+[y(10)-y(11)]^2+[y(11)-y(9)]^2\}/3}/480-y(21)\Big)\; \mathbf{zed18}\;\Big],
\end{aligned}
\tag{8.21}
$$

where ω_{co} is the cut–of frequency of the voltage feedback filter and **zed18** is a 1x8 matrix of zeros. Row 22 is

$$
\mathbf{GB(22)} = \Big[\mathbf{zed19} \quad k_i \quad \mathbf{zed17}\Big],
\tag{8.22}
$$

where k_i is the AC8B voltage regulator integrator gain, and **zed19** is a 1x9 and **zed17** is a 1x7 matrix of zeros. Row 23 is

$$
\begin{aligned}
&\mathbf{GB(23)} = \\
&\Big[\; \mathbf{zed18} \;\; -(k_d/\tau_d)w_{co}\Big(\sqrt{\{[y(9)-y(10)]^2+[y(10)-y(11)]^2+[y(11)-y(9)]^2\}/3}/480-y(21)\Big)\; \mathbf{zed18}\;\Big],
\end{aligned}
\tag{8.23}
$$

where k_d is the derivative gain and τ_d is the derivative time delay for the AC8B voltage regulator. For row 24

$$
\mathbf{GB(24)} = \Big[\mathbf{zed19} \quad x(7)k_p K_A/T_A \quad \mathbf{zed15} \quad -1/T_A \quad 0\Big],
\tag{8.24}
$$

where **zed15** is a 1x5 matrix of zeros and the balance of terms are defined in Section 5.3. Row 25 is

$$
\mathbf{GB(25)} = \Big[\mathbf{zed17} \quad -polyval(p5,x25,s5,u5) \quad \mathbf{zed17} \quad 1/T_E \quad -K_E/T_E\Big],
\tag{8.25}
$$

where **zed17** is a 1x7 matrix of zeros, polyval(p5,x25,s5,u5) returns the fifth order estimate of the exciter saturation function evaluated at x25, and the balance of terms are defined in Section 5.3. Rows 26–28 are

$$
\mathbf{GB(26\!:\!28)} = \Big[\mathbf{zed317}\Big],
\tag{8.26}
$$
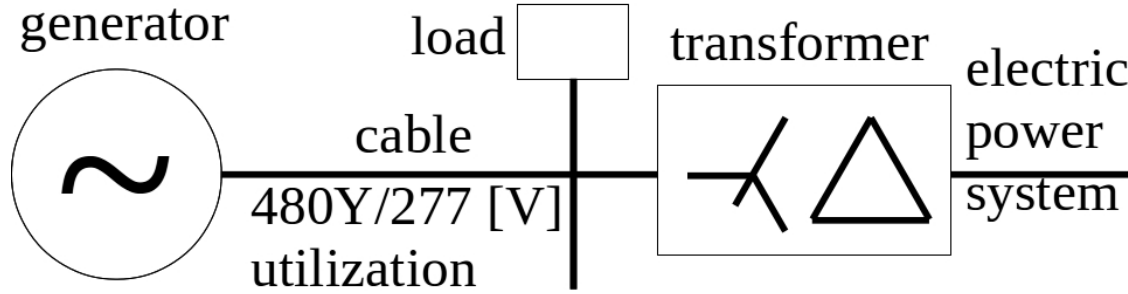
Figure 8.1: One–line diagram representation of the system used to simulate phase–to–neutral faults performed in Section 8.1.

where **zed317** is a 3x17 matrix of zeros. Row 29 is

$$\mathbf{GB(29)} = \begin{bmatrix} \mathbf{zed110} & P_{max}/\tau_{g1} & P_{max}/(R\tau_{g1}) & \mathbf{zed15} \end{bmatrix}, \tag{8.27}$$

where **zed110** is a 1x10 matrix of zeros and the balance of terms are defined in Section 5.5. Rows 30–32 are

$$\mathbf{GB(30:32)} = \begin{bmatrix} \mathbf{zed312} & L_t^{-1} & \mathbf{zed32} \end{bmatrix}, \tag{8.28}$$

where **zed312** is a 3x12 and **zed32** is a 3x2 matrix of zeros.

The model equations are written into a Matlab® function file invoked by a Matlab® script file. Generator and electric power system parameters are defined in Matlab® function files. The contents of these files[1] may be found in Appendix D.

8.1.2 Model Validation

The model comparison is imperfect because a single damper q axis damper winding models the parallel combination of the 2 damper windings on the q axis for the generator described in [16]. Another difference is that in [36] the generator connects to an infinite bus, where simulations performed assumed a 600 [MVA], 3%Z, X/R=40 transformer impedance to the infinite bus. However, the simulated current magnitudes are close to those published in [36].

---

[1]Files containing Regal Beloit Corp. proprietary information have been redacted
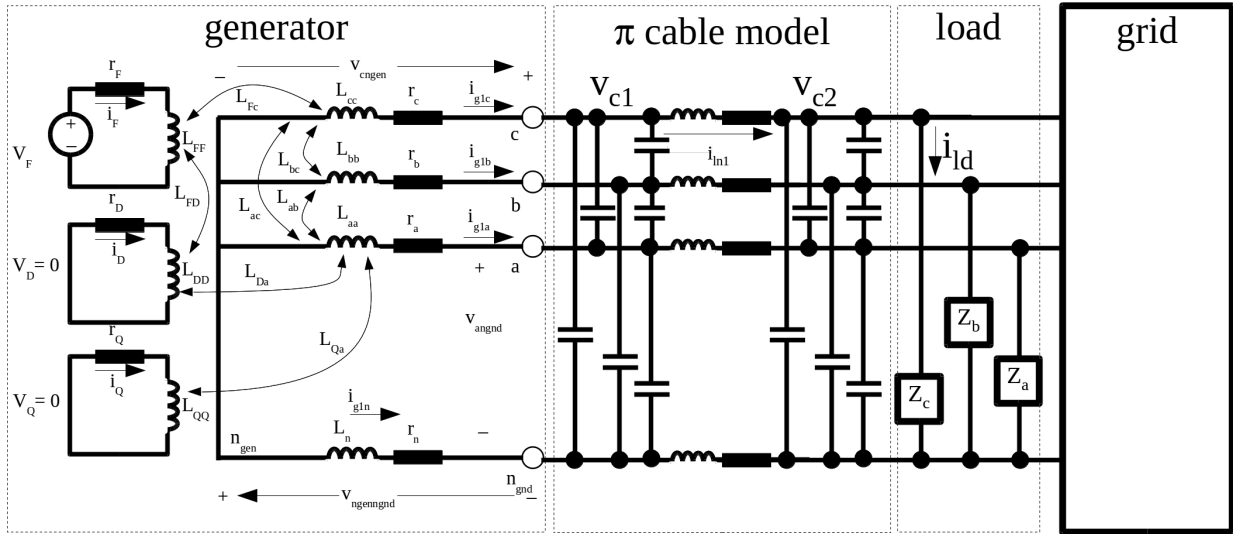
Figure 8.2: Four–wire diagram representation of the system used for simulating phase–to–neutral faults in Section 8.1.

The model validation simulation data is shown in Figure 8.3 on Page 125. The setup follows [36]: the generator is connected to a bus without load when a phase a to neutral fault occurs. Data in [36] is not reproduced here due to copyright infringement concerns. The simulated results are compared to [36] in Table 8.2 on Page 125, and a close magnitude match – 2.5% difference – and sinusoidal shape of the a–phase and b–phase currents is noted[2]. While simulated field current *peak* magnitude is within 10% of [36], the shape is quite different: the simulated data has a more severely pronounced second harmonic as shown in Figure 8.3 on Page 125. The electromagnetic torque comparison indicates a full order of magnitude difference between the simulated data and [36], and shares the pronounced second harmonic seen in the field current.

Since phase a current is the critical quantity, the proposed model seems a fair match. There are a number of alterations, unknowns and differences which might account for the field current departure, the pronounced second harmonic content, and the gap between the torque values. The consolidation of two damper windings into one has already been mentioned, and that may contribute to the second harmonic. In [36], there is no mention

---

[2]Data from [36] is interpreted from images, not tabular.

Table 8.2: Generator Zero–Sequence Model Validation: Phase "a" to Neutral Fault

State	From [36]	Simulated	% error
i_a	64 [kA]	65.6 [kA]	2.5
i_b	9 [kA]	8.9 [kA]	1.1
i_F	60 [kA]	54 [kA]	10
T_{em}	5 [MNm]	0.57 [MNm]	$\gg 1$
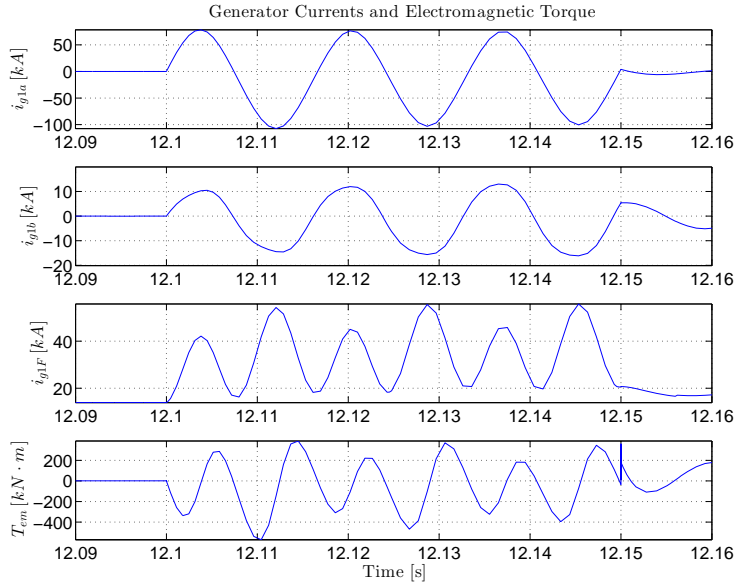
Figure 8.3: Generator model validation simulation results using data from [16].

of voltage regulation, so it is unclear how field excitation is controlled. This could have a dramatic effect on the field current magnitude and shape. Also in [36] the authors state that the generator is connected to an infinite bus, where simulations are performed assuming a finite impedance transformer. This too could impact the field current. Another potential source for error is timing of the fault inception. Finally, there is no mention of a prime mover in [36]. This could have a profound impact on the electromechanical torque experienced by the generator.

Performance was also checked against manual calculations to ascertain the model validity. The generator is now the Regal Beloit model with parameters listed in Table A1 on Page 151. Similar to the previous simulation, the generator is operating at rated voltage and

speed under light load conditions. Impedance to the infinite bus is a 3 [MVA], Δ–Y, 2.5%Z, X/R=10 transformer plus a positive sequence system impedance $Z_s = 0.054 + j0.54 \, [m\Omega]$. The circuit diagram is shown in Figure 8.2 on Page 124. A phase a to neutral fault is imposed on the system and fault current magnitude extracted from the simulation results.

The manual calculation of fault current magnitude starts with Figure 8.4 on Page 128. The impedance values are defined in Table 8.3 on Page 127. To calculate the total fault current, add the positive and negative sequence impedances in the left branch:

$$Z_{es1} = Z_{s1} + Z_{t1} \tag{8.29a}$$

$$Z_{es2} = Z_{s2} + Z_{t2}. \tag{8.29b}$$

Next find the equivalent positive, negative and zero sequence impedances:

$$Z_{1eq} = \frac{Z_{es1}Z_{g1}}{Z_{es1} + Z_{g1}} \tag{8.30a}$$

$$Z_{2eq} = \frac{Z_{es2}Z_{g2}}{Z_{es2} + Z_{g2}} \tag{8.30b}$$

$$Z_{0eq} = \frac{Z_{t0}Z_{g0}}{Z_{t0} + Z_{g0}}. \tag{8.30c}$$

Calculate the positive, negative and zero sequence fault current:

$$\hat{I}_{lnf} = \hat{I}_{lnf1} = \hat{I}_{lnf2} = \hat{I}_{lnf0} = \frac{3 * V_{ln}}{Z_{1eq} + Z_{2eq} + Z_{0eq}}. \tag{8.31}$$

Substituting the $V = 277 \angle 0 \quad [V]$ and impedance values into (8.31), $\hat{I}_{lnf} = 161 \angle -84.6°$ [kA]. To calculate the generator sequence currents use current divider calculations:

$$\hat{I}_{g1} = \hat{I}_{lnf} \frac{Z_{es1}}{Z_{es1} + Z_{g1}} = 13.2 \angle -86.0°[kA] \tag{8.32a}$$

$$\hat{I}_{g2} = \hat{I}_{lnf} \frac{Z_{es2}}{Z_{es2} + Z_{g2}} = 13.2 \angle -86.0°[kA] \tag{8.32b}$$

$$\hat{I}_{g0} = \hat{I}_{lnf} \frac{Z_{t0}}{Z_{t0} + Z_{g0}} = 13.6 \angle -85.0°[kA]. \tag{8.32c}$$

Table 8.3: Generator Manual Fault Current Calculation Impedance Data

Parameter	Value [mΩ]
Z_{s1}	$0.054 + j0.54$
Z_{s2}	$0.054 + j0.54$
Z_{t1}	$0.191 + j1.91$
Z_{t2}	$0.191 + j1.91$
Z_{t0}	$0.191 + j1.91$
Z_{g1}	$0.52 + j7.58$
Z_{g2}	$0.52 + j7.58$
Z_{g0}	$0.52 + j5.64$

The phase "a" fault current is the sum:

$$\hat{I}_{ga,flt} = \hat{I}_{g1} + \hat{I}_{g2} + \hat{I}_{g0} = 39.9 \angle -85.6°\,[kA]. \tag{8.33}$$

The system simulation results are shown if Figure 8.5 on Page 129. Close inspection reveals that the fault current magnitude is increasing with fault duration due to field response. To mimic the manual calculations as nearly as possible, the two current peaks immediately following the fault inception are used to calculate fault magnitude:

$$\left|i_{flt}\right| = \frac{\left|i_{pk1}\right| + \left|i_{pk2}\right|}{\sqrt{8}} = \frac{60.7 + 51.0\,[kA]}{\sqrt{8}} = 39.5\,[kA]. \tag{8.34}$$

The difference in magnitudes between (8.33) and (8.34) is 1.0%.

8.1.3 Simulated Faults

A 3–phase fault and a phase–to–neutral fault with the synchronous machine isolated from the grid are simulated to establish baseline current magnitudes. Then the generator is interconnected with a grid system – modeled as ideal sources behind finite positive, negative and zero–sequence impedances – and a single phase fault is again simulated to determine if the grid connection adds to the fault current seen by the generator. The transformer
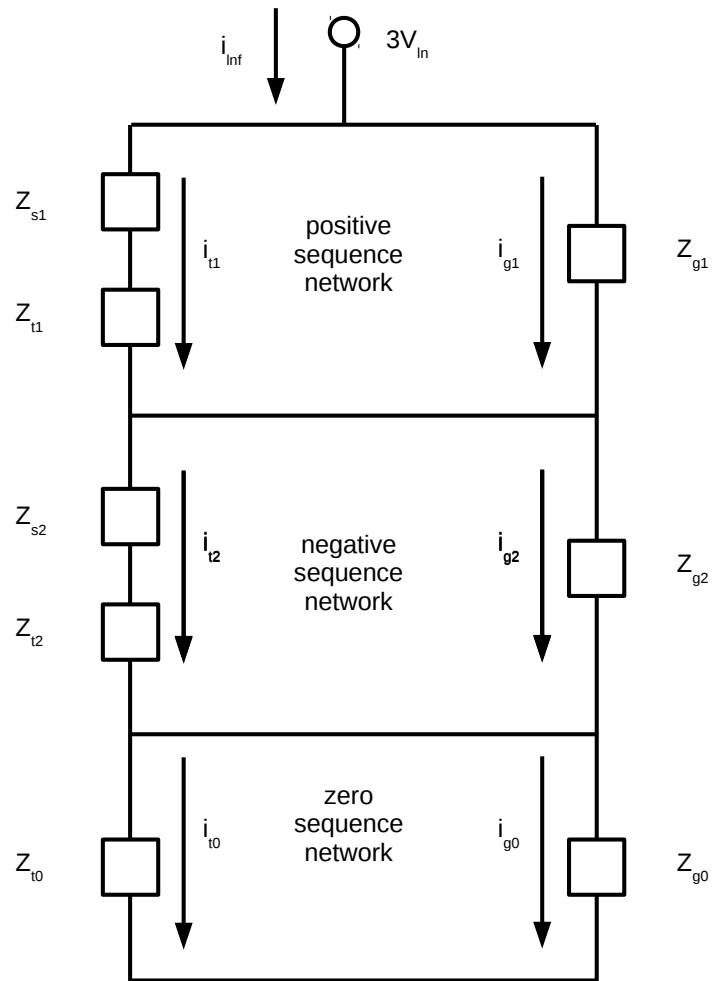
Figure 8.4: Sequence network for single line to ground fault – generator in parallel with transformer and grid.
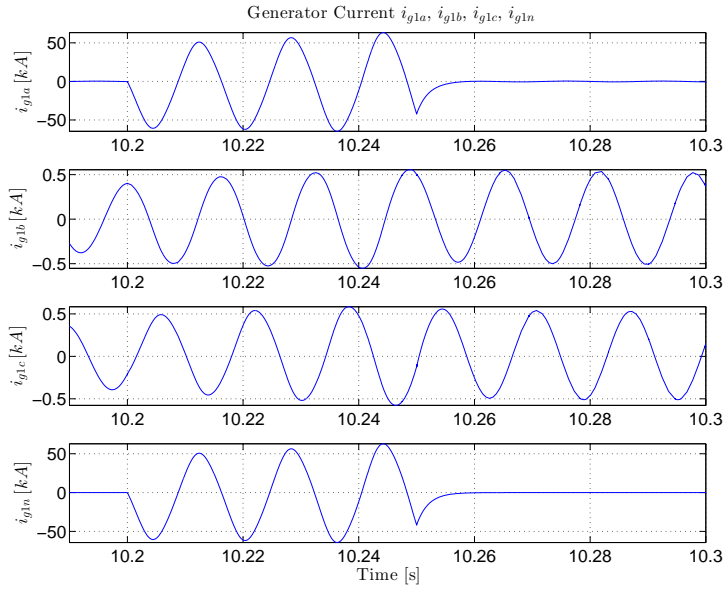
Figure 8.5: Simulation data for model validation employing a line to neutral fault.

and grid impedances are changed to examine the effect on fault current magnitude in the generator. The model for simulations is shown in Figure 8.2 on Page 124. A one (1) foot length of 500 [MCM] cable with impedance data listed in Table A5 on Page 153 is used to connect the generator to the micro–grid bus.

Fault duration for each simulation is 3 cycles. Prior to the fault the voltage behind the reactance of the generator will be established by the AC8B regulator and will impact the fault current flowing in the generator during the fault. The loading on the generator immediately prior to the fault is 2 + j1.5 [MVA] in each case.

AC fault current magnitude is gauged by examining the peaks in the current waveforms. A current magnitude is calculated for each cycle while the fault is impressed. The equivalent AC RMS value is calculated using (8.34).

Samples of the simulated data are shown in Figures 8.6–8.8. The baseline for 3 phase fault magnitude is set by Figure 8.6 on Page 131, and for the line–to–ground fault in Figure 8.7 on Page 131. A sample simulation for a phase–to–neutral fault is shown in Figure 8.8 on Page 132. The transformer connection is Δ-Y, and it is rated 3 [MVA], 5%Z,

X/R=10. System impedance to the infinite bus is 0.54 + j5.4 [mΩ].

Electric power system and transformer impedances, and fault magnitude data is summarized in Table 8.4 on Page 132. For this Regal Beloit generator, the data demonstrate that the current magnitude for a phase–to–neutral fault exceeds that of a three phase fault in agreement with [23, 37, 2]. Both faults are applied near to the generator terminals. The data also show that placing this generator in parallel with another zero–sequence source *reduces* the fault current experienced by the generator. The latter conclusion is in conflict with positions taken in [23, 37, 2].

Two factors help to explain the disagreement. In [23], the generator zero sequence impedance magnitude is 0.71 that of the electric power system zero sequence impedance. Using the impedance data from Row 8 in Table 8.4 on Page 132 as an example, the generator zero sequence impedance magnitude is 3.0 that of the system zero sequence impedance. A lower relative generator zero sequence impedance will raise the total fault current magnitude, raise the generator zero sequence current magnitude, increasing the fault current magnitude seen by the generator. Because the Regal Beloit generator has a relatively high zero sequence impedance, the fault magnitude is reduced as is the current flow through the generator zero sequence network.

8.2 Micro–grid as an Island

After tuning PID controllers in the AC8B exciter and voltage regulator, the energy storage device primary control system, and the secondary control system, the complete complex system is simulated to determine the impact of the secondary control network.

8.2.1 Model Implementation

The one–line diagram for the model implementation is shown in Figure 8.9 on Page 133. More details on the equation based model for the micro–grid electric power system current
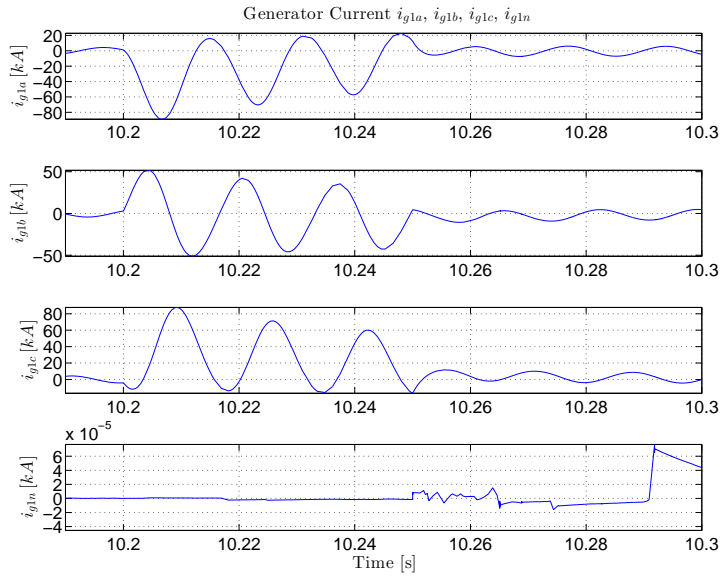
Figure 8.6: 3–phase generator fault current corresponding to Rows 1–4 in Table 8.4 on Page 132.
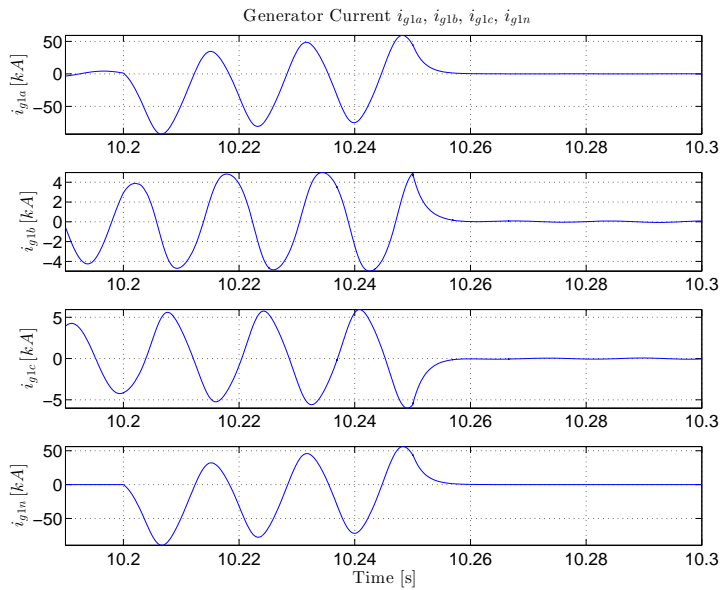
Figure 8.7: Line–to–neutral fault at the generator terminals with a 3 [MVA], 20 [pu] impedance transformer to grid connection.
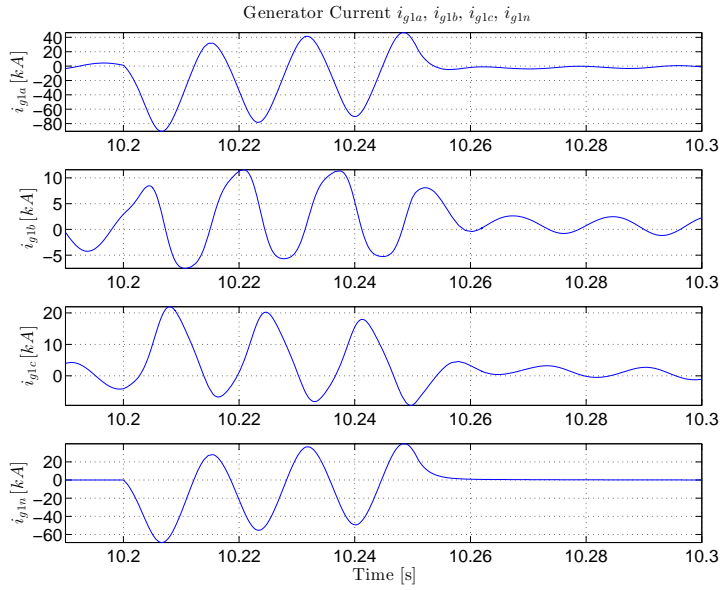
Figure 8.8: Line–to–neutral fault at the generator terminals with a 3 [MVA], 5% impedance transformer to grid connection corresponding to Row 6 in Table 8.4 on Page 132.

Table 8.4: Summary of Generator Terminal Fault Data

			Three Phase Fault				
		System Z	XFMR	Cycle 1	Cycle 2	Cycle 3	Average
Row	Phase	[mΩ]	3 [MVA] X/R=10	[kA]	[kA]	[kA]	[kA]
1	a	$0.54 + j5.4$	5% Z	37.1	31.6	28.3	32.3
2	b	$0.54 + j5.4$	5% Z	36.4	31.1	27.7	31.7
3	c	$0.54 + j5.4$	5% Z	35.6	30.2	26.9	30.7
4	AVG	$0.54 + j5.4$	5% Z	36.2	31.0	27.6	31.6

			Line–to–Neutral Fault				
		System Z	XFMR	Cycle 1	Cycle 2	Cycle 3	Average
Row	Phase	[mΩ]	3 [MVA] X/R=10	[kA]	[kA]	[kA]	[kA]
5	a	$0.54 + j5.4$	2000% Z	45.0	45.8	47.5	46.1
6	a	$0.54 + j5.4$	5% Z	43.4	42.3	41.3	42.3
7	a	$0.54 + j5.4$	2.5% Z	42.4	40.9	39.6	40.9
8	a	$0.054 + j0.54$	2.5% Z	44.8	42.5	40.7	42.7
9	a	$0.054 + j0.54$	7.5% Z	44.8	44.9	44.3	44.7
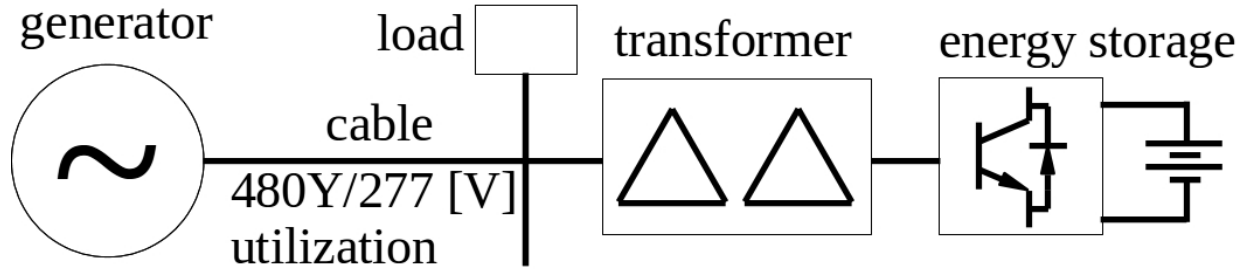
Figure 8.9: One–line diagram representation of the system used to simulate balanced three–phase conditions in Section 8.2.

carrying elements are shown in Figure 8.10. Details of other components – secondary control module, primary control for the energy storage device, AC8B regulator, and internal combustion engine – are shown in previous sections. The models for simulations performed in Section 8.2 are built in Simulink®, and the diagrams may be found in Appendix D.

8.2.2 Steady State Conditions

In Table 8.5, simulated steady state loading of the energy storage device and the generator are presented. Participation and weighting factors assigned to the power compensation for the simulations are defined and listed in Table 8.6.

The system was simulated first with the secondary control deactivated, and then with secondary control active. Without secondary control, it is evident that active power is primarily provided by the energy storage device, despite a generator set–point requesting 40 [kW]. Reactive power is also being supplied by the energy storage device, and in fact the generator is taking in VARs. When the secondary control is active, the devices share active and reactive loading more equitably. The steady state values are taken from the step response simulation described in Section 8.2.3

8.2.3 Step Load Change

A step change in load is simulated for two micro–grids conditions. The first uses all components listed with the exception of secondary control. In the latter, secondary control is

133
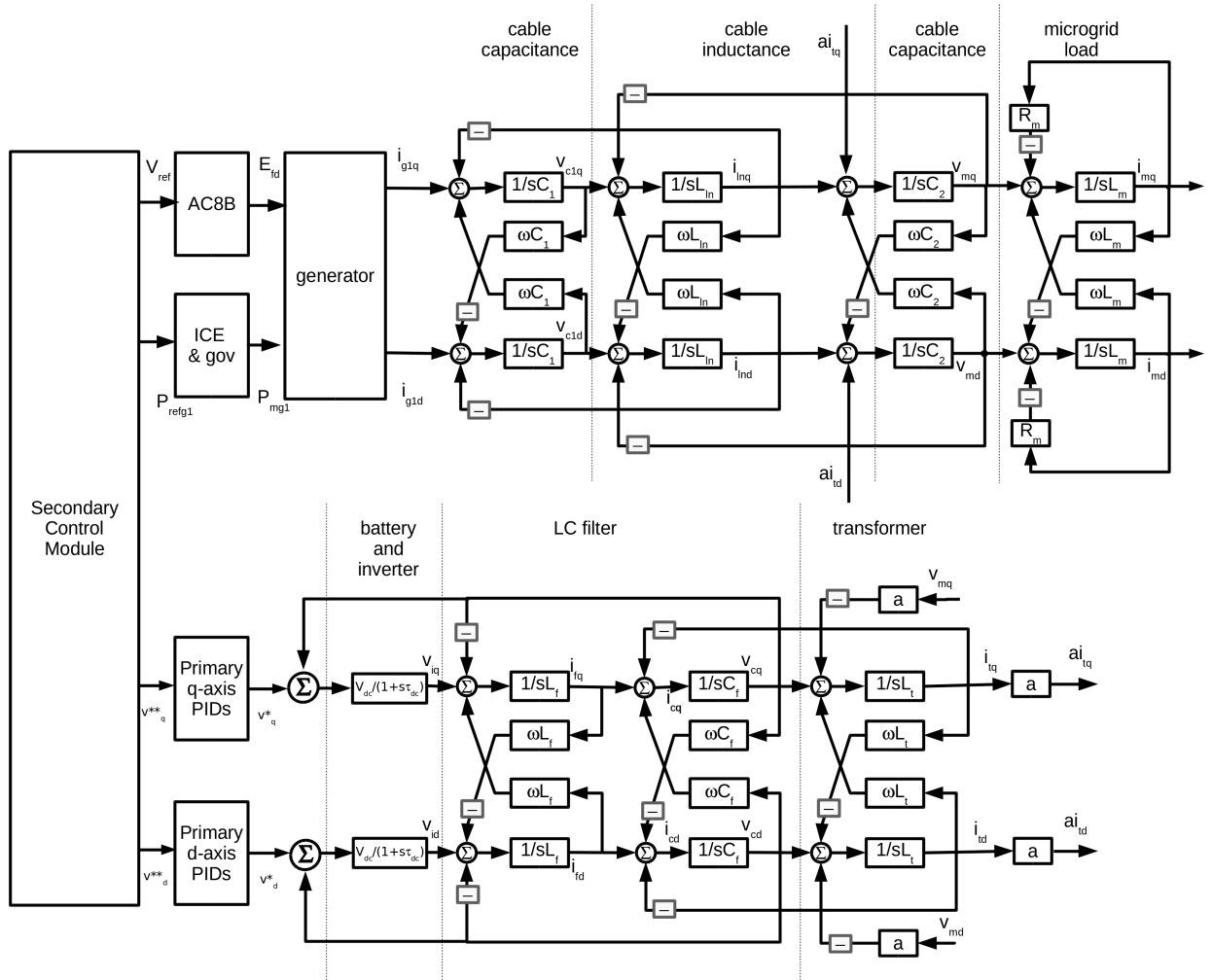
Figure 8.10: A diagram of the micro–grid as simulated in Section 8.2. Details of the secondary control module, primary control for the energy storage device, AC8B regulator, and internal combustion engine are shown in previous sections.

Table 8.5: Steady State Loading

	No Secondary Control		With Secondary Control	
S_m [kVA]	50 + j37.5	100 + j75	50 + j37.5	100 + j75
S_{es} [kVA]	50 + j50	97 + j79	36 + j32	73 + j70
S_{gen} [kVA]	0 – j12	0 – j4	14 + j6	29 + j7

enabled. Referring to Figures 8.11 through 8.13 on Pages 136 through 137, at t = 100 [s] the micro–grid load is increased from 50 + j37.5 [kVA] to 100 + j75 [kVA]. Fig. 8.11 shows the energy storage system power response without and with secondary control. Fig. 8.12 shows the generator power response without and with the secondary control. Transient

Table 8.6: Participation and Weighting Factors

Participation Factors		
Symbol	Definition	Value
$f_{p,g1}$	Generator Active Power	40,000
$f_{q,g1}$	Generator Reactive Power	30,000
$f_{p,es}$	Energy Storage Active Power	100,000
$f_{q,es}$	Energy Storage Reactive Power	75,000
$f_{p,tot}$	$f_{p,g1} + f_{p,es}$	140,000
$f_{q,tot}$	$f_{q,g1} + f_{q,es}$	105,000
Weighting Factors		
Symbol	Definition	Value
W_{Pg1}	Generator Active Power	0.5
W_{Qg1}	Generator Reactive Power	0.5
W_{Pes}	Energy Storage Active Power	1
W_{Qes}	Energy Storage Reactive Power	2

response in the energy storage and generator power does not appear to change radically with the secondary control enabled, but steady state loading is impacted as outlined in Section 8.2.2.

The load frequency is affected in a positive manner in that frequency deviations following a step load change is much smaller in magnitude. A bit of oscillation is apparent in the generator speed. Referring to Fig.8.13, the scheduled frequency is restored within 0.5 second and the load frequency dips to 0.975 [pu] without secondary control. Because load frequency barely moves with secondary control enabled, frequency restoration is instantaneous.

Load terminal voltage is shown in Figure 8.14. Load terminal voltage without secondary control enabled starts at about 0.99 [pu], and achieves steady state rather quickly following a step increase in load. But the steady state level drops about 0.5% as a result of the load step. With secondary control enabled, the voltage prior to the step load increase is near 1.0 [pu], rising to 1.005 [pu] following the increase. The rise time is on the order of 5 seconds, as the load d and q axis voltages adjust to satisfy the active power, frequency,
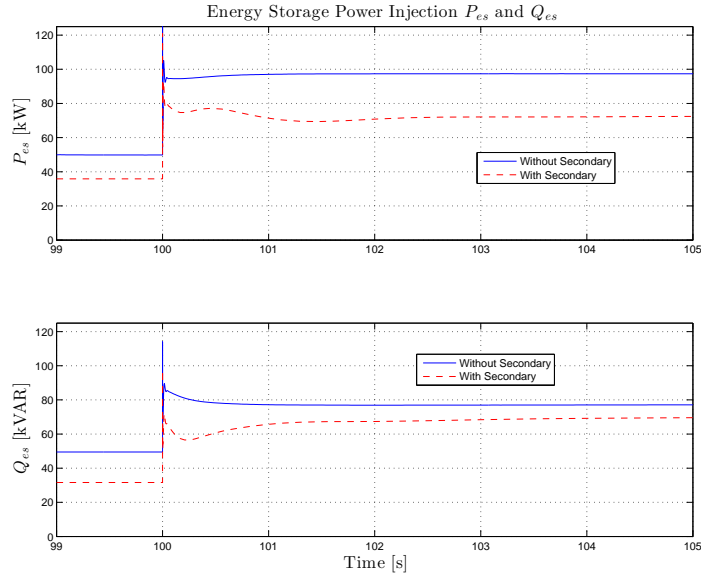
Figure 8.11: Energy storage system active and reactive power response to a step load change.

reactive power and voltage commands biased by the weighting factors at the generator and energy storage device. Since there is more than one control objective on each axis, steady state conditions represent a compromise of the control objectives. A voltage reference of one (1) [pu] is akin to the base setting, with deviations occurring because of competing control objectives.

While the energy storage LCL filter and generator stator impedances have a relatively high X/R ratio, the cable connecting the generator to the micro–grid bus does not. So there is strong cross coupling between the active power flow and voltage rise, and reactive power flow and power angle when comparing the generator bus to the load bus.

Based on simulation, the stability limit for step load change is 130% of the energy storage device rating. To design a high reliability micro–grid, the energy storage device should be capable of carrying the micro–grid load without assistance from other sources, implying a step load limit of 100% of the energy storage device rating.
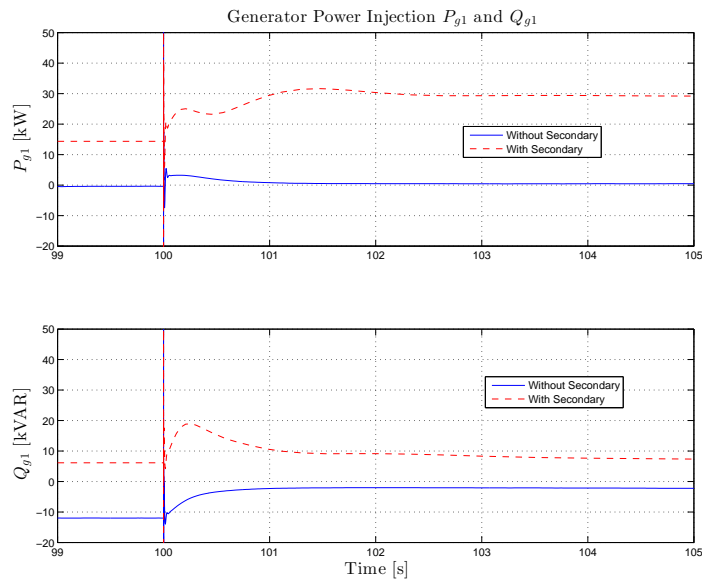
Figure 8.12: Generator active and reactive power response to a step load change.
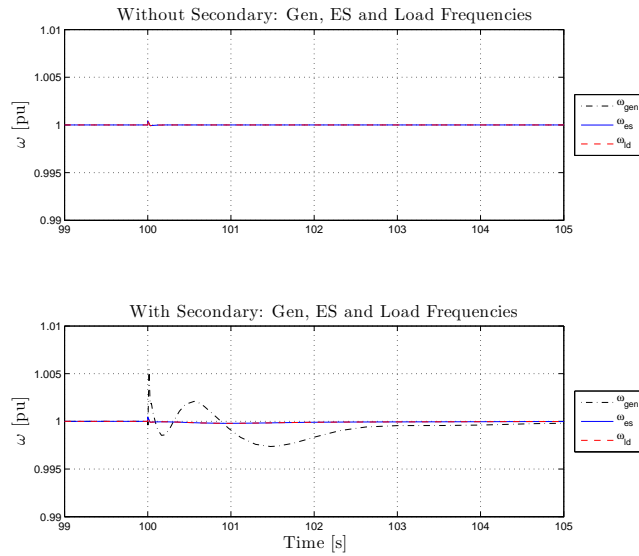
Figure 8.13: Generator, energy storage device, and load frequency response to a step load change.

8.2.4 Step Change in Command

For the simulation data presented in In Figures 8.15 and 8.16 on Pages 139 and 140, the micro–grid is loaded at $100 + j75$ [kVA] throughout, with initial set–point values as
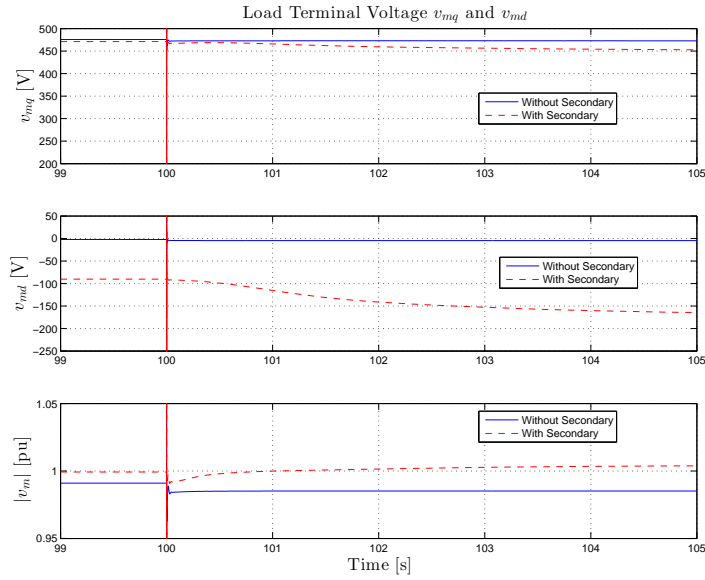
Figure 8.14: Load voltage magnitude response to a step load change.

indicated in Table 8.7 on Page 139. At t = 100 [s], the active and reactive power reference values for the energy storage device are reduced by 35% so that $P_{ref,es}$ = 70 [kW] and $Q_{ref,es}$ = 52.5 [kVAR]. The dispatch of the devices changes: the generator changes from S_{g1} = 29 + j6.8 [kVA] to S_{g1} = 38 + j4.0 [kVA], and the energy storage device changes from S_{es} = 73 + j70 [kVA] to S_{es} = 65 + j74 [kVA]. The power responses are shown in Figure 8.15, and frequency response is shown in Figure 8.16.

While the simulations indicate stable response, certain combinations of power references lead to unstable simulations. For example, if set–points for the energy storage device are less than 0.7 [pu] of the device rating while the generator set–point remain at 1.0 [pu], the simulations indicated instability. However, simulations where the energy storage set–points remain at 1.0 [pu] were stable even when the generator set–points dropped to 0 [pu]. With proper vetting, restricted ranges would ensure stable operation over a broad range of load values.

Table 8.7: Reference Values

Symbol	Definition	Value
ω_{ref}	Frequency	1 [pu]
$P_{ref,g1}$	Generator 1 Active Power	40 [kW]
$v_{ref,g1}$	Generator 1 Terminal Voltage	480 [V]
$Q_{ref,g1}$	Generator 1 Reactive Power	30 [kVAR]
$P_{ref,es}$	Energy Storage Active Power	100 [kW]
$v_{ref,es}$	Energy Storage Voltage	208 [V]
$Q_{ref,es}$	Energy Storage Reactive Power	75 [kVAR]
$P_{ref,tot}$	$P_{ref,g1} + P_{ref,es}$	140 [kW]
$Q_{ref,tot}$	$Q_{ref,g1} + Q_{ref,es}$	105 [kVAR]
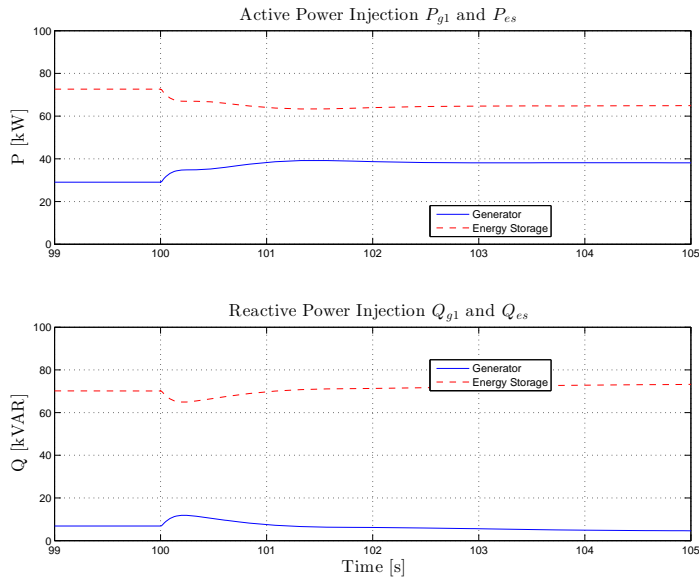
Figure 8.15: Changes in generator and energy storage power output in response to step changes in energy storage active and reactive power set–points.
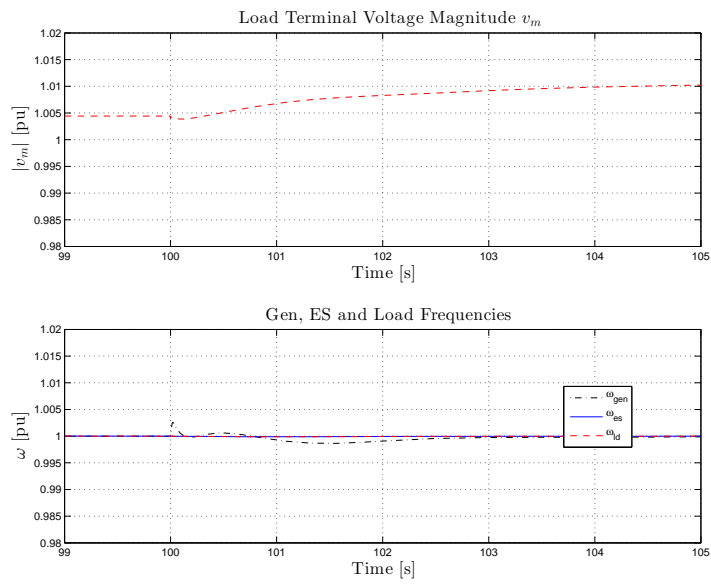
Figure 8.16: Frequency change in response to step changes in energy storage active and reactive power set–points.

Chapter 9

Conclusions

The scope of the work is represented by the

- development of a mathematical model for a salient pole, 2 damper winding synchronous generator with d axis saturation suitable for transient analysis,

- the development of a mathematical model for a voltage regulator and excitation system using the IEEE AC8B voltage regulator ans excitation system template,

- development of mathematical models for an energy storage primary control system, LC filter and transformer suitable for transient analysis,

- combination of generator and energy storage models in a micro–grid context,

- development of mathematical models for electric system components in the stationary abc frame and rotating dq reference frame,

- development of a secondary control network for dispatch of micro–grid assets,

- establishment of micro–grid limits of stable operation for step changes in load and power commands based on simulations assuming net load on the micro–grid, and

- use of generator and electric system models to assess the generator current magnitude during phase–to–ground faults.

Areas where further research is warranted are

- Model validation of the component and composite generator systems: permanent magnet generator, exciter and main generator. This should include load application and rejection, 3 phase fault inception, and phase–to–neutral fault inception.

- Model validation of the energy storage system.

- Implementation of the secondary control network in a micro–grid context and performance validation.

- Investigation of micro–grid stability when the energy storage device is in charging mode.

Bibliography

[1] IEEE Recommended Practice for Electric Power Distribution for Industrial Plants. *IEEE Std. 141–1993*, pages i –744, 1993.

[2] IEEE Recommended Practices for Protection and Coordination of Industrial and Commercial Power Systems. *IEEE Std. 242–2001*, pages i –739, 2001.

[3] IEEE Guide for Synchronous Generator Modeling Practices and Applications in Power System Stability Studies. *IEEE Std. 1110–2002*, pages i –72, 2002.

[4] IEEE Recommended Practice for Excitation System Models for Power System Stability Studies. *IEEE Std. 421.5–2005*, pages i –85, 2005.

[5] IEEE Recommended Practice for Grounding of Industrial and Commercial Power Systems. *IEEE Std. 142–2007*, pages i –215, 2007.

[6] P. M. Anderson and A. A. Fouad. *Power System Control and Stability, Second Edition.* John Wiley and Sons, Inc., New York, New York, 2003.

[7] T. Bach, D. Wohner, K. Takahashi, K. Hattori, M. Liese, and W. Hofmann. Determining Negative Sequence Currents of Turbine Generator Rotors. In *Electric Machines and Systems, 2009. ICEMS 2009. International Conference on*, pages 1–6, 2009.

[8] K. H. Chan, E. Acha, M. Madrigal, and J. A. Parle. The Use of Direct Time–Phase Domain Synchronous Generator Model in Standard EMTP–Type Industrial Packages. *Power Engineering Review*, 21, Issue 6:63–65, June 2001.

[9] Chien-Lang Chen, Yubin Wang, Jih-Sheng Lai, Yuang-Shung Lee, and Daniel Martin. Design of Parallel Inverters for Smooth Mode Transfer Microgrid Applications. *Power Electronics, IEEE Transactions on*, 25, Issue 1:6–15, January 2014.

[10] Manjula Dewadasa, Ritwik Majumder, Arindam Ghosh, and Gerard Ledwich. Control and Protection of a Microgrid with Converter Interfaced Micro Sources. In *Power Systems, 2009. ICPS '09. International Conference on*, pages 1–6, 2009.

[11] Donald. J. Dobner and Roger. D. Fruechte. An Engine Model for Dynamic Engine Control Development. In *American Control Conference, 1983*, pages 73–78, 1983.

[12] C. L. Fortescue. Method of Symmetrical Co-Ordinates Applied to the Solution of Polyphase Networks. *American Institute of Electrical Engineers, Transactions of the*, XXXVII, No. 2:1027–1140, July 1918.

[13] John J. Grainger and William D. Stevenson. *Power System Analysis*. McGraw–Hill, New York, New York, 1994.

[14] Paul C. Krause, Oleg Wasynczuk, and Scott D. Sudhoff. *Analysis of Electric Machinery*. Institute of Electrical and Electronic Engineers, Inc., New York, New York, 1995.

[15] Paul C. Krause, Oleg Wasynczuk, and Scott D. Sudhoff. *Analysis of Electric Machinery and Drive Systems, Second Edition*. John Wiley and Sons, Inc., New York, New York, 2002.

[16] Prabha Kundur. *Power System Stability and Control*. McGraw–Hill, Inc., New York, New York, 1994.

[17] R. H. Lasseter, J. H. Eto, B. Schenkman, J. Stevens, H. Vollkommer, D. Klapp, E. Linton, H. Hurtado, and J. Roy. CERTS Microgrid Laboratory Test Bed. *Power Delivery, IEEE Transactions on*, 26, No. 1:325–332, January 2011.

[18] Robert H. Lasseter. CERTS Microgrid. In *System of Systems, 2007 IEEE International Conference on*, pages 1–5, 2007.

[19] R. F. Lawrence and R. W. Ferguson. Generator Negative–Sequence Currents for Line–to–Line Faults. In *Power Apparutus and Systems, Part III. Transactions of the American Institute of Electrical Engineers*, volume 72, pages 9–16, 2009.

[20] J. Liang, T. C. Green, G. Weiss, and Q. C. Zhong. Hybrid Control of Multiple Inverters in an Island–Mode Distribution System. In *Power Electronics Specialist Conference, 2003. PESC '03. 2003 IEEE 34th Annual*, volume 1, pages 61–66, 2003.

[21] M. N. Marwali, Jin-Woo Jung, and A. Keyhani. Control of distributed generation systems–Part II: Load sharing control. *Power Electronics, IEEE Transactions on*, 19, Issue 6:1551–1561, November 2004.

[22] NEMA. National Electrical Manufacturers Association Standard MG 1-2009. 2009.

[23] Neil Nichols. The Electrical Considerations in Cogeneration. *IEEE Journal of Industry Applications*, IA-21, No. 4:754–761, May/June 1985.

[24] Hassan Nikkhajoei and Robert H. Lasseter. Distributed Generation Interface to the CERTS Microgrid. *Power Delivery, IEEE Transactions on*, 24, No. 3:1598–1608, July 2009.

[25] Central Station Engineers of the Westinghouse Electric Corporation. *Electrical Transmission and Distribution Reference Book*. Westinghouse Electric Corporation, East Pittsburgh, Pennsylvania, 1964.

[26] Chee Mun Ong. *Dynamic Simulation of Electric Machinery Using Matlab®/Simulink*. Prentice–Hall, Inc., Upper Saddle River, New Jersey, 1998.

[27] Gerardus C. Paap. Symmetrical Components in the Time Domain and Their Application to Power Network Calculations. *IEEE Transactions on Power Systems*, 15, No. 2:522–528, May 2000.

[28] R. H. Park. Two–Reaction Theory of Synchronous Machines. In *American Institute of Electrical Engineers, Transactions of the*, volume 48, pages 716–727, 1929.

[29] B. K. Powell. A Dynamic Model for Automotive Engine Control Analysis. In *Decision and Control including the Symposium on Adaptive Proceses, 1979 18th IEEE Conference on*, volume 2, pages 120–126, 1979.

[30] Romeu Reginatto and Rodrigo A. Ramos. On electrical power evaluation in dq coordinates under sinusoidal unbalanced conditions. *Generation, Transmission and Distribution, IET 2014*, 8, Issue 5:976–982, July 2014.

[31] O. Rodriguez and A. Medina. Synchronous Machine Stability Analysis Using an Efficient Time Domain Methodology: Unbalanced Operation Analysis. *Power Engineering Society Summer Meeting, 2002 IEEE*, 2:677–681, July 2002.

[32] O. Rodriguez and A. Medina. Efficient methodology for stability analysis of synchronous machines. *Generation, Transmission and Distribution, IEE Proceedings on*, 150, Issue 4:405–412, June 2003.

[33] Rodrigo Hartstein Salim and Rodrigo Andrade Ramos. A Framework for Analyzing the Small–Signal Dynamic Perfromance of Unbalanced Power Systems. In *Power and Energy Society General Meeting, 2011 IEEE*, pages 1–8, 2011.

[34] Rodrigo Hartstein Salim and Rodrigo Andrade Ramos. A Model Based Approach for Small–Signal Stability Assessment of Unbalanced Power Systems. *Power Systems, Transactions on*, 27, No 4:2006–2014, November 2012.

[35] Ashishkumar Solanki, Adel Nasiri, Vijay Bhavaraju, Yakov Familiant, and Qiang Fu. A New Framework for Microgrid Management: Virtual Droop Control. *Smart Grid, IEEE Transactions on*, 7, Issue 2:554–566, March 2016.

[36] Liwei Wang, Juri Jatskevich, and Hermann W. Dommel. Re–examination of Synchronous Machine Modeling Techniques for Electromagnetic Transient Simulations. *Power Systems, IEEE Transactions on*, 22, No. 3:1221–1230, August 2007.

[37] Frank A. Woodbury. Grounding Considerations in Cogeneration. *IEEE Journal of Industry Applications*, IA-21, No. 6:1523–1532, November/December 1985.

[38] Dan Wu, Fen Tang, Tomislav Dragicevic, Juan C. Vasquez, and Josep M. Guerrero. A Control Architecture to Coordinate Renewable Energy Sources and Energy Storage Systems in Islanded Microgrids. *Smart Grid, IEEE Transactions on*, 6, Issue 3:1156–1166, May 2015.

Appendix A: Calculating $\dot{\boldsymbol{P}}\boldsymbol{P}^{-1}$

In transforming circuit equations from abc to dq0 coordinates, evaluation of $\dot{\boldsymbol{P}}\boldsymbol{P}^{\text{-1}}$ is required. Taking the time derivative of (5.4):

$$\dot{\boldsymbol{P}} = \sqrt{2/3} \begin{bmatrix} 0 & 0 & 0 \\ -\omega\sin\left(\omega t\right) & -\omega\sin\left(\omega t - 2\pi/3\right) & -\omega\sin\left(\omega t + 2\pi/3\right) \\ \omega\cos\left(\omega t\right) & \omega\cos\left(\omega t - 2\pi/3\right) & \omega\cos\left(\omega t + 2\pi/3\right) \end{bmatrix} \tag{A1}$$

And the inverse of (5.4) is:

$$\boldsymbol{P}^{\text{-1}} = \sqrt{2/3} \begin{bmatrix} 1/\sqrt{2} & \cos\left(\omega t\right) & \sin\left(\omega t\right) \\ 1/\sqrt{2} & \cos\left(\omega t - \frac{2\pi}{3}\right) & \sin\left(\omega t - \frac{2\pi}{3}\right) \\ 1/\sqrt{2} & \cos\left(\omega t + \frac{2\pi}{3}\right) & \sin\left(\omega t + \frac{2\pi}{3}\right) \end{bmatrix} \tag{A2}$$

Calculation of first row terms a_{11}, a_{12} and a_{13} in $\dot{\boldsymbol{P}}\boldsymbol{P}^{\text{-1}}$ is trivial, resulting in three entires of zero (0). The terms a_{21} and a_{31} in column 1 are also trivial being the sum of three (3) sinusoids of equal magnitude displaced by $\frac{2\pi}{3}$ [radians]. The main diagonal terms are:

$$a_{22} = -a_{33} = -\frac{2\omega}{3}\left[\sin\left(\omega t\right)\cos\left(\omega t\right)\right.$$
$$+ \sin\left(\omega t - \frac{2\pi}{3}\right)\cos\left(\omega t - \frac{2\pi}{3}\right) \tag{A3}$$
$$\left. + \sin\left(\omega t + \frac{2\pi}{3}\right)\cos\left(\omega t + \frac{2\pi}{3}\right)\right]$$

Invoking Euler's identity:

$$\cos\left(\theta\right) = \frac{1}{2}\left(e^{j\theta} + e^{-j\theta}\right)$$
$$\sin\left(\theta\right) = \frac{1}{2j}\left(e^{j\theta} - e^{-j\theta}\right) \tag{A4}$$

Multiplying the two lines of (A4) together:

$$\sin(\theta)\cos(\theta) = \frac{1}{4j}\left(e^{j\theta} + e^{-j\theta}\right)\left(e^{j\theta} - e^{-j\theta}\right)$$
$$= \frac{1}{4j}\left(e^{j2\theta} - e^{-j2\theta} + 1 - 1\right) \tag{A5}$$
$$= \frac{1}{2}\sin(2\theta)$$

Substituting (A5) into (A3):

$$a_{22} = -a_{33} = -\frac{2\omega}{3}\left\{\frac{1}{2}\left[\sin(2\omega t) + \sin\left(2\omega t - \frac{4\pi}{3}\right) + \sin\left(2\omega t + \frac{4\pi}{3}\right)\right]\right\} \tag{A6}$$

And terms a_{22} and a_{33} are zero (0) being the sum of three (3) equal magnitude sinusoidal signals displaced by $\frac{2\pi}{3}$ [radians]. Moving to term a_{23}:

$$a_{23} = -\frac{2\omega}{3}\left[\sin^2(\omega t) + \sin^2\left(\omega t - \frac{2\pi}{3}\right) + \sin^2\left(\omega t + \frac{2\pi}{3}\right)\right] \tag{A7}$$

Invoking (A4) a second time:

$$\sin^2(\theta) = \left(\frac{1}{2j}\right)^2\left(e^{j\theta} - e^{-j\theta}\right)\left(e^{j\theta} - e^{-j\theta}\right)$$
$$= -\frac{1}{4}\left(e^{j2\theta} + e^{-j2\theta} - 1 - 1\right) \tag{A8}$$
$$= -\frac{1}{2}\left[\cos(2\theta) - 1\right]$$

Substituting (A8) into (A7):

$$a_{23} = \frac{2\omega}{3}\frac{1}{2}\left[\cos(2\omega t) - 1 + \cos\left(2\omega t - \frac{4\pi}{3}\right) - 1 + \cos\left(2\omega t + \frac{4\pi}{3}\right) - 1\right] = -\omega \tag{A9}$$

Where in (A9) the sinusoidal terms sum to zero (0). Evaluating term a_{32}:

$$a_{32} = \frac{2\omega}{3}\left[\cos^2(\omega t) + \cos^2\left(\omega t - \frac{2\pi}{3}\right) + \cos^2\left(\omega t + \frac{2\pi}{3}\right)\right] \tag{A10}$$

Invoking (A4) a third time:

$$\cos^2(\theta) = \left(\frac{1}{2}\right)^2 \left(e^{j\theta} + e^{-j\theta}\right)\left(e^{j\theta} + e^{-j\theta}\right)$$

$$= \frac{1}{4}\left(e^{j2\theta} + e^{-j2\theta} + 1 + 1\right) \tag{A11}$$

$$= \frac{1}{2}\left[\cos(2\theta) + 1\right]$$

Substituting (A11) into (A10):

$$a_{32} = \frac{2\omega}{3}\frac{1}{2}\left[\cos(2\omega t) + 1 + \cos\left(2\omega t - \frac{4\pi}{3}\right) + 1 + \cos\left(2\omega t + \frac{4\pi}{3}\right) + 1\right] = \omega \tag{A12}$$

Where in (A12) the sinusoidal terms sum to zero (0). In matrix form

$$\dot{P}P^{-1} = \begin{bmatrix} 0 & 0 & 0 \\ 0 & 0 & -\omega \\ 0 & \omega & 0 \end{bmatrix} \tag{A13}$$

Appendix B: Parameter Tables

Parameter	Value	Description
X_q	0.883 [pu]	q axis synchronous reactance
X_l	0.063 [pu]	armature leakage reactance
R_l	0.52 [mΩ]	armature line–neutral resistance
X'_d	0.124 [pu]	d axis transient reactance
R_f	1.509 [Ω]	field winding resistance
X_{lD}	0.0836 [pu]	stator referred d axis damper leakage reactance
X_{lQ}	0.0738 [pu]	stator referred q axis damper leakage reactance
X_{lF}	0.129 [pu]	stator referred field axis damper leakage reactance
T_{st}	0.024 [s]	subtransient short circuit time constant

Table A1: Parameters for the Regal Beloit 2.57 [MVA], 480 [V], 0.85 pf, 60 [Hz], 1800 [rpm] synchronous generator.

Parameter	Value	Description
K_A	290 [·]	regulator voltage gain
T_A	0 [s]	regulator time constant
V_{RMIN}	0 [V]	PM generator lower voltage limit
V_{RMAX}	275.5 [V]	PM generator upper voltage limit
T_E	0.14 [s]	self excited time constant
K_E	0 [·]	self excited constant
K_D	0.57 [A⁻¹]	exciter demagnetizing factor
K_C	0.53 [·]	rectifier loading factor related to commutating reactance
V_{EMIN}	0 [V]	exciter lower voltage limit

Table A2: Parameters for the Regal Beloit AC8B Excitation System Model.

Parameter	Value	Description
X_d	3.087 [pu]	d axis synchronous reactance
X_q	1.506 [pu]	q axis synchronous reactance
R_l	4.8 [mΩ]	armature line–neutral resistance
X'_{du}	0.358 [pu]	unsaturated transient reactance
X'_d	0.315 [pu]	saturated transient reactance
X''_d	0.160 [pu]	unsaturated transient reactance
X''_q	0.141 [pu]	saturated transient reactance
R_f	2.610 [Ω]	field winding resistance
X_2	0.150 [pu]	negative sequence reactance
X_0	0.012 [pu]	zero sequence reactance

Table A3: Parameters for the Kohler REZG40, 50 [kVA], 480 [V], 0.85 pf, 60 [Hz], 1800 [rpm] synchronous generator.

Parameter	Value	Description
L_{ad}	1.66 [pu]	d axis mutual inductance
L_{aq}	1.61 [pu]	q axis mutual inductance
L_l	0.15 [pu]	armature leakage reactance
R_a	0.003 [pu]	armature resistance
L_{fd}	0.165 [pu]	field leakage inductance
R_{fd}	0.0006 [pu]	field resistance
L_{1d}	0.1713 [pu]	d axis damper leakage inductance
R_{1d}	0.0284 [pu]	d axis damper resistance
L_{1q}	0.7252 [pu]	q axis damper 1 leakage inductance
R_{1q}	0.00619 [pu]	q axis damper 1 resistance
L_{2q}	0.125 [pu]	q axis damper 2 leakage inductance
R_{2q}	0.02368 [pu]	q axis damper 2 resistance

Table A4: Parameters taken from [16] Chapter 3 for a 555 [MVA], 24 [kV], 0.9 pf, 60 [Hz], 3600 [rpm] turbine–generator.

		Pos & Neg Sequence			Zero Sequence		
Volt.	Cond.	Series	Series	Shunt	Series	Series	Shunt
Class	Size	R	X	C	R	X	C
$[kV]$		$[\frac{\Omega}{mile}]$	$[\frac{\Omega}{mile}]$	$[\frac{\Omega}{mile}]$	$[\frac{\Omega}{mile}]$	$[\frac{\Omega}{mile}]$	$[\frac{\Omega}{mile}]$
1	#2 [AWG]	0.987	0.165	4700	6.99	0.273	9000
1	500 [MCM]	0.134	0.123	1300	3.11	0.208	2100

Table A5: Cable parameters taken from [25] Table 6 Chapter 4 page 79.

Appendix C: Time Based Linearizations

To extract stability information, linearizing non–linear energy storage device and generator models at desirable operating points may be employed. To assure development of the correct model, one of several techniques is used:

1. Manual calculation using maxim

2. Model linearization using Matlab® and Simulink®

3. Extraction of the numerical Jacobian from the selected Matlab® ordinary differential equation algorithm using the *numjac* function

A second order system was used to validate the methodologies. Given the system described by the set of equations:

$$\dot{x}_1 = -x_1 + 2x_1^3 + x_2 + u$$
$$\dot{x}_2 = -x_1 - x_2^2$$

(A14)

with output defined as

$$y = x_1$$

(A15)

find the state space model of the system at equilibrium when $u = 0.1$.

Setting the left side of (A14) to zero (0) and solving the two equations

$$-x_1 + 2x_1^3 + x_2 + 0.1 = 0$$
$$x_1 = -x_2^2$$

(A16)

Substituting $-x_2^2$ for x_1:

$$2x_2^6 - x_2^2 - x_2 - 0.1 = 0$$

(A17)

yields two real–valued solutions for x_2. The two equilibrium points are[1]

1. $x(1) = [-0.012700 \quad -0.112696]^T$

2. $x(2) = [-1.021584 \quad 1.010734]^T$

To arrive at the small signal state space model, first order Taylor's series expansion Jacobian matrices are formed and evaluated at x(1)

$$
\begin{aligned}
a &= \left.\frac{\partial \dot{x}}{\partial x}\right|_{x=x(1)} = \left.\begin{bmatrix} -1 + 6x_1^2 & 1 \\ -1 & -2x_2 \end{bmatrix}\right|_{x=x(1)} = \begin{bmatrix} -0.999032 & 1 \\ -1 & 0.225393 \end{bmatrix} \\
b &= \left.\frac{\partial \dot{x}}{\partial u}\right|_{x=x(1)} = \begin{bmatrix} 1 \\ 0 \end{bmatrix} \\
c &= \left.\frac{\partial y}{\partial x}\right|_{x=x(1)} = \begin{bmatrix} 1 & 0 \end{bmatrix} \\
d &= \left.\frac{\partial y}{\partial u}\right|_{x=x(1)} = \begin{bmatrix} 0 \end{bmatrix}
\end{aligned}
\tag{A18}
$$

The Simulink® non–linear model realization is shown in Figure A1 on Page 157 and simulation results with initial conditions set to zero (0) are shown in Figure A2 on Page 158. The time–based linearization occurs at $t = 30\,[seconds]$, and the equilibrium point values for x_1 and x_2 are shown in Figure A2 on Page 158. For initial conditions of zero (0), the simulated equilibrium point corresponds to that calculated for $x_2(1)$ and $x_1(1)$

---

[1]The equilibrium point corresponding to x(1) is stable with eigenvalues at -0.385 ± 0.7904, while equilibrium point x(2) is unstable with eigenvalues at -1.8815 and 5.1218.

The state space matrices are read from the Matlab® workspace

$$a = \begin{bmatrix} -0.999032 & 1 \\ -1 & 0.225393 \end{bmatrix}$$

$$b = \begin{bmatrix} 1 \\ 0 \end{bmatrix}$$

$$c = \begin{bmatrix} 1 & 0 \end{bmatrix}$$ (A19)

$$d = \begin{bmatrix} 0 \end{bmatrix}$$

This demonstrates that the linearized system representations (A18) and (A19) are equivalent.

A third method to extract the numerical Jacobian using the Matlab® function *numjac* yields the simulation results in Figure A3 on Page 159, showing a system response identical to the Simulink® results in Figure A2 on Page 158. Extracting the Jacobian matrix at operating point x(1)

$$a = \begin{bmatrix} -0.999032 & 1 \\ -1 & 0.225395 \end{bmatrix}$$ (A20)

which is the same *a* matrix as in (A18) and (A19) to five (5) significant digits.

156
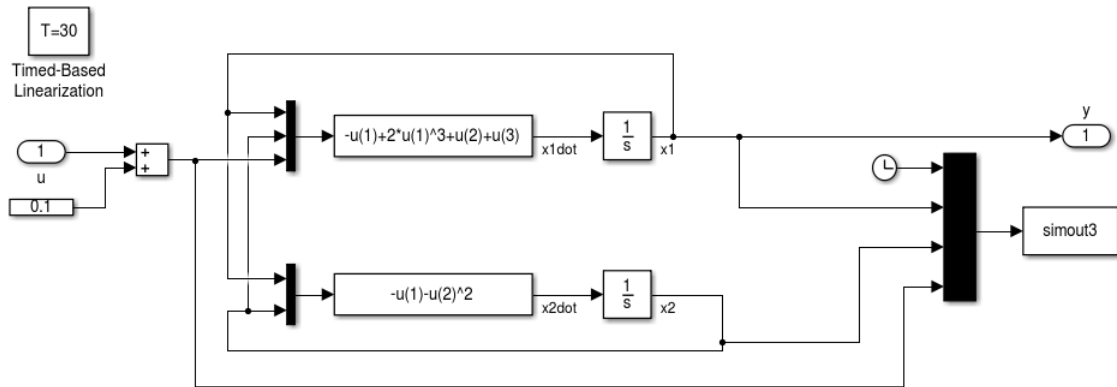
Figure A1: The Simulink® realization of the sample non–linear system.
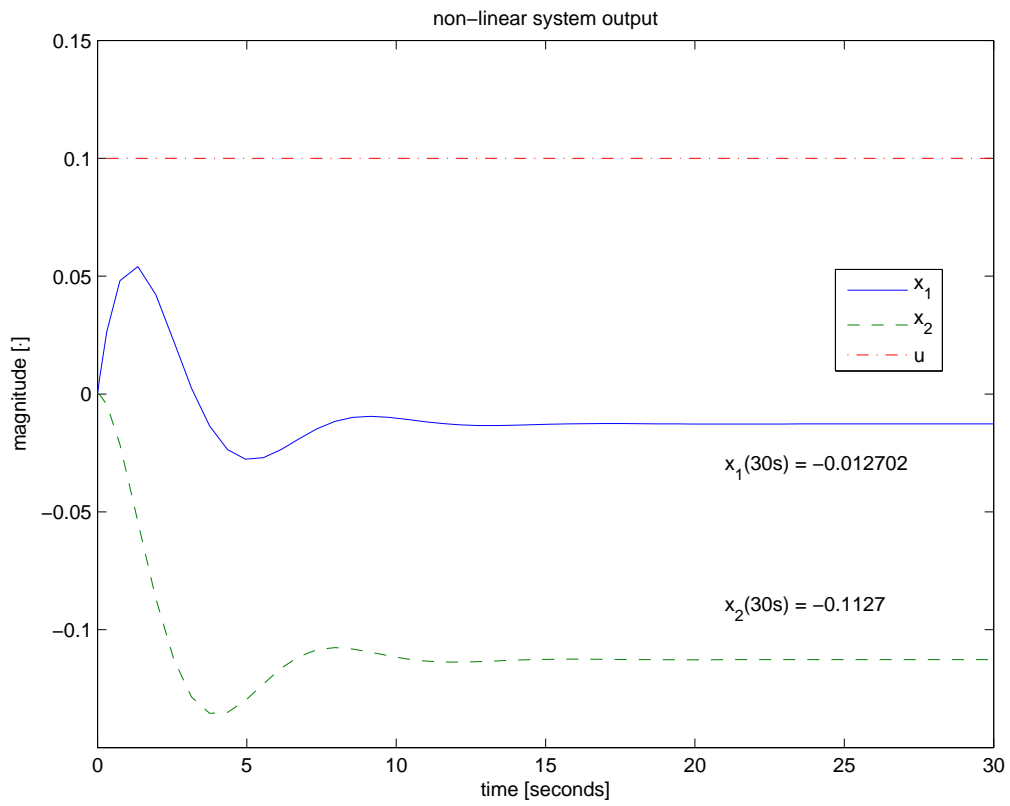
Figure A2: The simulation results for Figure A1.
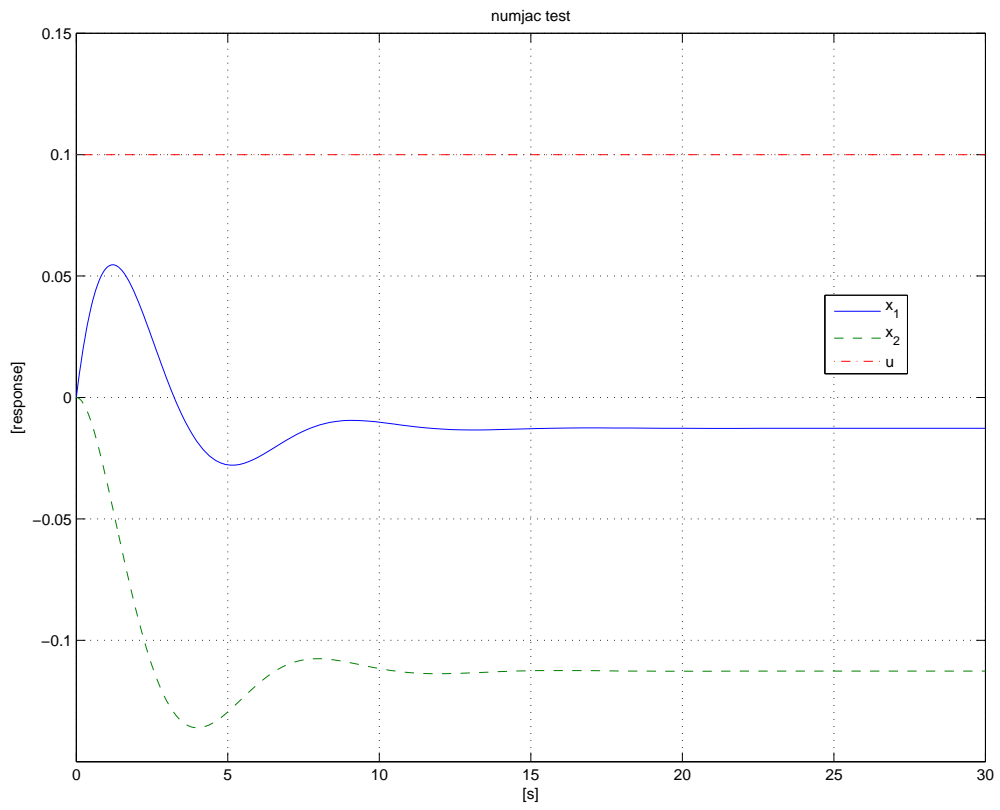
Figure A3: The simulation results for the call to ode23tb in Matlab®.

Appendix D: Matlab® Files and Simulink® Models

Main Matlab® file for simulating four–wire systems:

```
% General simulation of abc three phase system

% System model with generator source modeled in 0dq reference frame

% pid control of generator terminal voltage

% AC8B exciter model

% Line charging at generator terminals

% Line impedance

% Line charging at load end

% Wye connected load

% grid is an infinite source behind an RL impedance connected at load


clear all

tstart = 10;

tinit = tstart;

step = 1e-4;

tplot = 0.1;

tfinal = tstart+tplot;

t = tstart:step:tfinal;


% load('carp9_4b.mat');


% global zed31 zed33 zed62 zed69 zed610 zed35 zed312 zed314 zed621 zed1316

zed32 = zeros(3,2);

zed33 = zeros(3);
```

```
zed62 = zeros(6,2);

zed611 = zeros(6,11);

zed35 = zeros(3,5);

zed312 = zeros(3,12);

zed314 = zeros(3,14);

zed621 = zeros(6,21);

zed1317 = zeros(13,17);


% ig00 = 0; %y1

% igd0 = 0; %y2

% igq0 = 0; %y3

% igF0 = 0; %y4

% igD0 = 0; %y5

% igQ0 = 0; %y6

% w0 = pi*60; %y7

% theta0 = 0; %y8

% vc1a0 = 0; %y9

% vc1b0 = 0; %y10

% vc1c0 = 0; %y11

% iln1a0 = 0; %y12

% iln1b0 = 0; %y13

% iln1c0 = 0; %y14

% vc2a0 = 0; %y15

% vc2b0 = 0; %y16

% vc2c0 = 0; %y17

% ild1a0 = 0; %y18

% ild1b0 = 0; %y19
```

```
% ild1c0 = 0; %y20

% vg1fb0 = 0; %y21

% vg1i0 = 0; %y22

% vg1d0 = 0; %y23

% vg1R0 = 0; %y24

% vg1E0 = 0; %y25

% omegahati0 = 0; %y26

% thetahat0 = 0; %y27

% omegahatlpf0 = 0; %y28

% Pmechg10 = 0; %y29

%

% ic = [ig00 igd0 igq0 igF0 igD0 igQ0 w0 theta0 ...

%        vc1a0 vc1b0 vc1c0 iln1a0 iln1b0 iln1c0 vc2a0 vc2b0 vc2c0 ...

%        ild1a0 ild1b0 ild1c0 vg1fb0 vg1i0 vg1d0 vg1R0 vg1E0 ...

%        omegahati0 thetahat0 omegahatlpf0 Pmechg10]';


load('initcond9_4a.mat');

ic = finstate;


% start the generator isolated from the grid


options = odeset('NonNegative',[24 25],'RelTol',1e-1,'AbsTol',1e-1);


% [s,y] = ode23tb(@abcflow9_4,[tstart tfinal],ic,options); % Solve ODE


    [s,yout]=ode23tb(@abcflow9_4a,[tstart tfinal],ic,options); % Solve ODE
```

```
finstate = yout(length(yout),:)';

% save initcond9_4a_12s_nl_100pu_v.mat finstate;


    tout = s;

    touta = s;

    youta = yout;


%%

[rln1,lln1,c,g,rld1,lld1,rld2,lld2,wco,kipll,kppll,tauf,tevent,...

    tflt,rt,lt,omega] = eps9_4();

[ra,ld,Lq,J,we,kMQ,rF,rD,rQ,lF,lD,LQ,L0,D,rn,Ln,p,kfd,Lmd,p6,s6,mu6,...

    R,taug1,Pmax,pref] = rb_hsg_740066_V9_4();

[kiss,kp,kd,taud,Vrb,Irb,KAow,TA,Vrmax,Vrmin,Vfemax,Vemin,TE,p5,s5,mu5,...

    KE,KD,KC,vrp,vrs,vrmu] = rb_5_inch_exciter9_4();

p= 4;

vg10dq = zeros(length(yout),3);

ig1abc = zeros(length(yout),3);

pang = zeros(length(yout),3);

% pout = zeros(length(yout),3);

% qout = zeros(length(yout),3);

for n = 1:length(yout);

vg10dq(n,:) = sqrt(2/3)*[1/sqrt(2) 1/sqrt(2) 1/sqrt(2);...

cos(p/2*yout(n,8)+pi/2) cos(p/2*yout(n,8)-pi/6) cos(p/2*yout(n,8)+7*pi/6);...

sin(p/2*yout(n,8)+pi/2) sin(p/2*yout(n,8)-pi/6) sin(p/2*yout(n,8)+7*pi/6)]...

*yout(n,9:11)';

ig1abc(n,:) = sqrt(2/3)*[1/sqrt(2) 1/sqrt(2) 1/sqrt(2);...

cos(p/2*yout(n,8)+pi/2) cos(p/2*yout(n,8)-pi/6) cos(p/2*yout(n,8)+7*pi/6);...
```

```
sin(p/2*yout(n,8)+pi/2) sin(p/2*yout(n,8)-pi/6) sin(p/2*yout(n,8)+7*pi/6)]...

\yout(n,1:3)';

pout(n,1) = vg10dq(n,1:3)*yout(n,1:3)';

qout(n,1) = -vg10dq(n,3)*yout(n,2)+vg10dq(n,2)*yout(n,3);

pang(n,1) = 2*yout(n,8)-yout(n,27);

end


tem = pout./yout(:,7);

pouta = pout;

qouta = qout;

tema = tem;

vg10dqa = vg10dq;

ig1abca = ig1abc;

panga = pang;

% save data9_4a_slgf_nl_3mva7_5pct_lowzs.mat touta youta vg10dqa ig1abca panga;

% save data9_4a_1pgt3mva5pct_lowzs.mat touta youta vg10dqa ig1abca panga;

% save data9_4a_1pgt_ng.mat touta youta vg10dqa ig1abca panga;



%%


% find an angle for synchronizing to the grid

theta = -pi:2*pi/1000:pi;

vs0 = 480*sqrt(2/3)*[cos(theta); cos(theta-2*pi/3); cos(theta+2*pi/3)];

for m = 1:length(theta);

    err(m) = norm(vs0(1:3,m)-finstate(15:17));

end
```

```
errtrac = 1e5;

for q = 1:length(err)-1;

    if err(q+1) < errtrac;

        errtrac = err(q+1);

        count = q+1;

    else

    end

end

global teta

teta = theta(count);

save theta9_4a.mat teta;




% tfinal = 12;

tstart1 = tfinal;

tinit  = tfinal;

tsim = 0.5;

tfinal = tfinal+tsim;


ita0 = 0; %y30

itb0 = 0; %y31

itc0 = 0; %y32


ic = [finstate; ita0; itb0; itc0];


% load('initcond9_4b_12s_nl.mat')

% ic = finstate;
```

```
% connect the generator to the grid and continue simulation

clear yout teout yeout ieout
options = odeset('NonNegative',[24 25],'RelTol',1e-1,'AbsTol',1e-1);


    [s,yout]=ode23tb(@abcflow9_4b,[tstart1 tstart1+tsim],ic,options);


%     tstart1 = s(nt);


finstate = yout(length(yout),:)';
% save initcond9_4b_13s_nl.mat finstate;
%     tout = s;
    toutb = s;
    youtb = yout;



%%
p = 4;
vg10dq = zeros(length(yout),3);
ig1abc = zeros(length(yout),3);
pang = zeros(length(yout),3);
vs = zeros(length(yout),3);
for n = 1:length(yout);
vg10dq(n,:) = sqrt(2/3)*[1/sqrt(2) 1/sqrt(2) 1/sqrt(2);...
cos(p/2*yout(n,8)+pi/2) cos(p/2*yout(n,8)-pi/6) cos(p/2*yout(n,8)+7*pi/6);...
sin(p/2*yout(n,8)+pi/2) sin(p/2*yout(n,8)-pi/6) sin(p/2*yout(n,8)+7*pi/6)]...
```

```
*yout(n,9:11)';
ig1abc(n,:) = sqrt(2/3)*[1/sqrt(2) 1/sqrt(2) 1/sqrt(2);...
cos(p/2*yout(n,8)+pi/2) cos(p/2*yout(n,8)-pi/6) cos(p/2*yout(n,8)+7*pi/6);...
sin(p/2*yout(n,8)+pi/2) sin(p/2*yout(n,8)-pi/6) sin(p/2*yout(n,8)+7*pi/6)]...
\yout(n,1:3)';
pout(n,1) = vg10dq(n,1:3)*yout(n,1:3)';
qout(n,1) = -vg10dq(n,3)*yout(n,2)+vg10dq(n,2)*yout(n,3);
pang(n,1) = 2*yout(n,8)-yout(n,27);
end


tem = pout./yout(:,7);
poutb = pout;
qoutb = qout;
temb = tem;
vg10dqb = vg10dq;
ig1abcb = ig1abc;
pangb = pang;


% save data9_4b_1pgt3mva5pct_lowzs.mat toutb youtb vg10dqb ig1abcb pangb;
% save data9_4b_1pgt_ng.mat toutb youtb vg10dqb ig1abcb pangb;
%
% % tout = s;
tout = [touta; toutb];
len = length(tout);
yout = zeros(len,length(finstate));
yout(1:length(touta),1:29) = youta;
yout(length(touta)+1:len,1:length(finstate)) = youtb;
```

```
vg10dq = [vg10dqa; vg10dqb];

ig1abc = [ig1abca; ig1abcb];

% pout = [pouta; poutb];

% qout = [qouta; qoutb];

% tem = [tema; temb];

pang = [panga; pangb];
```

Matlab® file abcflow9_4a.m

```matlab
function dy = abcflow9_4a(t,y)
%%%%%%%%%%%%%%%%%%%%%%%%%%%%%%%%%
[rln1,lln1,c,g,rld1,lld1,rldf2,lld2,wco,kipll,kppll,tauf,tevent,tflt,...
    rt,lt,omega] = eps9_4();
[ra,ld,Lq,J,we,kMQ,rF,rD,rQ,lF,lD,LQ,L0,D,rn,Ln,p,kfd,Lmd,p6,s6,mu6,...
    R,taug1,Pmax,pref] = rb_hsg_740066_V9_4();
[kiss,kp,kd,taud,Vrb,Irb,KAow,TA,Vrmax,Vrmin,Vfemax,Vemin,TE,p5,s5,mu5,...
    KE,KD,KC] = rb_5_inch_exciter9_4();
if t<=tevent;
    r1 = rld1;
    l1 = lld1;
else
    if (tevent<t)&&(t<=tevent+tflt);
        r1 = rldf2;
        l1 = lld2;
    else
        r1 = rld1;
        l1 = lld1;
    end
end


vref = 1;
% bring generator voltage and power up in 3 seconds
if t<=3;
    vr = vref*t/3;
    prefg1 = pref*t/3;
```

```
    ki=0;
else
    vr = vref;
    ki=kiss;
    prefg1 = pref;
end


% avoid division by 0
if TA == 0;
    TA = 1e-3;
end


ki=kiss;
prefg1 = pref;



% enable for generating open circuit characteristics
% if t<=40.01;
%     vr = 1.10*vref;
% else if (40.01<t)&&(t<=41);
%         vr = 1.10*vref+0.05*(t-40);
%     else if (41<t)&&(t<=45);
%             vr = 1.15;
%         else if (45.01<t)&&(t<=46);
%                 vr = 1.15+0.05*(t-45);
%             else vr = 1.2;
%             end
```

```matlab
%          end
%      end
% end


zed33 = zeros(3);

zed62 = zeros(6,2);

zed35 = zeros(3,5);

zed39 = zeros(3,9);

zed618 = zeros(6,18);

zed1312 = zeros(13,12);


Irb = Irb*kfd;

Vrb = Vrb/kfd;


% commutation calculations associated with AC8B model
IN = KC*(y(4)/Irb)/y(25);
if IN<=0.433;
    FEX = 1-(1/sqrt(3)*IN);
else
    if (IN>0.433)&&(IN<=0.75);
        FEX = sqrt(0.75-IN);
    else
        if (IN>0.75)&&(IN<=1.0);
            FEX = sqrt(3)*(1.0-IN);
        else
            FEX = 0;
```

```
            end

        end

    end


% u = [1vg10in 2vg1din 3vg1qin 4vg1Fin 5vg1Din 6vg1Qin 70 8~Pin 9VFEmult

%10g1vrefpu 11Prefg1pu 12wrefpu 13Prefespu 14Qrefespu 15Qrefg1pu 16vesref]'


u = [0; 0; 0; FEX*y(25)*Vrb; 0; 0; 0; 1; 1; vr; prefg1; 1];


LAD = polyval(p6,480*y(21),s6,mu6);


    rgen = [ra+3*rn 0 0 0 0 0

        0 ra we*Lq 0 0 we*kMQ

        0 -we*(ld+LAD) ra -we*LAD -we*LAD 0

        0 0 0 rF 0 0

        0 0 0 0 rD 0

        0 0 0 0 0 rQ];


    lgen = [L0+3*Ln 0 0 0 0 0

        0 ld+LAD 0 LAD LAD 0

        0 0 Lq 0 0 kMQ

        0 LAD 0 lF+LAD LAD 0

        0 LAD 0 LAD lD+LAD 0

        0 0 kMQ 0 0 LQ];


lgeni = lgen\eye(6);
```

```
% NL first order DE
dy = [-lgen\rgen zed62 [-sqrt(2/3)*lgeni(1:3,1:3)*...
    [1/sqrt(2) 1/sqrt(2) 1/sqrt(2);...
    cos(p/2*y(8)+pi/2) cos(p/2*y(8)-pi/6) cos(p/2*y(8)+7*pi/6);...
    sin(p/2*y(8)+pi/2) sin(p/2*y(8)-pi/6) sin(p/2*y(8)+7*pi/6)]
    -sqrt(2/3)*lgeni(4:6,1:3)*[1/sqrt(2) 1/sqrt(2) 1/sqrt(2);...
    cos(p/2*y(8)+pi/2) cos(p/2*y(8)-pi/6) cos(p/2*y(8)+7*pi/6);...
    sin(p/2*y(8)+pi/2) sin(p/2*y(8)-pi/6) sin(p/2*y(8)+7*pi/6)]]...
    zed618 % 1 to 6 [ig10 ig1d ig1q ig1F ig1D ig1Q]'
    -1/(sqrt(3)*J*y(7))*(y(9)+y(10)+y(11))...
    -sqrt(2)/(sqrt(3)*J*y(7))*(y(9)*cos(p/2*y(8)+pi/2)...
    +y(10)*cos(p/2*y(8)-pi/6)+y(11)*cos(p/2*y(8)+7*pi/6))...
    -sqrt(2)/(sqrt(3)*J*y(7))*(y(9)*sin(p/2*y(8)+pi/2)...
    +y(10)*sin(p/2*y(8)-pi/6)+y(11)*sin(p/2*y(8)+7*pi/6))...
    0 0.0 0 -D*y(7)/J 0 0 0.0 ...
    0 0 0 0 0.0 0 0 0 0 0.0 0 0 0 0 0.0 0 0 0 1/(J*y(7)) % 7 [omegam]
    0 0 0 0 0.0 0 1 0 0 0.0 0 0 0 0 0.0 0 0 0 0 0.0...
    0 0 0 0 0.0 0 0 0 0 % 8 [thetam]
    sqrt(2/3)*c\([1/sqrt(2) 1/sqrt(2) 1/sqrt(2);...
    cos(p/2*y(8)+pi/2) cos(p/2*y(8)-pi/6) cos(p/2*y(8)+7*pi/6);...
    sin(p/2*y(8)+pi/2) sin(p/2*y(8)-pi/6) sin(p/2*y(8)+7*pi/6)]\eye(3))...
    zed35 -c\g -c\eye(3) zed33 zed33 zed39 % 9 to 11 [vc1a vc1b vc1c]'
    zed33 zed35 lln1\eye(3) -lln1\rln1 -lln1\eye(3) zed33 zed39...
    % 12 to 14 [iln1a iln1b iln1c]'
    zed33 zed35 zed33 c\eye(3) -c\g -c\eye(3) zed39...
    % 15 to 17 [vc2a vc2b vc2c]'
    zed33 zed35 zed33 zed33 l1\eye(3) -l1\r1 zed39...
```

% 18-20 [ild1a ild1b ild1c]'

0 0 0 0 0.0 0 0 0 0 0.0 0 0 0 0 0.0 0 0 0 0 0.0 0 0 0 0 0.0 0 0 0 0 ...

% 21 [vg1fb]

0 0 0 0 0.0 0 0 0 0 0.0 0 0 0 0 0.0 0 0 0 0 0.0 -ki 0 0 0 0.0 0 0 0 0 ...

% 22 [vg1i*]

0 0 0 0 0.0 0 0 0 0 0.0 0 0 0 0 0.0 0 0 0 0 0.0 0 0 -1/taud...

0 0.0 0 0 0 0 0 % 23 [vg1d*]

0 0 0 0 0.0 0 0 0 0 0.0 0 0 0 0 0.0 0 0 0 0 0.0 ...

-kp*KAow*y(7)/TA KAow*y(7)/TA KAow*y(7)/TA -1/TA 0.0 0 0 0 0 0 % 24 [vg1R]

0 0 0 -KD/(TE*Irb) 0.0 0 0 0 0 0.0 0 0 0 0 0.0 0 0 0 0 0.0 ...

0 0 0 1/TE -(KE/TE) 0 0 0 0 0 % 25 [vg1E]

0 0 0 0 0.0 0 0 0 0 0.0 0 0 0 0 ...

kipll*sqrt(2/3)*cos(y(27)+pi/2) kipll*sqrt(2/3)*cos(y(27)-pi/6)...

kipll*sqrt(2/3)*cos(y(27)+7*pi/6) 0 0 0.0 0 0 0 0 0.0 0 0 0 0 ...

% 26 [omega_hati]

0 0 0 0 0.0 0 0 0 0 0.0 0 0 0 0 ...

kppll*sqrt(2/3)*cos(y(27)+pi/2) kppll*sqrt(2/3)*cos(y(27)-pi/6)...

kppll*sqrt(2/3)*cos(y(27)+7*pi/6) 0 0 0.0 0 0 0 0 0.0 1 0 0 0 ...

% 27 [theta_hat]

0 0 0 0 0.0 0 0 0 0 0.0 0 0 0 0 kppll/tauf*sqrt(2/3)*cos(y(27)+pi/2)...

kppll/tauf*sqrt(2/3)*cos(y(27)-pi/6)...

kppll/tauf*sqrt(2/3)*cos(y(27)+7*pi/6) 0 0 0.0 ...

0 0 0 0 0.0 1/tauf 0 -1/tauf 0 % 28 [omega_hatlpf]

0 0 0 0 0.0 0 -Pmax/(R*taug1*60*pi) 0 0 0.0 0 0 0 0 0.0 0 0 0 0 0.0 ...

0 0 0 0 0.0 0 0 0 -1/taug1]*y+... % 29 [Pmechg1]

[lgeni zed62 zed62 zed62 % 1 to 6 [ig10 ig1d ig1q ig1F ig1D ig1Q]'

0 0 0 0 0.0 0 0 0 0 0.0 0 0 0 % 7 [omegam]

174

```matlab
      zed1312 % 8-20
      0 0 0 0 0 0.0 0 0 0 ...
      wco*(sqrt(((y(9)-y(10))^2+(y(10)-y(11))^2+(y(11)-y(9))^2)/3)/480 ...
      -y(21)) 0.0 0 0 % 21 [vg1fb]
      0 0 0 0 0 0.0 0 0 0 0 ki 0 0 % 22 [vg1i*]
      0 0 0 0 0 0.0 0 0 0 ...
      -(kd/taud)*wco*(sqrt(((y(9)-y(10))^2+(y(10)-y(11))^2+(y(11)...
      -y(9))^2)/3)/480-y(21)) 0.0 0 0 % 23 [vg1d*]
      0 0 0 0 0 0.0 0 0 0 0 kp*KAow*y(7)/TA 0 0 % 24 [vg1R]
      0 0 0 0 0 0.0 0 0 -polyval(p5,y(25),s5,mu5) 0 0.0 0 0 % 25 [vg1E]
      0 0 0 0 0 0.0 0 0 0 0 0.0 0 0 % 26 [omega_hati]
      0 0 0 0 0 0.0 0 0 0 0 0.0 0 0 % 27 [theta_hat]
      0 0 0 0 0 0.0 0 0 0 0 0.0 0 0 % 28 [omega_hatlpf]
      0 0 0 0 0.0 0 0 0 0 0.0 Pmax/taug1 Pmax/(R*taug1)]*u; % 29 [Pmechg1]
return
```

Matlab® file abcflow9_4b.m

```matlab
function dy = abcflow9_4b(t,y)
%%%%%%%%%%%%%%%%%%%%%%%%%%%%%%%%
[rln1,lln1,c,g,rld1,lld1,rld2,lld2,wco,kipll,kppll,tauf,tevent,tflt,...
    rt,lt,omega] = eps9_4();
[ra,ld,Lq,J,we,kMQ,rF,rD,rQ,lF,lD,LQ,L0,D,rn,Ln,p,kfd,Lmd,p6,s6,mu6,R,...
    taug1,Pmax,pref] = rb_hsg_740066_V9_4();
[kiss,kp,kd,taud,Vrb,Irb,KAow,TA,Vrmax,Vrmin,Vfemax,Vfemin,TE,p5,s5,mu5...
    ,KE,KD,KC] = rb_5_inch_exciter9_4();


load('theta9_4a.mat');
% global r1 l1 vr ki prefg1 TA Irb Vrb IN wye24 LAD


if t<=tevent;
    r1 = rld1;
    l1 = lld1;
else
    if (tevent<t)&&(t<=tevent+tflt);
        r1 = rld2;
        l1 = lld2;
    else if tevent+tflt<t;
            r1 = 1e5*rld1;
            l1 = 1e5*lld1;
        end
    end
end
```

176

```matlab
vref = 1;
if t<=3;
    vr = vref*t/3;
    prefg1 = pref*t/3;
    ki=0;
else
    vr = vref;
    ki=kiss;
    prefg1 = pref;
end



if TA == 0;
    TA = 1e-3;
end


Irb = Irb*kfd;
Vrb = Vrb/kfd;

% wye24 = polyval(vrp,y(24),vrs,vrmu);
% wye24 = y(24);
if y(24)<=Vrmin;
    wye24 = Vrmin;
else
    if (y(24)>Vrmin)&&(y(24)<=Vrmax);
        wye24 = y(24);
    else
```

```
        wye24 = Vrmax;

    end

end




Vemax = (Vfemax-kd*y(4)/Irb)/(KE+polyval(p5,y(25),s5,mu5));



if y(25)<=Vfemin;

    wye25 = Vfemin;

else

    if (y(25)>Vfemin)&&(y(25)<=Vemax);

        wye25 = y(25);

    else

        wye25 = Vfemax;

    end

end



IN = KC*(y(4)/Irb)/wye25;

if IN<=0.433;

    FEX = 1-(1/sqrt(3)*IN);

else

    if (IN>0.433)&&(IN<=0.75);

        FEX = sqrt(0.75-IN);

    else

        if (IN>0.75)&&(IN<=1.0);

            FEX = sqrt(3)*(1.0-IN);

        else
```

```
                 FEX = 0;

             end

         end

end


zed32 = zeros(3,2);

zed33 = zeros(3);

zed62 = zeros(6,2);

zed611 = zeros(6,11);

zed35 = zeros(3,5);

zed312 = zeros(3,12);

zed314 = zeros(3,14);

zed621 = zeros(6,21);

zed1317 = zeros(13,17);


% u = [1vg10in 2vg1din 3vg1qin 4vg1Fin 5vg1Din 6vg1Qin 70 8~Pin 9VFEmult...

% 10g1vrefpu 11Prefg1pu 12wrefpu 13Prefespu 14Qrefespu...

% 15Qrefg1pu 16wye24 17wye25]'


u = [0; 0; 0; FEX*wye25*Vrb; 0; 0; 0; 1; 1; vr; prefg1; 1;...
480*sqrt(2/3)*[cos(omega*t+teta); cos(omega*t+teta-2*pi/3);...
cos(omega*t+teta+2*pi/3)]; wye24; wye25];


% LAD = Lmd;

LAD = polyval(p6,480*y(21),s6,mu6);


    rgen = [ra+3*rn 0 0 0 0 0
```

```
        0 ra we*Lq 0 0 we*kMQ

        0 -we*(ld+LAD) ra -we*LAD -we*LAD 0

        0 0 0 rF 0 0

        0 0 0 0 rD 0

        0 0 0 0 0 rQ];


    lgen = [L0+3*Ln 0 0 0 0 0

        0 ld+LAD 0 LAD LAD 0

        0 0 Lq 0 0 kMQ

        0 LAD 0 lF+LAD LAD 0

        0 LAD 0 LAD lD+LAD 0

        0 0 kMQ 0 0 LQ];


lgeni = lgen\eye(6);


% NL first order DE
dy = [-lgen\rgen zed62 [-sqrt(2/3)*lgeni(1:3,1:3)...
    *[1/sqrt(2) 1/sqrt(2) 1/sqrt(2); cos(p/2*y(8)+pi/2) cos(p/2*y(8)-pi/6)...
    cos(p/2*y(8)+7*pi/6); sin(p/2*y(8)+pi/2) sin(p/2*y(8)-pi/6)...
    sin(p/2*y(8)+7*pi/6)]
    -sqrt(2/3)*lgeni(4:6,1:3)*[1/sqrt(2) 1/sqrt(2) 1/sqrt(2);...
    cos(p/2*y(8)+pi/2) cos(p/2*y(8)-pi/6) cos(p/2*y(8)+7*pi/6);...
    sin(p/2*y(8)+pi/2) sin(p/2*y(8)-pi/6) sin(p/2*y(8)+7*pi/6)]] zed621...
    % 1 to 6 [ig10 ig1d ig1q ig1F ig1D ig1Q]'
    -1/(sqrt(3)*J*y(7))*(y(9)+y(10)+y(11))...
    -sqrt(2)/(sqrt(3)*J*y(7))*(y(9)*cos(p/2*y(8)+pi/2)...
    +y(10)*cos(p/2*y(8)-pi/6)+y(11)*cos(p/2*y(8)+7*pi/6))...
```

```
-sqrt(2)/(sqrt(3)*J*y(7))*(y(9)*sin(p/2*y(8)+pi/2)...

+y(10)*sin(p/2*y(8)-pi/6)+y(11)*sin(p/2*y(8)+7*pi/6))...

0 0.0 0 -D*y(7)/J 0 0 0.0 ...

0 0 0 0 0.0 0 0 0 0 0.0 0 0 0 0 0.0 0 0 0 1/(J*y(7)) 0.0 0 0 0 % 7 [omegam]

0 0 0 0 0.0 0 0 1 0 0 0.0 0 0 0 0 0.0 0 0 0 0 0.0 0 0 0 0 0.0 ...

0 0 0 0 0.0 0 0 0 % 8 [thetam]

sqrt(2/3)*c\([1/sqrt(2) 1/sqrt(2) 1/sqrt(2);...

cos(p/2*y(8)+pi/2) cos(p/2*y(8)-pi/6) cos(p/2*y(8)+7*pi/6);...

sin(p/2*y(8)+pi/2) sin(p/2*y(8)-pi/6) sin(p/2*y(8)+7*pi/6)]...

\eye(3)) zed35 -c\g -c\eye(3) zed33 zed33 zed312...

% 9 to 11 [vc1a vc1b vc1c]'

zed33 zed35 lln1\eye(3) -lln1\rln1 -lln1\eye(3) zed33 zed312...

% 12 to 14 [iln1a iln1b iln1c]'

zed33 zed35 zed33 c\eye(3) -c\g -c\eye(3) zed33 zed33 zed33 c\eye(3)...

% 15 to 17 [vc2a vc2b vc2c]'

zed33 zed35 zed33 zed33 l1\eye(3) -l1\r1 zed312...

% 18-20 [ild1a ild1b ild1c]'

0 0 0 0 0.0 0 0 0 0 0.0 0 0 0 0 0.0 0 0 0 0 0.0 0 0 0 0 0.0 ...

0 0 0 0 0.0 0 0 0 % 21 [vg1fb]

0 0 0 0 0.0 0 0 0 0 0.0 0 0 0 0 0.0 0 0 0 0 0.0 -ki 0 0 0 0.0 ...

0 0 0 0 0.0 0 0 0 % 22 [vg1i*]

0 0 0 0 0.0 0 0 0 0 0.0 0 0 0 0 0.0 0 0 0 0 0.0 0 0 0 -1/taud 0 0.0 ...

0 0 0 0 0.0 0 0 0 % 23 [vg1d*]

0 0 0 0 0.0 0 0 0 0 0.0 0 0 0 0 0.0 0 0 0 0 0.0 ...

-kp*KAow*y(7)/TA KAow*y(7)/TA KAow*y(7)/TA 0 0.0 0 0 0 0 0.0 0 0 0 ...

% 24 [vg1R]

0 0 0 -KD/(TE*Irb) 0.0 0 0 0 0 0.0 0 0 0 0 0.0 0 0 0 0 0.0 ...
```

```
0 0 0 0 0.0 0 0 0 0 0.0 0 0 % 25 [vg1E]

0 0 0 0 0.0 0 0 0 0 0 0.0 0 0 0 0 ...

kipll*sqrt(2/3)*cos(y(27)+pi/2) kipll*sqrt(2/3)*cos(y(27)-pi/6)...

kipll*sqrt(2/3)*cos(y(27)+7*pi/6) 0 0 0.0 0 0 0 0 0.0 0 0 0 0 0.0 0 0 ...

% 26 [omega_hati]

0 0 0 0 0.0 0 0 0 0 0.0 0 0 0 0 ...

kppll*sqrt(2/3)*cos(y(27)+pi/2) kppll*sqrt(2/3)*cos(y(27)-pi/6)...

kppll*sqrt(2/3)*cos(y(27)+7*pi/6) 0 0 0.0 0 0 0 0 0.0 1 0 0 0 0.0 ...

0 0 % 27 [theta_hat]

0 0 0 0 0.0 0 0 0 0 0.0 0 0 0 0 ...

kppll/tauf*sqrt(2/3)*cos(y(27)+pi/2)...

kppll/tauf*sqrt(2/3)*cos(y(27)-pi/6)...

kppll/tauf*sqrt(2/3)*cos(y(27)+7*pi/6) 0 0 0.0 0 0 0 0 0.0 ...

1/tauf 0 -1/tauf 0 0.0 0 0 % 28 [omega_hatlpf]

0 0 0 0 0.0 0 -Pmax/(R*taug1*60*pi) 0 0 0.0 0 0 0 0 0.0 0 0 0 0 0 0.0 ...

0 0 0 0 0.0 0 0 0 -1/taug1 0.0 0 0 0 % 29 [Pmechg1]

zed314 -lt\eye(3) zed312 -lt\rt]*y+... % 30-32 [ita itb itc]'

[lgeni zed611 % 1-6

0 0 0 0 0.0 0 0 0 0 0 0.0 0 0 0 0 0 0.0 0 0 0 % 7

zed1317 % 8-20

0 0 0 0 0.0 0 0 0 ...

wco*(sqrt(((y(9)-y(10))^2+(y(10)-y(11))^2+(y(11)-y(9))^2)/3)/480 ...

-y(21)) 0.0 0 0 0 0 0 0.0 0 0 0 % 21 [vg1fb]

0 0 0 0 0.0 0 0 0 0 ki 0 0 0 0 0.0 0 0 0 % 22 [vg1i*]

0 0 0 0 0.0 0 0 0 ...

-(kd/taud)*wco*(sqrt(((y(9)-y(10))^2+(y(10)-y(11))^2+(y(11)...

-y(9))^2)/3)/480-y(21)) 0.0 0 0 0 0 0 0.0 0 0 0 % 23 [vg1d*]
```

182

```
0 0 0 0 0.0 0 0 0 0 kp*KAow*y(7)/TA 0 0 0 0 0 0.0 -1/TA 0 % 24 [vg1R]

0 0 0 0 0.0 0 0 -polyval(p5,wye25,s5,mu5) 0 0.0 0 0 0 0 0.0 ...

1/TE -(KE/TE)% 25 [vg1E]

0 0 0 0 0.0 0 0 0 0 0.0 0 0 0 0 0.0 0 0 % 26 [omega_hati]

0 0 0 0 0.0 0 0 0 0 0.0 0 0 0 0 0.0 0 0 % 27 [theta_hat]

0 0 0 0 0.0 0 0 0 0 0.0 0 0 0 0 0.0 0 0 % 28 [omega_hatlpf]

0 0 0 0 0.0 0 0 0 0 0.0 Pmax/taug1 Pmax/(R*taug1) 0 0 0.0 ...

0 0 % 29 [Pmechg1]

zed312 lt\eye(3) zed32]*u; % 30-32 [ita itb itc]'
```
return

Matlab® file eps9_4.m for electric power system parameters

```
function [rln,lln,c,g,rld1,lld1,rld2,lld2,wco,kipll,kppll,tauf,...
    tevent,tflt,rt,lt,omega] = eps9_4()

l = 1/5280; % cable length in miles

% circuit impedances

% from Westinghouse T&D Table 6 Chapter 4 p79

wco = 150;

kipll = 100;

kppll = 10;

tauf = 1/125;

tevent = 10.2;

omega = 2*pi*60;

tflt = 3/60;


% 500MCM CU 1kV 60Hz impedance

r0 = 2.74; % = rs+2rm [ohms/mile]

xln0  = 0.208; % = xs+2xm [ohms/mile]

r1 = 0.1354; %  = r2 = rs-rm [ohms/mile]

xln1 = 0.123; %  = x2 = xs-xm [ohms/mile]


% 500MCM CU 1kV 60Hz shunt capacitance

xc0 = 2600; % [ohms/mile]

xc1 = 1300; % [ohms/mile]

bc0 = 1/xc0; % [S/mile]

bc1 = 1/xc1; % [S/mile]


% 500MCM CU 1kV 60Hz shunt resistance
```

```
rl0 = 9000; % [ohms*mile]

rl1 = 4700; % [ohms*mile]

gl0 = 1/rl0; % [S/mile]

gl1 = 1/rl1; % [S/mile]


% % #2 CU 1KV 60Hz impedance
% r0 = 6.99; % = rs+2rm [ohms/mile]
% xln0  = 0.273; % = xs+2xm [ohms/mile]
% r1 = 0.987; %  = r2 = rs-rm [ohms/mile]
% xln1 = 0.165; %  = x2 = xs-xm [ohms/mile]
%
% % #2 CU 1kV 60Hz shunt capacitance
% xc0 = 9000; % [ohms*mile]
% xc1 = 4700; % [ohms*mile]
% bc0 = 1/xc0; % [S/mile]
% bc1 = 1/xc1; % [S/mile]
%
% % #2 CU 1kV 60Hz shunt resistance
% rl0 = 9000; % [ohms*mile]
% rl1 = 4700; % [ohms*mile]
% gl0 = 1/rl0; % [S/mile]
% gl1 = 1/rl1; % [S/mile]


% Assume l mile
rs = l*(r0+2*r1)/3; % [ohms]
ls = l*(xln0+2*xln1)/(3*omega); % [H]
rm = l*(r0-r1)/3; % [ohms]
```

```
lm = l*(xln0-xln1)/(3*omega); % [H]


% Assume 1 mile using lumped parameter pi model

cm = l*(bc1-bc0)/(3*omega*2); % [F]

cs = l*(2*bc1+bc0)/(3*omega*2); % [F]

gm = l*(gl1-gl0)/(3*2); % [S]

gs = l*(2*gl1+gl0)/(3*2); % [S]

rln = [rs rm rm; rm rs rm; rm rm rs];

lln = [ls lm lm; lm ls lm; lm lm ls];

c = [cs -cm -cm; -cm cs -cm; -cm -cm cs];

g = [gs -gm -gm; -gm gs -gm; -gm -gm gs];


% s1 = 39e3 + 1i*0.75*39e3;

% z1 = 480^2/conj(s1);

% r1 = real(z1);

% l1 = imag(z1)/omega;

%

% rld1 = [r1 0 0; 0 r1 0; 0 0 r1];

% lld1 = [l1 0 0; 0 l1 0; 0 0 l1];


% s2 = 2e6 + 1i*0.75*2e6;

% z2 = 480^2/conj(s2);

% r2 = real(z2);

% l2 = imag(z2)/omega;


s2 = 2000 + 1i*0.75*2000;

z2 = 480^2/conj(s2);
```

```
r2 = real(z2);

l2 = imag(z2)/omega;

% x2 = imag(z2);


% s2 = 40e3 + 1i*30e3;

% z2 = 480^2/conj(s2);

% r2 = real(z2);

% l2 = imag(z2)/omega;

% x2 = imag(z2);


rld1 = [r2 0 0; 0 r2 0; 0 0 r2];

lld1 = [l2 0 0; 0 l2 0; 0 0 l2];


% a phase line to neutral fault

% rldflt = [1e-4 0 0;0 rldb 0; 0 0 rldc];

% lldflt = [1e-6 0 0; 0 lldb 0; 0 0 lldc];


% rldflt = [r2 0 0; 0 r2 0; 0 0 r2];

% lldflt = [l2 0 0; 0 l2 0; 0 0 l2];

% m = 100;

% rld2 = [m*r1 0 0; 0 m*r1 0; 0 0 m*r1];

% lld2 = [m*l1 0 0; 0 m*l1 0; 0 0 m*l1];


% % phase to neutral fault - full load

% m = 1e-6;

% rld2 = [m*r2 0 0; 0 r2 0; 0 0 r2];

% lld2 = [m*l2 0 0; 0 l2 0; 0 0 l2];
```

```matlab
% phase to neutral fault - no load

m = 1e-8;

rld2 = [m*r2 0 0; 0 r2 0; 0 0 r2];

lld2 = [m*l2 0 0; 0 l2 0; 0 0 l2];


% 3 phase fault

% m = 1e-5;

% rld2 = m*rld1;

% lld2 = m*lld1;


% % three phase fault

% rldflt = [1e-7 0 0;0 1e-7 0; 0 0 1e-7];

% lldflt = [1e-9 0 0; 0 1e-9 0; 0 0 1e-9];


% impedance to the infinite bus - assume delta-wye transformer with no leakage

% capacitance

Rs1 = 5.4e-5; % [ohms] electric power system positive sequence resistance

Xs1 = 5.4e-4; % [ohms] electric power system positive sequence reactance

Ztmag = 0.075; % [pu] transformer impedance

Sbase = 3e6; % [VA] transformer rating

XtoR = 10; % assume X/R = 10

Vbase = 480; % [V]

Ztbase = Vbase^2/Sbase; % [ohms]

Ztohm = Ztmag*Ztbase; % [ohms]

Rt = Ztohm/sqrt(XtoR^2+1); % [ohms]

Xt = Rt*XtoR; % [ohms]
```

```
% rt0 = Rt+Rs1; % = rts+2rtm [ohms] for wye-wye

% xt0  = Xt+Xs1; % = xts+2xtm [ohms] for wye-wye

rt0 = Rt; % = rts+2rtm [ohms] for delta-wye gnd

xt0  = Xt; % = xts+2xtm [ohms] for delta-wye gnd

rt1 = Rt+Rs1; %  = rt2 = rts-rtm [ohms]

xt1 = Xt+Xs1; %  = xt2 = xts-xtm [ohms]


rts = (rt0+2*rt1)/3; % [ohms]

lts = (xt0+2*xt1)/(3*omega); % [H]

rtm = (rt0-rt1)/3; % [ohms]

ltm = (xt0-xt1)/(3*omega); % [H]


rt = [rts rtm rtm; rtm rts rtm; rtm rtm rts];

lt = [lts ltm ltm; ltm lts ltm; ltm ltm lts];


end
```

Matlab® files rb_hsg_740066_V9_4.m containing main generator parameters and rb_5_inch_exciter9_4.m containing exciter parameters are withheld as they contain proprietary information.
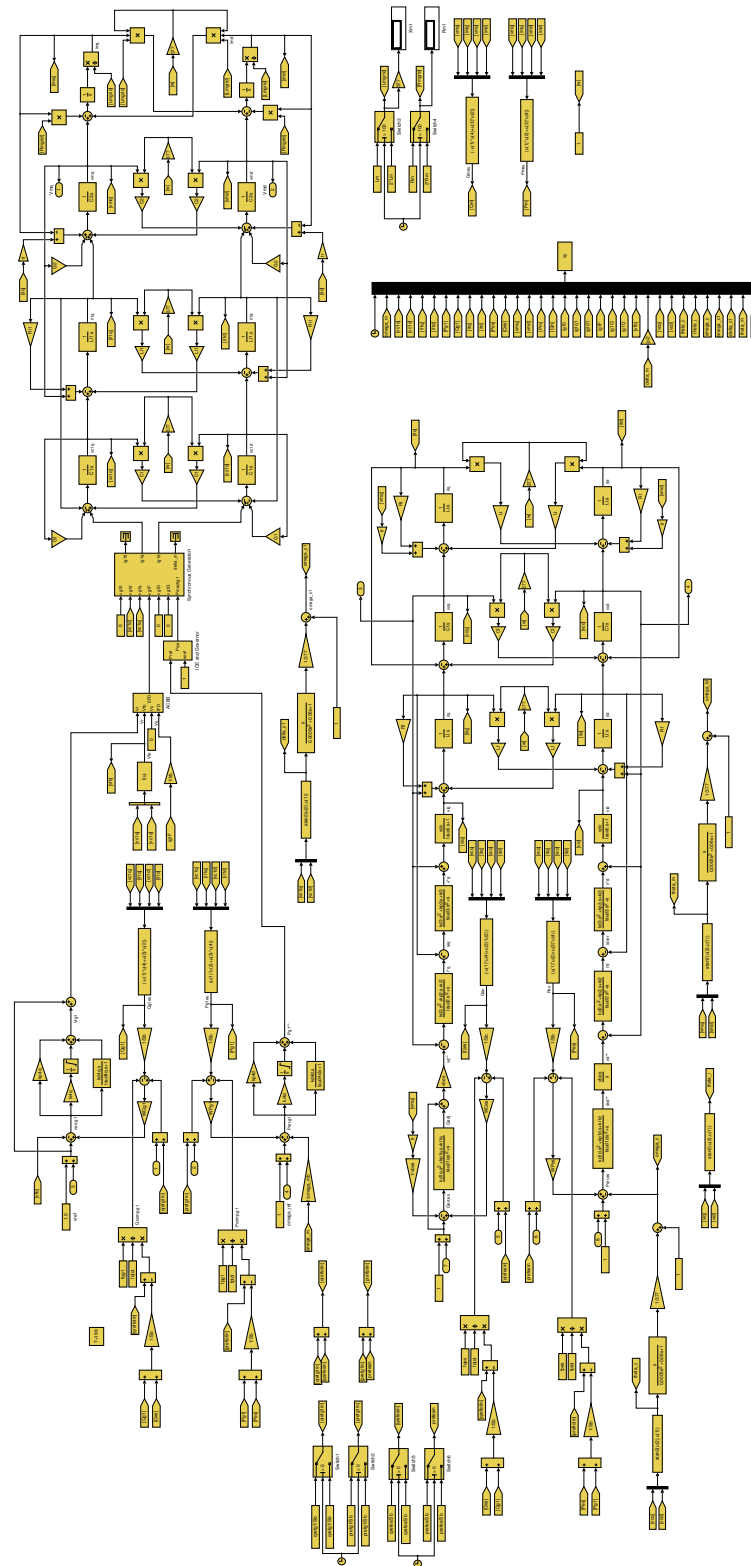
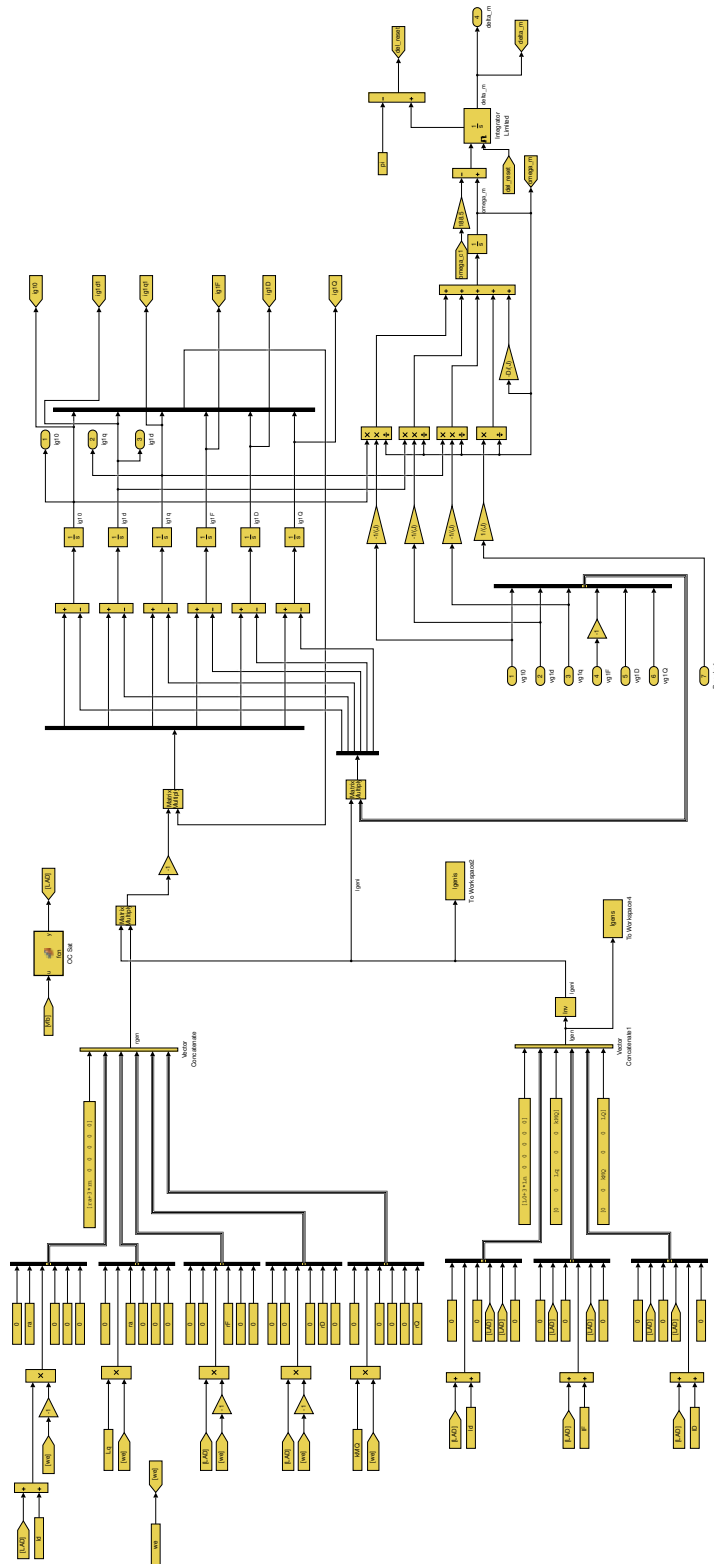Figure A4: Diagram of the main Simulink® model for the micro–grid.

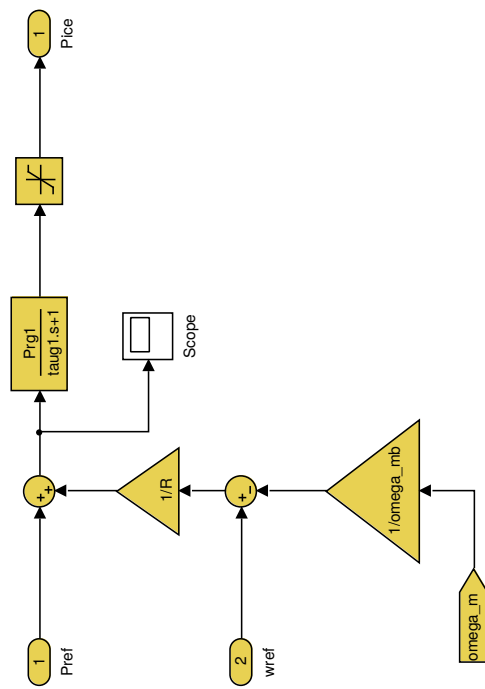Figure A5: Diagram of the synchronous generator model for the micro–grid.

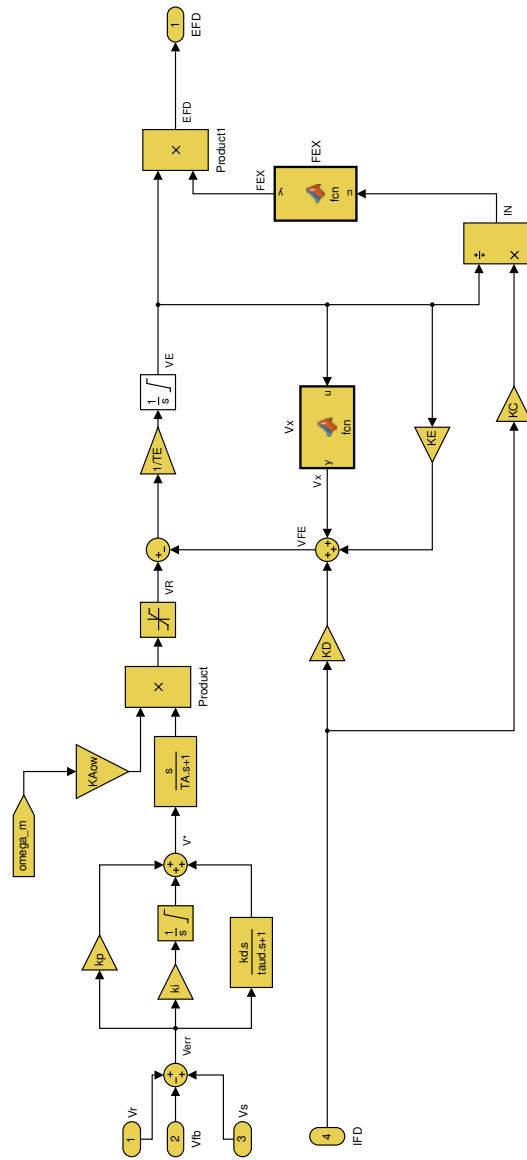Figure A6: Diagram of the internal combustion engine and governor model for the micro–grid.

Figure A7: Diagram of the AC8B voltage regulator and excitation system model for the micro–grid.

<div align="center">

CURRICULUM VITAE

</div>

Education

University of Wisconsin Milwaukee *August 2016*

PhD Electrical Engineering

Business Minor

Cumulative GPA 4.0/4.0

University of Wisconsin Milwaukee *December 2009*

MS in Electrical Engineering

Cumulative GPA 4.0/4.0

Marquette University *December 1985*

BS in Electrical Engineering, Cum Laude

Cumulative GPA 3.5/4.0

Experience

Milwaukee School of Engineering University

December 2013 – Present

Adjunct Assistant Professor

Milwaukee WI

- Classes Taught:

- EE253 and EE3401 – Electromechanical Energy Conversion and Control

- EE2050 – Linear Circuits – Steady State I (DC)

- EE2060 – Linear Circuits – Steady State II (AC)

- EE499 – Independent Study – Bulk Power System Stability

- EE499 – Independent Study – Transmission System Sequence Components and Relaying

- Other Contributions

  - With John Wheeldon, developed EE3401 syllabus based on Umans' text

  - Engaged student Alex Andrews to improve National Instruments motor tachometer in the power lab

L7 Consulting LLC

July 2013 – Present

Sole Member

Milwaukee WI Owner of a consulting business specializing in commercial and utility electrical equipment specification, system studies and analysis, protection, and power quality analysis

University of Wisconsin Milwaukee

January 2014 – Present

Research Assistant

Milwaukee WI

Research focused on micro–grid control and generator models for unbalanced system conditions

University of Wisconsin Milwaukee

August 2013 – January 2014

Teaching Assistant

Milwaukee WI

- Taught Introduction to Control Systems Laboratory with emphasis on discovery learning

- Awarded Outstanding Teaching Assistant 2013

We Energies

February 2007 – June 2013

Project Manager Operational SupportMilwaukee WI

- Negotiated agreements with operating entities adjacent to and contained within the WEC Balancing Authority Area

- Built models for energy accounting systems to track generation, interchange, and load for the WEC Balancing Authority and several Load Serving Entities

- Led a cross functional team with external partners that developed plans to restore power to southeast Wisconsin following a blackout event

- Researched and co–wrote the May, 2012 North American Electric Reliability Corporation Severe Impact Resilience Task Force (SIRTF) report in collaboration with an international team of industry experts and federal and state regulators

- Presented the SIRTF report at the Edison Electric Institute April, 2012 Business Continuity and Mutual Assistance Conference

- Developed and communicated a suite of emergency operating procedures compliant to enforceable standards

- Served as a subject matter expert for ReliabilityFirst audits and achieved 100% compliance.

- Served as subject matter expert for preparation of the blackout report on power loss to Michigan's Upper Peninsula occurring May 10, 2011

We Energies

October 2004- February 2007

Power System Supervisor

Milwaukee WI

- Directed power plant output and interchange transactions in real time to minimize production costs while maintaining acceptable system reliability

- Operated and maintained real time and study environment state estimator programs

- Developed situational awareness tools to expedite problem resolution for display 24x7 in the control room

We Energies

January 2002 - October 2004

Construction and Maintenance Supervisor

Milwaukee WI

- Created mechanism and meetings to coordinate substation construction activity between distinct groups that improved communication between groups, and established common understanding of goals, deadlines and priorities

- Utilized innovative work practices to share resources across labor union boundaries to complete high priority projects on time and within budget

- Reassigned crews to capital and external customer projects to minimize operating and maintenance expenditures - saving $50,000-$100,000 annually in O&M expenses

We Energies

May 1999 – January 2002 and September 1982 – 1994

Engineering Roles with Increasing Responsibilities

Milwaukee WI

- Developed new and revised existing standards for customer and utility interface equipment – switchgear, transformers, metering equipment, protection, and grounding

- Provided outstanding customer service by trouble shooting and resolving power quality issues at large customer locations

- Acted as technical interface and coordinator for new equipment installed at large customers in southeast Wisconsin

- Managed hands on equipment start–up – switchgear, transformers, voltage regulators and protection devices

Luke Weber Photography

February 1994-May 1999

Self Employed

Milwaukee WI Focus on editorial and commercial photography for Milwaukee area corporations and organizations

Professional Engagement

Licensure   State of Wisconsin Professional Engineer No. 26824–6

since January 26,1990

IEEE   Member Power Engineering Society

IEEE   Member Control Systems Society

Publications

- *Modeling and Control of a Synchronous Generator in an AC Micro–grid Environment*, Luke Weber, Adel Nasiri, David Hyypio, and William Dittman, 2016 IEEE Energy Conversion Congress and Expo, *Not Yet Published*

- *Chapter 18 Uninterruptible power supplies, Power Electronic Converters and Systems: Frontiers and applications*, Luke G. Weber and Adel Nasiri, Edited by Andrzej M. Trzynadlowski, IET Press, 2015

- *Micro–grids: Architectures, Controls, Protection, and Demonstration*, Qiang Fu, Adel Nasiri, Ashishkumar Solanki, Abedalsalam Bani–Ahmed, Luke Weber, and Vijay Bhavaraju, Electric Power Components and Systems, 2015

- *Micro–grid Communications: State of the Art and Future Trends*, A. Bani–Ahmed, L. Weber, A. Nasiri, H. Hosseini, International Conference on Renewable Energy and Research and Applications, October 2014

- *EV Charging Station Integrating Renewable Energy and Second–Life Battery*, Ahmad Hamidi, Luke Weber, Adel Nasiri, International Conference on Renewable Energy Research and Applications, October 2013

- *Severe Impact Resilience: Considerations and Recommendations*, Severe Impact Resilience Task Force, NERC Special Report, May 9, 2012